Pharmacokinetics and efficacy of a tunable curcumin-loaded polymeric nanoparticle for neonatal neuroprotection

Nuo Xu

A dissertation

submitted in partial fulfillment of the

requirements for the degree of

Doctor of Philosophy

University of Washington

2025

Reading Committee:

Elizabeth Nance, Chair

Cole DeForest

Suzie Pun

Thomas Ragnar Wood

Program Authorized to Offer Degree:

Chemical Engineering

University of Washington

Abstract

Pharmacokinetics and efficacy of a tunable curcumin-loaded polymeric nanoparticle for neonatal neuroprotection

Nuo Xu

Chair of the Supervisory Committee:

Elizabeth Nance

Chemical Engineering

Newborns with neurological disorders are in particular need of therapeutic intervention, due to the immaturity and rapid brain development in the perinatal period, which can increase risk of long-term neurodevelopmental disability. In many neurological disorders, including neonatal or perinatal brain injury, inflammation results in sustained activation of pro-inflammatory microglia that drives ongoing pathology and worse outcomes. This thesis research focused on using anti-inflammatory small molecules-loaded polymeric nanoparticles as potential neuroprotective agents for neonatal or perinatal brain disease and injury. Firstly, we quantified the pharmacokinetics (PK) and biodistribution of polymeric nanoparticles formulated using different surfactants as stabilizers, and investigated the effects of surfactants on PK profiles and biodistribution of polymeric nanoparticles in the term-equivalent rat. Our

results show that the PK and biodistribution of polymeric nanoparticles can be adjusted by changing the surfactant. To increase the systemic half-life of polymeric nanoparticles and formulate nanoparticles with improved bioavailability, Pluronic F127 (F127) should be used as the stabilizer. Next, using F127 as the stabilizer, we investigated the effects of PLGA length, stabilizer concentration, polymer functionalization, and formulation method on curcumin loading. Upon successful optimization of a PLGA-PEG nanoparticle with high curcumin encapsulation efficiency and drug loading, we assessed particle PK and biodistribution in term pigs. To move into a clinical-trial ready model, we also assessed particle accumulation in the fetal growth restricted (FGR) piglet brain following different administration routes. We found curcumin-loaded nanoparticles were colocalized with microglia after intranasal administration, which demonstrated the potential of our polymeric nano-platform to be used as a microglia-targeting vehicle for hydrophobic molecules in perinatal brain injury. Finally, we used the curcumin-loaded nanoparticles with optimized curcumin loading and systemic circulation half-life to evaluate the neuroprotective effects in neonatal rats with brain injury at different developmental ages. The relationship between developmental age and neuroprotective effect of the nano-therapy was revealed: after a single dose of curcumin-loaded nanoparticles, neuroprotective effects were only observed in the acute period in late preterm-equivalent rats with hypoxic-ischemic (HI) brain injury, but not in term-equivalent or late-term equivalent rats with HI. Our results suggest that 1) neonatal dose determination should be based on developmental age, and 2) multiple doses of curcumin-loaded polymeric nanoparticles are needed for neonatal neuroprotection after HI.

Acknowledgements

This thesis marks the end of the journey, and I am grateful to everyone who supported me along the way.

First and foremost, I would like to thank my supervisor, Dr. Elizabeth Nance, for the invaluable guidance, encouragement, and support. I joined Nance Lab as an MS student in March 2020, and I chose to continue my PhD here because I believed – with Elizabeth's mentorship – I would thrive throughout this journey. That belief has carried me through.

I am also sincerely grateful to my collaborators – this work would not have been possible without you. Thank you, Julie and Kirat, for working together to make the international collaboration a reality and for collecting the data used in Chapter 3. Thank you, Tommy, Kylie, and the entire Neonatal Neuroscience Lab, for our teamwork and efforts in collecting the data presented in Chapter 4.

I would like to thank my parents for their unconditional and unwavering support. A special thanks to my mom, Xiang, for being my constant source of strength and motivation throughout this journey.

This has been an incredible journey. Thank you to everyone who has been part of this journey. I could not have done this without you.

Table of Contents

Chapter 1: Introduction

Over 600 neurological disorders can occur throughout a person's lifetime. In the US, the annual cost of neurological disorders is $800 billion. Newborns with neurological disorders are receiving increasing focus, due to the immaturity and the rapid development of their brains around the perinatal period, which are associated with long-term neurodevelopmental disabilities. However, there are no curative treatments, motivating the need for innovative, effective, and non-invasive therapeutic options for these patients. Polymer based nanomedicine is a controlled and sustained drug delivery system that can provide neuroprotection in a highly-efficient and non-invasive manner. Polymer nanomedicine use in the neonatal population has not yet been explored, primarily due to limited preclinical data. The scope of this thesis is to expedite the clinical translation of the neuroprotective polymeric nanoparticles for use in neonates. In the introduction to this thesis, we provide background on neurological disorders in neonates, the use of therapeutic polymer nanoparticles in clinical settings, and the state-of-the-art preclinical animal models used to study perinatal brain injury. We then quantify the preclinical pharmacokinetics (PK) and biodistribution of these nanoparticles in term-equivalent rats to provide guidance for efficacy and toxicity evaluation. Following that, the physicochemical properties of nanoparticles were optimized with the guide of PK and biodistribution data. Using the optimal polymeric nano-platform with reproducibility, tunability, shelf-life stability, and high hydrophobic cargo loading and encapsulation efficiency, we characterized preclinical PK and biodistribution in a piglet model to generate more human-comparable preclinical data. Lastly, we analyzed, the impact of developmental stage on neuroprotective effects of drug-loaded polymer nanoparticles in a rat model of perinatal brain injury. These data will contribute to the accelerated clinical translation of polymer-based nanomedicine and provide guidance for the translational study in the nanomedicine field.

1.1. Neurological disorders in neonates

Around 3 in every 1000 pregnant women have fetuses with various brain abnormalities[1]. The abnormal brain development during fetal life will contribute to many neurological disorders and may last throughout the lifespan[2]. The common types of neurological disorders in neonates include fetal growth restriction (FGR), hypoxic-ischemic encephalopathy (HIE), premature birth, and seizures[3, 4]. HIE and seizures are caused by loss of oxygen or blood flow to the brain or premature birth, and HIE is a major cause of neonatal seizures[5].

1.1.1. FGR

Fetal growth restriction (FGR) occurs when a fetus is unable to grow normally due to inadequate nutrient and oxygen supply[6]. FGR is a condition that affects 5-10% of pregnancies in developed countries and up

to 25% of pregnancies in low to middle income countries[7]. Globally, around 20 million babies are born growth restricted every year and FGR is a leading cause of perinatal mortality and long-term disability. FGR is often defined as an estimated fetal weight less than the 10th percentile for gestational age and is determined by prenatal ultrasound evaluation in clinical practice. However, due to the variability of clinical presentation, up to 50% of FGR fetuses remain undiagnosed, and are first recognized in late pregnancy or at birth[6-8]. The brain is particularly vulnerable to prolonged hypoxic FGR conditions, and adverse outcomes cause life-long complications that range from learning and behavioral issues to cerebral palsy[9-11]. It is vital to treat FGR newborns early to prevent or reduce life-long disorders; however, there are no treatments to protect the FGR newborn brain. Wixey et al. have previously shown neuroprotective effects using anti-inflammatory treatments such as ibuprofen[12, 13], and placental-derived stem cells[14], in the FGR newborn pig. However, the dosing requirements to achieve these effects and the adverse effects associated with these treatment strategies indicate that an alternative safe and effective neuroprotective agent is critically needed.

1.1.2. HIE

Neonatal HIE is the neurological syndrome that occurs in the newborn infant subject to different degrees of a hypoxic-ischemia event. HIE is associated with loss of consciousness; decrease of spontaneous movements, tone, and reflexes; and appearance of convulsions in the more severe cases[15]. HIE occurs in 2 to 4 per 1000 live births in developed countries[16, 17]. Without treatment, two thirds of affected infants die or develop severe neurodevelopmental impairments including intellectual disability, cerebral palsy, epilepsy, and hearing or vision impairment[18, 19]. Therapeutic hypothermia (TH) is now a standard treatment strategy for HIE, which aims to improve neurodevelopment outcomes in infants with HIE. TH is the only approved treatment in clinical practice. However, TH requires intensive care support that necessitate appropriate resources, instrumentation and trained personnel, and TH is only therapeutically effective for treating moderate or severe HIE[15]. TH is only approved for term infants with HIE, but not for pre-term infants who suffer from brain injury. As a result, it is not an ideal treatment for patients in low- and middle-income countries, or preterm infants with brain injury. Therefore, it is necessary to develop easily administrable novel therapeutics with high treatment efficacy and low cost such that a clinician can make rapid decisions at birth to ensure intervention within the therapeutic window prior to the secondary brain injury[20].

1.1.3. Premature birth

Preterm birth, defined as delivery of an infant before 37 gestational weeks, have an increased risk of neurodevelopmental disorders[21, 22]. The global preterm birth rate is about 11%[23]. Neurodevelopmental disorders is a group of lifelong conditions include the impairments of cognitive,

communication, behavior and motor skills[24]. This risk might be related with the sudden and premature exposure of the rapidly developing brain to the extrauterine environment during a critical period for synaptic formation, dendritic differentiation, layering of cortical neurons and glial proliferation[25-27]. Cerebral palsy is the most significant neurological disorder associated with preterm birth, resulting in a huge economic and social burden. Some studies have shown that some antenatal neuroprotection strategies, such as magnesium sulphate and antenatal corticosteroids for fetal neuroprotection, may have favorable influence for the preterm brain[28, 29]. Postnatal management options such as TH, stem cells, and anti-inflammatory interventions are also being explored[30]. However, considering the wide range of developmental stages defined as preterm and the current preclinical adverse effects observed following therapies, there are no effective therapeutic options for preterm brain injury. Therefore, a more effective neuroprotective strategy is needed. Neuroprotective polymeric nanoparticles are one promising neuroprotective approach that have excellent bioavailability and biocompatibility and can be administered systemically or locally to maximize therapeutic accumulation in the brain[31].

1.1.4. Seizures

Although seizures are not a focus of this thesis, it is important to note seizures are a common type of neurological disorder associated with preterm birth and HIE. Seizures incidence is higher during the neonatal period than at any other time of the life. Seizures are the most common neurological emergency in the newborn period, which are associated with a high risk of mortality and morbidity[32]. Neonatal seizures occur in 1 to 3 per 1000 live births for babies born at full term, and with a significantly higher rate in premature neonates. Post-asphyxia encephalopathy, cerebral dysgenesis and meningitis/encephalitis are the most common adverse neurodevelopmental outcomes consistently associated with neonatal seizures[33]. Although many causes can give rise to neonatal seizures, most seizures are caused by hypoxic-ischemic encephalopathy, stroke or hemorrhage, infections, cortical malformations, errors of metabolism, and genetic etiologies. Additionally, neonatal drug withdrawal and birth-related head trauma can also lead to neonatal seizures[32]. The treatment for neonatal seizures might be time-critical[34], so it can be favorable to treat the neonatal seizures as early as possible.

For FGR, HIE, and brain injury associated with preterm birth, there are no effective therapies. Nanomedicine offers a promising platform to safely and effectively deliver therapies to the perinatal brain to improve neurological outcomes in this patient population.

1.2. Therapeutic nanoparticles and polymeric nanoparticles

Due to the rapid neurodevelopment in the perinatal period, cost-effective and easy-to-access strategies for monitoring, assessing and treating neurodevelopmental disorders are important to provide timely

interventions[35]. Conventional therapeutics exhibit limitations of their solubility, stability, bioavailability etc., and thus have low therapeutic efficiency. Accordingly, therapeutic delivery systems with high efficiency and low cost and toxicity are needed. The application of nanotechnology to drug delivery shows significant advantages in pharmaceutical and biotechnology industries, such as improved delivery efficacy of hydrophobic drugs, greater stability and biocompatibility of drug products, extended route of administration, reduced toxicity, and effective targeted delivery to disease site [36, 37].

Therapeutic nanoparticles are nanoparticles used to deliver drugs and other therapeutic agents for disease treatment. Among the 75 of therapeutic nanoparticles approved by the Food and Drug Administration (FDA) or European Medicines Agency (EMA), 25 (33.3%) are lipid-based (Table 1-1), and 24 (32.0%) are polymer-based nanoparticles (Table 1-2). As of February 2024, search results with the keyword 'nanoparticle' on ClinicalTrials.gov produced 164 clinical trials for systemically administered therapeutic nanoparticles (Table S1-1) out of 640 clinical trials containing nanoparticles. Lipid-based nanoparticles are the most common vehicles for the systemic use of therapeutic nanomedicine. This may be due to advantages including low immunogenicity, the ability to encapsulate hydrophilic and hydrophobic active agents, and ease of manufacturing scalability[38-40]. Despite their wide use, lipid-based nanoparticles have drawbacks such as short systemic circulation time, instability *in vivo*, and active agent release during storage[41, 42].

Polymeric nanoparticles are the next most widely used nanoparticles[43]. Polymeric nanoparticles have 1 to 1000 nm diameters, which have a polymer-based core and can encapsulate and/or adsorb active ingredients within the core and/or on the particle surface. Advantages of polymeric nanoparticles include their capability to provide controlled and sustained drug release, protect the cargo against the bioenvironment, improve the bioavailability and physicochemical properties of the drug[44]. Hence, polymeric nanoparticles can be used as drug delivery vehicles to treat disease such as cancer, infections, blood disorders, endocrine and metabolic diseases, nervous system diseases and mental diseases, immunological diseases and inflammation, cardiovascular diseases, ocular diseases, and skin diseases, etc[44]. Polymer-based formulations in the market or clinical trials (Table 1-2, Table S1-1) demonstrate the potential of polymeric nanoparticles to be translated from laboratory results to clinical applications. Similarly, polymeric nanoparticles have drawbacks, including toxicity, limited encapsulation efficiency for hydrophilic cargos, and lack of scalability[45]. Polymeric lipid hybrid nanoparticles are an emerging platform for active agent delivery that combines the properties of lipid- and polymer-based nanoparticles by having a polymeric core and lipid-polyethylene glycol (PEG) shell[46]. Notably, 18 PEGylated nanoparticles are among the 75 approved nano-formulations, constituting a large number (24.0%) of nano-formulations.

Besides lipid- and polymer-based nanoparticles, protein-based nanoparticles (5.3%), nanocrystals (20.0%), and inorganic nanoparticles (9.3%) comprise the remaining third of therapeutic nanoparticles in the global market (Table 1-3). Since both nanocrystals and inorganic nanoparticles are formulated using inorganic materials, their therapeutic applications are confined by the short systemic circulation time and poor biocompatibility. These nanoparticles are more frequently used for imaging-based applications[46, 47].

In this thesis, we focus on the use of polymeric nanoparticles for non-invasive delivery to the brain. Polymer nanoparticles can carry cargo across the blood-brain barrier (BBB), and their tunable size provides them with good diffusivity in brain parenchyma, which ensures polymer-based nanoparticles can be used for neuroprotection and neurological diseases treatment [48-50]. Our pervious studies indicates that 1) nanoparticles should be smaller than 114 nm to freely diffuse in brain parenchyma[51], and 2) surfactants can determine the biodistribution of nanoparticles[50]. So, here, we aim to develop a polymeric nano-platform with a sub-100 nm particle size, prolonged systemic half-life, high anti-inflammatory drug loading, sustained release profile, and shelf-life stability. After the formulation, the PK and efficacy of this nano-platform will be characterized in preclinical animal models to help expedite its clinical translation.

Table 1-1. Lipid-based therapeutic nanoparticles approved by FDA or EMA.

Trade name	Particle type	Active ingredients	Application/Indication	Approval year	Particle size
AmBisome®	Liposomes	Amphotericin B	Fungal infections	EMA (1990), FDA (1997)	Less than 100 nm[52, 53]
Doxil® (Caelyx®)	PEGylated nano-liposomes	Doxorubicin hydrochloride	Ovarian cancer; multiple myeloma; HIV-associated Kaposi's sarcoma (KS)	FDA (1995), EMA (1996)	Less than 100 nm[54]
Abelcet®	Lipids	Amphotericin B	Fungal infections	FDA (1995)	1600 to 11000 nm[53, 55]
DaunoXome®	Liposomes composed of a lipid bilayer of distearoylphosphatidylcholine and cholesterol (2:1 molar ratio)	Daunorubicin citrate	Advanced HIV-associated KS	FDA, EMA (1996)	45 nm[53]
Amphotec	Liposomes	Amphotericin B	Fungal infections	FDA (1996)	130 nm[53]
Caelyx®	PEGylated liposomes	Doxorubicin hydrochloride	Metastatic breast cancer; advanced ovarian cancer; HIV-associated KS; multiple myeloma	EMA (1996)	90 nm[56]

Inflexal® V	Lecithin-phospholipid liposomes	Haemagglutinin surface molecules of the influenza viruses	Influenza	EMA (1997)	About 150 nm[53]
Curosurf®	Liposomes	Poractant alfa	Respiratory distress syndrome (RDS) in premature infants	FDA (1999)	Size distribution centered on 80 and 800 nm[57]
Visudyne®	Liposomes	Verteporfin	Age-related macular degeneration (AMD)	FDA, EMA (2000)	150 to 300 nm[53]
Myocet®	Liposomes	Doxorubicin hydrochloride	Metastatic breast cancer	EMA (2000)	180 nm[53, 58]
DepoCyt®	Liposomes	Cytarabine	Lymphomatous meningitis	EMA (2002), FDA (2007)	10 to 20 μm[53]
DepoDur®	Liposomes	Morphine sulphate	Post-operative pain	FDA (2004), EMA (2006)	17 to 23 μm[53]
Mepact®	Liposomes	Mifamurtide	Osteosarcoma	EMA (2009)	2 to 3.5 μm[53, 59]
Exparel®	Liposomes	Bupivacaine	Pain management	FDA (2011)	24 to 31 μm[53]
Marqibo®	Sphingomyelin/Cholesterol liposomes	Vincristine sulfate	Acute lymphoblastic leukemia	FDA (2012). Approval is withdrawn as of May 2, 2022.	About 100 nm[53, 60]
Lipodox® (generic version of Doxil®/Caelyx®)	PEGylated nano-liposomes	Doxorubicin hydrochloride	Ovarian cancer; metastatic breast cancer; HIV-associated KS	FDA (2013)	180 nm[61]

Onivyde®	Liposomes	Irinotecan	Metastatic pancreatic cancer	FDA (2015)	110 nm[53]
Lipusu®	Liposomes	Paclitaxel	Breast cancer; lung squamous cell carcinoma	FDA (2016)	About 400 nm[62]
Vyxeos®	Liposomes	Daunorubicin and cytarabine	Acute myeloid leukemia (t-AML) or AML with myelodysplasia-related changes (AML-MRC)	FDA (2017), EMA (2018)	About 100 nm[63]
Shingrix®	3-O-desacyl-4'-monophosphoryl lipid	Recombinant varicella zoster virus surface glycoprotein E (gE) antigen	Prevention of herpes zoster (HZ)	FDA (2017), EMA (2018)	163 nm[64]
Onpattro® (patisiran)	PEGylated lipid	siRNA targeting transthyretin	Transthyretin-mediated amyloidosis	FDA, EMA (2018)	60 to 100 nm
Arikayce®	Liposomes	Amikacin	Mycobacterium avium complex (MAC) lung disease	FDA (2018)	About 300 nm
Comirnaty™ (Pfizer-BioNTech Vaccine)	Lipids	Nucleoside-modified mRNA (modRNA)	Covid-19	FDA, EMA (2021)	60 to 65 nm[65]

Spikevax™ (Moderna COVID-19 Vaccine)	Lipids	Nucleoside-modified mRNA (modRNA)	Covid-19	FDA, EMA (2022)	30 to 1000 nm[65]
Zolsketil®	PEGylated liposomes	Doxorubicin hydrochloride	Breast cancer; advanced ovarian cancer; multiple myeloma; HIV-associated KS	EMA (2022)	About 100 nm[66]

FDA: Food and Drug Administration. EMA: European Medicines Agency. HIV: Human Immunodeficiency Virus. KS: Kaposi's Sarcoma. siRNA: small interfering RNA. mRNA: messenger RNA. N/A: no data available.

Table 1-2. Polymer-based therapeutic nanoparticles approved by FDA or EMA.

Trade name	Particle type	Active ingredients	Application/Indication	Approval year	Particle size
Diprivan®	Micellar nanoparticle	Propofol	Anesthesia or sedation	FDA (1989), EMA (2001)	30 nm[67]
Adagen®	Polymeric conjugate (PEGylated)	Adenosine deaminase (ADA)	Severe combined immunodeficiency disease (SCID)	FDA (1990)	N/A
Oncaspar®	Polymeric conjugate (PEGylated)	Asparaginase	Acute leukemia; hypersensitivity to asparaginase	FDA (1994), EMA (2016)	50 to 200 nm
Apelea®	Micellar paclitaxel	Paclitaxel	Ovarian cancer	2018 (EMA)	20 to 30 nm

Copaxone®	Polypeptides	Glatiramer acetate	Multiple sclerosis (MS)	FDA (1996), EMA (2016)	Around 5 and 111 nm[68]
Renagel®	Sevelamer (consists of polyallylamine that is crosslinked with epichlorohydrin)	Sevelamer hydrochloride	Hyperphosphatemia caused by chronic kidney disease	FDA, EMA (2000)	23 μm[69]
PegIntron®	Polymeric conjugate (PEGylated)	Interferon alfa-2a	Chronic hepatitis C	EMA (2000), FDA (2001)	N/A
Pegasys®	Polymeric conjugate (PEGylated)	Interferon alfa-2a	Chronic hepatitis C; chronic hepatitis B	FDA, EMA (2002)	0.5 to 23 nm[70]
Zevalin®	Polymeric conjugate	β-emitting isotope, (90)Y, linked to the anti-CD20 monoclonal antibody (mAb), rituximab	Non-Hodgkin's lymphoma (NHL)	FDA (2002) (Discontinued), EMA (2004)	N/A
Somavert®	Polymeric conjugate (PEGylated)	Growth hormone receptor antagonist	Acromegaly	EMA (2002), FDA (2003)	N/A
Avinza®	Polymer beads constituted by ammonium-methacrylate copolymers	Morphine sulphate	Moderate to severe pain	FDA (2002) (Discontinued)	N/A

Neulasta®	Polymeric conjugate (PEGylated)	Filgrastim	Neutropenia caused by receiving chemotherapy	FDA (2002)	6 nm[71]
Estrasorb™	Micellar nanoparticle	Estradiol hemihydrate	Moderate to severe hot flashes after menopause	FDA (2003)	About 1 μm
Macugen®	Polymeric conjugate (PEGylated)	Anti-vascular endothelial growth factor (VEGF) aptamer	Wet age-related macular degeneration	FDA (2004)	N/A
Genexol-PM®	Micellar nanoparticle	Paclitaxel	Lung cancer	FDA (2007)	24 nm[72]
Renvela®	Sevelamer (consists of polyallylamine that is crosslinked with epichlorohydrin)	Sevelamer carbonate	Hyperphosphatemia caused by chronic kidney disease	FDA (2007), EMA (2009)	25 to 65 μm
Mircera®	Polymeric conjugate (PEGylated)	Epoetin beta	Anemia	EMA (2007), FDA (2018)	N/A
Cimzia®	Polymeric conjugate (PEGylated)	Tumor necrosis factor (TNF) blocker	Crohn's disease; arthritis; active ankylosing spondylitis; plaque psoriasis	FDA (2008), EMA (2009)	9 nm
Krystexxa®	Polymeric conjugate (PEGylated)	Porcine-like recombinant uricase	Gout	FDA (2010)	N/A

Plegridy®	Polymeric conjugate (PEGylated)	Interferon beta 1a	MS	FDA (2014)	N/A
Adynovate®	Polymeric conjugate (PEGylated)	Recombinant antihemophilic factor	Bleeding episodes; Perioperative management	FDA (2015)	N/A
VivaGel® BV	Dendrimer based nanoparticulate	Astodrimer sodium	Bacterial vaginosis	FDA (2015)	9 nm
Rebinyn®	Polymeric conjugate (Glycopegylated)	Recombinant DNA-derived coagulation factor IX	Hemophilia B	FDA (2017)	N/A
Zilretta®	PLGA (LA:GA=75:25) microspheres	Triamcinolone acetonide	Osteoarthritis pain of the knee	FDA (2017)	About 45 μm[73]
Apealea®	Micellar nanoparticle	Paclitaxel	Platinum-sensitive epithelial ovarian cancer; primary peritoneal cancer; fallopian tube cancer	EMA (2018)	20 to 60 nm

FDA: Food and Drug Administration. EMA: European Medicines Agency. DNA: deoxyribonucleic acid. PLGA: Poly(lactic-co-glycolic acid). N/A: no data available.

Table 1-3. Other therapeutic nanoparticles approved by FDA or EMA.

Trade name	Particle type	Active ingredients	Application/Indication	Approval year	Particle size

Protein-based nanoparticles					
Ontak®	Protein nanoparticle	Recombinant DNA-derived cytotoxic protein composed of diphtheria toxin and human interleukin-2 (IL-2)	Cutaneous T-cell lymphoma	FDA (1999)	N/A
Abraxane	Albumin-bound particle	Paclitaxel	Advanced cancer of breast, lung, or pancreas	FDA (2005), EMA (2008)	130 nm[74]
Rapamune®	Protein-bound particle	Sirolimus (rapamycin)	Kidney transplant; lymphangioleiomyomatosis (LAM)	EMA (2001), FDA (2010)	250 nm
Fyarro™	Albumin-bound particle	Sirolimus (rapamycin)	Perivascular epithelioid cell tumor	FDA (2021)	Less than 100 nm
Nanocrystals					
Ritalin LA®	Nanocrystalline	Methylphenidate	Attention deficit hyperactivity disorder (ADHD)	FDA (2002)	N/A
Zanaflex®	Nanocrystalline	Tizanidine hydrochloride	Spasticity	FDA (2002)	N/A
OsSatura®	Nanocrystalline	Hydroxyapatite	Bone voids or defects	FDA (2003)	N/A

Emend®	Nanocrystalline	Aprepitant	Nausea and vomiting caused by chemotherapy	FDA, EMA (2003)	120 nm
Vitoss®	Nanocrystalline	Bovine skin collagen (type I) with a porous tricalcium phosphate inorganic phase	Bony voids or gaps arise due to trauma, tumors or osteolysis	FDA (2003)	100 nm
Ostim®	Nanocrystalline	Hydroxyapatite	Bone defect	FDA (2004)	19 nm
TriCor®	Nanocrystalline	Fenofibrate	High levels of cholesterol and triglycerides	FDA (2004)	412 nm[75]
Focalin XR®	Nanocrystalline	Dexmethylphenidate hydrochloride	ADHD	FDA (2005)	N/A
Megace ES®	Nanocrystalline	Megestrol acetate	Loss of appetite and wasting syndrome in people with AIDS	FDA (2005)	Less than 2000 nm
NanOss®	Nanocrystalline	Hydroxyapatite granules	Advanced bone graft substitute	FDA (2005)	15 to 100 nm
Invega®	Nanocrystalline	Paliperidone	Schizophrenia	FDA (2006)	N/A
Ivemend®	Nanocrystalline	Fosaprepitant dimeglumine	Nausea and vomiting caused by chemotherapy	FDA, EMA (2008)	N/A
Invega Sustenna®	Nanocrystalline	Paliperidone palmeitate	Schizophrenia	FDA (2009)	2.5 μm

EquivaBone®	Nanocrystalline	Calcium phosphate, carboxymethyl cellulose and human demineralized bone matrix	Bone voids or defects	FDA (2009)	Less than 100 nm
Ryanodex®	Nanocrystalline	Dantrolene sodium	Malignant hyperthermia	FDA (2014)	407 nm
Inorganic nanoparticles					
Infed® (CosmoFer®)	Iron dextran colloid		Iron deficiency anemia (IDA) and iron deficiencies (ID)	FDA (1992)	About 15nm[76]
Dexferrum®	Iron dextran		IDA and ID	FDA (1996)	31.5 to 36.5 nm[77]
Ferrlecit®	Sodium ferric gluconate		IDA and ID	FDA (1999), EMA (2013)	12 nm[78]
Venofer®	Iron sucrose nanocolloidal		IDA in people with kideny disease	FDA (2000)	7 nm[77]
Feraheme®	Iron oxide nanoparticles (coated with polyglucose sorbitol carboxymethylether)		IDA	FDA (2009)	17 to 31 nm[77]
Ferinject®	Ferric carboxymaltose nanoparticle (Ferric hydroxide core with a carbohydrate shell)		IDA and ID	FDA, EMA (2013)	23 to 25 nm[79]
Hensify®	Hafnium oxide nanoparticles		Locally advanced soft tissue sarcoma	EMA (2019)	50 nm[63]

FDA: Food and Drug Administration. EMA: European Medicines Agency. AIDS: Acquired Immune Deficiency Syndrome. N/A: no data available.

1.3. Animal models for preclinical study

To translate therapeutic nanoparticles from laboratory results to clinical therapies, the PK and the efficacy of the nanoparticles will be evaluated after the design and formulation of nanoparticles. Robust preclinical data to demonstrate the efficacy and safety of the formulation plays a fundamental role on deciding the dose and schedule for further clinical investigation, which is especially important for phase I clinical trial. Compared with conventional drugs, nanomedicine is more prone to lack of predictability of efficacy when first used in human, and the variability is more obvious for the molecularly targeted therapeutics[80-82]. Furthermore, the safety issues for a formulation are not always able to be characterized during preclinical research studies, and these issues are one of the most common reasons causing the failure of phase I trial[80, 83]. Therefore, performing the efficacy and toxicity study in at least two animal models with multiple doses and extended evaluation time is considered as one of the methods to improve the predictability of nano-therapies [84]. A nano-formulation can cause the toxicity due to the local overexposure when it has a high accumulation in a specific organ or tissue. Therefore, pharmacokinetic and biodistribution analysis is necessary in the preclinical stage. In addition, preclinical studies in small laboratory rodents are not completely able to understand the interactions of nanoparticles and biological components relevant to human physiology. Hence, preclinical studies in more human-like animal models, such as pigs, can bridge the preclinical safety to patient safety[85]. Considering these factors, two animal models, the Vannucci rat model of hypoxic-ischemic (HI) injury and a piglet model of fetal growth restriction (FGR) are used in this thesis to characterize the efficacy and toxicity profiles of our neuroprotective polymeric nano-formulations.

1.3.1. Vannucci rat model of HI

Vannucci model is a model of HI brain damage in the immature rat. At postnatal day 7 (P7; day of birth = P1), the rat's brain is histologically similar to that of a 34- to 36-week gestation human fetus or newborn infant, i.e., cerebral cortical neuronal layering is complete, the germinal matrix is involuting, and white matter has undergone little myelination. Thus, the model was originally developed in the P7 rat, and then it is gradually applied to newborn rodents at all stages of development [86]. The method to produce HI brain entails ligation of one common carotid artery followed thereafter by systemic hypoxia. The insult produces permanent hypoxic-ischemic brain damage limited to the cerebral hemisphere ipsilateral to the carotid artery occlusion. The model has proved useful for numerous studies of perinatal hypoxic-ischemic brain damage and is presently utilized by numerous investigators throughout the globe [86, 87]. These make Vannucci model a favorable model for characterizing efficacy and safety of neuroprotective polymeric nanoparticles.

1.3.2. Piglet model of FGR

The piglet brain resembles the newborn human brain in terms of cortical surface area, histology, myelination, and vascularization: the newborn piglet brain is gyrenchephalic with a grey matter and white matter ratio similar to that of human infants. Human brain growth is greatest from a few weeks before to a few weeks after birth. Similarly, the piglet has a period of rapid brain growth extending from late prenatal to early postnatal life. Therefore, the piglet is an ideal animal to examine altered brain development arising from compromising perinatal events. In this thesis, we leverage a piglet model of FGR facilitated by our collaborators at the University of Queensland in Brisbane Australia. Approximately, 15–20% of piglets in a litter are born growth restricted. Growth restriction in the piglet occurs spontaneously obviating the need for surgical induction of growth retardation, so brain outcomes can be studied without confounding impacts of experimental interventions. The FGR piglet mimics many of the human pathophysiological outcomes associated with FGR including asymmetrical growth restriction with brain sparing. Inadequate fetal growth in pigs is caused by alterations associated with placental insufficiency similar to the human population. Therefore, Wixey et al. established a piglet model of FGR: FGR piglets are classically identified by their lower birth weights. Morphologically, FGR piglets can be characterized according to three criteria based on head morphology: "dolphin-like" head shape, bulging eyes, and wrinkles perpendicular to the mouth. Other measurements of growth restriction in the piglet in addition to <10th centile birth weight include relative brain to body weight and brain to liver weight ratio[88, 89]. With the efficacy and biodistribution study in the piglet model of FGR, the predictability of our polymeric nano-platform is further improved, which can increase the success of clinical translation.

1.4. Overview of project chapters

In Chapter 2, we quantify the PK and biodistribution of our neuroprotective polymeric nanoparticles in term-equivalent rats to optimize the therapeutic dose and schedule in following preclinical study. We also explore the effects of surfactant on the PK and biodistribution of formulations prepared with different stabilizers to improve formulation design.

In Chapter 3, we use curcumin as the model drug to develop a tunable, reproducible PLGA-PEG-based nano-platform with high hydrophobic drug loading and long-term stability, which has a higher potential to be scaled-up and transported without the cold-chain. Following that, we quantify the brain uptake and biodistribution of nano-formulated curcumin particles in the piglet model via different administration routes and assess its potential to treat neonatal brain injury and disease. This provides better predictability of the formulation in clinical application.

In Chapter 4, we evaluate the neuroprotective effects of curcumin-loaded polymeric nanoparticles in neonatal rats at different developmental stages, which explore the relationship of developmental age and

therapeutic dose and schedule in perinatal rats. A guideline for therapeutic dose and schedule design has been established for perinatal brain injury treatment.

In Chapter 5, we summarized the main conclusions of this thesis and the future directions.

In Chapter 6, the thesis research and other co-author manuscript contributions completed during this thesis work are summarized.

Chapter 2: Neonatal pharmacokinetics and biodistribution of polymeric nanoparticles and effect of surfactant

This chapter was published as: Xu, N.; Wong, M.; Balistreri, G.; Nance, E. Neonatal Pharmacokinetics and Biodistribution of Polymeric Nanoparticles and Effect of Surfactant. *Pharmaceutics* **2023**, *15*, 1176. https://doi.org/10.3390/pharmaceutics15041176

2.1. Introduction

In the last few decades, the Food and Drug Administration (FDA) has encouraged the development of formulations for the pediatric population, which has resulted in more rapid advancements [90]. Specifically, both US and European based pediatric formulation initiatives strive to investigate nanomedicine-based formulations for pediatric use [91-93]. Nanomedicine has undergone an explosive development in the past three decades [94, 95] and is a promising therapeutic platform for pediatric populations. In addition to improving therapeutic efficacy, nanomedicine can mask drug taste, improve drug bioavailability and permeability, and reduce off-site or off-target toxicity in children [96-98]. Currently most nanomedicine platforms are evaluated in adult models preclinically or in adults clinically and the off-label use of adult medications in pediatrics remains a significant clinical problem [99, 100]. Off-label use of a drug can cause a higher risk of adverse drug reactions for children, especially for neonates, infants, and children younger than two years old, even when the original purpose of off-label drug use is to benefit these patients [101-103].

The development of nanomedicine for pediatrics is challenged by the lack of pharmacokinetic (PK) data in the pediatric population [104], a gap in data even more significant for neonates due to the limited patient numbers and technical and ethical prerequisites of clinical trials in this patient population [99]. Even for well-established nanoparticle platforms such as liposomes and polymersomes, PK data is limited in pediatric and neonatal populations. To address this data gap, we sought to generate PK data in a neonatal model for polymer nanoparticles.

As one of the most commonly used polymeric nanoparticles, poly(lactic-*co*-glcyolic-acid)-polyethylene glycol (PLGA-PEG) nanoparticles play an important role in drug delivery due to the improvement to the physicochemical and PK properties of the cargo [105-107]. PLGA-based formulations have been approved for several biomedical applications, such as Decapeptyl®, Lupron Depot®, Nutropin Depot®, Suprecur® MP, Sandostatin® LAR Depot, Somatuline® LA, Trelstar™ Depot, Vivitrol® and Risperdal® Consta™, etc [108]. In addition, there are many PLGA-based formulations undergoing clinical trials, such as ciprofloxacin-loaded PLGA nanoparticles to treat E-Fecalis infections in endodontics, and

quercetin-encapsulated PLGA-PEG nanoparticles (Nano-QUT) for squamous cell carcinoma treatment (NCT05456022) [109]. PLGA-based nanoformulations have good biocompatibility and have been widely studied in adults; however, the application of PLGA-PEG nanoparticles in neonates is still limited [31]. Here, we quantified the PK parameters and biodistribution of PLGA-PEG nanoparticles in term-equivalent healthy rats.

We also investigated the effect of surfactant used as a stabilizer in the formulation process on PK parameters and biodistribution. Prior research has revealed surfactants used in the emulsification step have impact on the biodistribution of polymer nanoparticles [50, 110, 111]. We chose Pluronic® F127 (F127) surfactant in the Pluronic surfactant family and Tween® 80 (P80) from the polysorbate surfactant family to formulate PLGA-PEG nanoparticles with similar particle size and zeta potential. These surfactants are nonionic surfactants and are most frequently used in the field of nanomedicine, due to their relatively lower toxicity compared with ionic surfactants [112]. In addition, among nonionic surfactants, most nanoformulations include polysorbates, poly(vinyl alcohol), or Pluronics® as stabilizers, emphasized by the high frequency of use in literature [113]. Prior literature has also reported that polysorbate 80 (P80) formulated nanoparticles have higher affinity with apolipoprotein E (ApoE) in circulation, which is associated with enhanced brain targeting through greater blood-brain barrier (BBB) penetration [114-118]. Brain targeting has received increasing attention due to the difficulty for therapeutic agents in crossing the BBB. Therefore, we further focused this study on the effect of surfactant on the PK, biodistribution and cellular association of PLGA-PEG nanoparticles in the term-equivalent brain.

Our main results provide fundamental PK data in the term-equivalent rat, which can be used to build physiologically based pharmacokinetic (PBPK) models or similar models to support first-in-human predictions in neonates. Our findings also provide guidance for design and delivery of therapeutic polymeric nanoparticles for application in neonatal populations.

2.2. Materials and Methods

2.2.1. Animal Care and Ethics Statement

This study was performed in accordance with the guide for the care and use of laboratory animals of the National Institutes of Health (NIH). All animals were handled according to approved Institutional Animal Care and Use Committee (IACUC) protocols (#4383-01, approval date: 20 March 2022; #4383-02, approval date: 13 August 2020) of the University of Washington (UW), Seattle, WA. The UW has an approved Animal Welfare Assurance (#A3464-01) on file with the NIH Office of Laboratory Animal Welfare, is registered with the United States Department of Agriculture (certificate #91-R-0001), and is

accredited by AAALAC International. Time-mated pregnant female Sprague–Dawley rats (virus antibody-free CD® (SD) IGS, Charles River Laboratories, Raleigh, NC, USA) were purchased and arrived on postnatal day 5 (P5) with a litter of 10 sex-balanced pups. Dams were housed individually with their litter and allowed to acclimate to their environment. Before and after the experiment, each dam and her pups were housed under standard conditions with an automatic 12 h light/dark cycle, a temperature range of 20–26 °C, and access to standard chow and autoclaved tap water ad libitum. The pups were checked for health daily.

2.2.2. Polymer Activation and Labeling

PLGA-PEG (45k:5k, LA:GA = 50:50, Akina, Inc., West Lafayette, IN, USA) polymer was covalently labeled with fluorescent dye before nanoparticle formulation. To activate the PLGA-PEG polymer, the polymer was dissolved in a 20 mL glass scintillation vial with dichloromethane (DCM, Fisher Scientific, Pittsburgh, PA, USA) to create a 100 mg/mL polymer solution. P-nitrophenyl chloroformate (PNCF, Sigma-Aldrich, St. Louis, MO, USA) was dissolved in DCM to create a 10 mg/mL stock solution. PNCF solution was added to the polymer solution, followed by the immediate addition of pyridine (Sigma-Aldrich). The solution was stirred and reacted for 3 h at 200–300 rpm, and then the polymer reaction solution was slowly added to cold ethyl ether (Sigma-Aldrich) to stop the reaction. The solution was then centrifuged at 1000× g for 2 min and lyophilized overnight to dry the activated polymer. After polymer drying, CF647 Succinimidyl Ester (CF647®, Biotium, Fremont, CA, USA) was dissolved in dimethylformamide (DMF, Fisher Scientific) to make a 2 mg/mL stock solution. Activated polymer was dissolved in DMF, and then the CF647® solution was added to the polymer solution. Triethylamine (TEA, Sigma-Aldrich) was added immediately after CF647 and reacted for 4 h. The solution was lyophilized overnight to dry the dye-labeled polymer. CF647-labeled polymer was stored at −20 °C for future use.

2.2.3. Nanoparticle Preparation and Characterization

Nanoparticles were prepared using the standard nanoprecipitation method, as described previously [31]. Briefly, 20 mg PLGA-PEG was dissolved in 1 mL acetone (Sigma-Aldrich) to prepare a 20 mg/mL organic solution, and then this solution was added dropwise into 25 mL of 1% (*v*/*w*) P80 or 1% (*w*/*w*) F127 solution. The nanoparticles (PLGA-PEG/F127 and PLGA-PEG/P80) formed spontaneously in the surfactant solution. The solution was stirred magnetically at 500 rpm for 3 h, and any remaining organic solvent was removed by rotary evaporation at 4 °C under reduced pressure for 30 min. After that, nanoparticles were collected at 100,000× g for 60 min and washed at 100,000× g for 25 min by centrifugation. Nanoparticles were resuspended in 1× PBS after washing and then stored at 4 °C for future use.

The particle size and polydispersity index (PDI) of nanoparticles were measured using dynamic light scattering (DLS), and the zeta potential (ζ-potential) was determined using a zeta potential analyzer (NanoSizer Zeta Series, Malvern Instruments, Malvern, UK). Samples were diluted to appropriate concentrations to obtain accurate measurements in 10 mM sodium chloride (NaCl, Sigma-Aldrich), pH 7.0. Samples were also analyzed via transmission electron microscopy (TEM).

2.2.4. Transmission Electron Microscopy Method

To prepare nanoparticles for TEM, the samples were diluted to a 1:500 ratio (sample to DI water) from a batch concentration of 20 mg/mL. PLGA nanoparticles served as a control. PLGA-PEG and PLGA in DI water, 1% F127, and 1% P80 were adsorbed on a 200-mesh carbon film grid (Fisher Scientific, Hampton, NH, USA), negatively stained with uranyl acetate (Ted Pella Inc., Redding CA, USA), and then washed in DI water. Samples were prepared and imaged on the Tecnai F20 SuperTwin TEM instrument at the Molecular Analysis Facility (MAF) at the University of Washington.

2.2.5. Nanoparticle Administration and Tissue Extraction

Healthy rats (n = 4 per timepoint; 2F and 2M per timepoint) at P10 (term-equivalent to humans) received intraperitoneal (i.p.) injections of CF647-labeled PLGA-PEG/F127 or PLGA-PEG/P80 nanoparticles at a PLGA-PEG concentration of 150 mg/kg rat in 1× PBS. Tail veins are not accessible in this age of rat; therefore, i.p. was the chosen route of administration. Animals were returned to the dams after receiving a single dose of nanoparticles. Rats were sacrificed at the indicated time (30 min, 1 h, 4 h, 8 h, 24 h, 72 h) after injection by an overdose of euthanasia solution. For each rat, the brain, heart, lungs, liver, spleen, kidneys, and blood were collected. Blood was collected in a heparin-coated 1.5 mL tube, and serum was separated via 5 min of centrifugation at 3000× g.

2.2.6. High-Performance Liquid Chromatography (HPLC) Method

To verify the stability of the CF647-labeling on PLGA-PEG/F127 and PLGA-PEG/P80 after i.p. injection, CF647-labeled PLGA-PEG/F127 and PLGA-PEG/P80 nanoparticles were i.p. injected into P10 rats. The rats were sacrificed 4 h after the administration to collect blood. Serum extracts were collected using an Amicon filter tube (Ultracel® membrane, 3 kDa cutoff) to filter serum proteins. Free CF647, serum extract from whole blood (blank sample), and serum extracts from blood from nanoparticle-injected rats were analyzed using a C18-based column (Agilent Eclipse XDB-C18, 150 mm × 4.6 mm, 5 µm). The mobile phase consisted of 90% acetonitrile and 10% 10 mM aqueous ammonium acetate (pH 7.5 before mixing). The column temperature was set to 30 °C. The flow rate was 0.5 mL/min, and the injection volume was 10 µL. Absorbance detection was performed by UV at 650 nm, and the total run time was 10 min.

2.2.7. Tissue Processing for PK and Organ-Level Biodistribution Analysis

To quantify the PK profiles and organ-level biodistribution, one hemisphere of the brain, one lobe each of the lung and liver, one kidney, and the heart and spleen were homogenized in 1× PBS, and the supernatants were collected via centrifugation at 10,000× g for 10 min. The PK parameters of PLGA-PEG/F127 and PLGA-PEG/P80 in serum, brain, heart, lung, liver, spleen, and kidney tissues were calculated from a calibration curve for each tissue using UV-Vis spectrometry. Tissue from pups not injected with nanoparticles served as controls. The noncompartmental PK analysis method was used to determine the PK parameters in P10 rat serum, brain, and other organs, as described elsewhere [119]. A graphical relationship between PLGA-PEG concentration (y-axis) and time (x-axis) was established. Then, the data points from the terminal elimination phase were used to calculate the elimination rate constant (K_e).

$$K_e = \frac{lnC_1 - lnC_2}{t_2 - t_1} \text{ (2-1)}$$

C_1 and C_2 are the concentrations of PLGA-PEG in terminal elimination phase, and t_1 and t_2 are the corresponding times, respectively.

Area under the PLGA-PEG concentration versus time curve (AUC) from time zero (C_0) until 72 h ($AUC_{(0\text{-}72)}$) was calculated by GraphPad Prism (Version 9.4.1. GraphPad Software Inc, San Diego, CA, USA). Because no to minimal PLGA-PEG polymer was detectable at 72 h, total AUC was defined as:

$$\text{AUC} = \text{AUC}_{(0\text{-}72)} \text{ (2-2)}$$

Volume of distribution (V_d) and volume of distribution at steady state were calculated as:

$$V_d = \frac{\text{Injected dose}}{\text{AUC} \times K_e} \text{ (2-3),}$$

and

$$\text{V}_{\text{ss}} = \text{Cl} \times \text{MRT} \text{ (2-4)}$$

Clearance (Cl) was calculated as:

$$\text{Clearance} = \frac{\text{Injected dose}}{\text{AUC}} \text{ (2-5)}$$

Elimination half-life ($T_{1/2}$) was calculated as:

$$T_{1/2} = \frac{0.693}{K_e} \text{ (2-6)}$$

Area under the moment of PLGA-PEG concentration (PLGA-PEG × time) versus time curve (AUMC) from time zero until 72 h ($AUMC_{(0-72)}$) was calculated using GraphPad Prism. Similarly, total AUMC was defined as:

$$AUMC = AUMC_{(0-72)} \quad (2\text{-}7)$$

Mean residence time (MRT) of PLGA-PEG was calculated as:

$$MRT = \frac{AUMC}{AUC} \quad (2\text{-}8)$$

2.2.8. Immunohistochemistry

To characterize the tissue-level biodistribution, one hemisphere of the brain, one portion each of the lung and liver, and one kidney were placed in a formalin-to-30% sucrose gradient and cryosectioned on a Leica cryostat into 30 μm sections[31]. To evaluate brain distribution, primary antibodies for microglia (1:250 rabbit anti-Iba1, Wako, Fujifilm, Minato City, Tokyo, Japan) and neurons (1:250 donkey anti-NeuN, Abcam, Cambridge, UK) were prepared in 1× PBS containing 1% Triton X-100 (Sigma-Aldrich) and 3% normal goat serum (Sigma-Aldrich). Primary antibody solutions were added to tissue sections for 4–6 h at room temperature in a humified dark chamber. The tissue slices were washed twice in 1× PBS. Secondary antibodies were dissolved in 1× PBS containing 1% Triton X-100 and added to the tissue slices with 2 h incubation. The slices were washed twice in 1× PBS, then stained with 1:10,000 4′,6-diamidino-2-phenylindole (DAPI, Invitrogen, Waltham, MA, USA). The slides were washed and dried for 30 min in the dark. Mounting medium (Dako, Agilent Technologies, Santa Clara, CA, USA) was added to each slide, and a glass coverslip was placed on top. Slides were stored at 4 °C until imaged under an A1 confocal microscope (Nikon, Tokyo, Japan) and at −20 °C for long-term storage. For other organs, tissue sections were stained with DAPI and imaged using confocal microscopy.

2.2.9. Statistical analysis

Statistical analysis was performed using Welch's *t*-test. All statistical analyses were carried out using GraphPad Prism (GraphPad Software Inc., Version 9.4.1). A p-value of <0.05 was considered statistically significant. Calculated PK parameters are reported as mean ± standard deviation in all tables.

2.3. Results

2.3.1. Characterization and stability of CF647-labeled nanoparticles

CF647-labeled PLGA-PEG nanoparticles were formulated in 1% F127 surfactant and 1% P80 surfactant via standard nanoprecipitation method. Following formulation, hydrodynamic size, PDI, and zeta potential were determined by DLS and Zetasizer (Table 2-1). These two PLGA-PEG formulations had similar physicochemical properties: PLGA-PEG/F127 nanoparticles were 60.2 ± 0.8 nm, -2.6 ± 0.3 mV, and had a PDI of 0.2 ± 0.01. PLGA-PEG/P80 nanoparticles were 66.2 ± 1.4 nm, -2.0 ± 0.3 mV, and had a PDI of 0.2 ± 0.01. The stability of CF647 dye labeled nanoparticles were verified indirectly due to limited ability to visualize polymeric nanoparticles directly in tissue samples [120]. Detected at 650 nm absorbance, free CF647 dye had an absorbance peak at 650 nm (Fig 2-1A). The blank serum sample also showed no absorbance signal at 650 nm (Fig 2-1B). Serum extracts obtained from rat 4 h post i.p. injection of PLGA-PEG/F127 and PLGA-PEG/P80 nanoparticles (Fig 2-1C and D) showed no absorbance peaks, which indicates that there was no detectable free CF647 dye in serum following i.p. injection. No peak was identified with a fluorescence detector at Ex/Em 635 nm/665 nm (Fig S2-1) for the serum samples containing particles as well. These results suggest that CF647-labeled PLGA-PEG nanoparticles retain the CF647 label after i.p. injection. The colloidal stability of these particles in serum has previously been shown [50].

Table 2-1. Physicochemical properties of PLGA-PEG/F127 and PLGA-PEG/P80. All values are reported as mean ± standard error of the mean (SEM) (n=3).

Formulation	Size ± SEM (nm)	PDI ± SEM	Zeta potential ± SEM (mV)
PLGA-PEG/F127	60.2 ± 0.8	0.2 ± 0.01	-2.6 ± 0.3
PLGA-PEG/P80	66.2 ± 1.4	0.2 ± 0.01	-2.0 ± 0.3

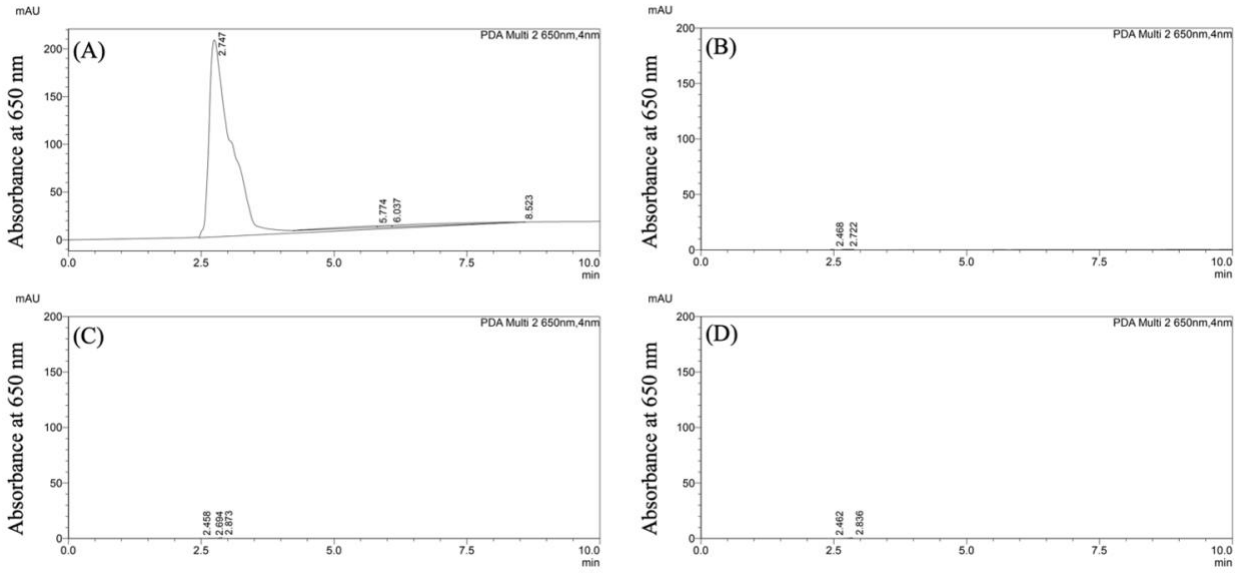

Figure 2-1. Representative HPLC chromatograms acquired based on absorbance at 650 nm for: (A) Free CF647 dye at a 20 nmol/mL concentration, (B) blank serum extracts, (C) serum extracts obtained from rat 4 h post injection of PLGA-PEG/F127 at a 150 mg/kg dosage, and (D) serum extracts obtained from rat 4 h post injection of PLGA-PEG/P80 at a 150 mg/kg dosage.

2.3.2. PK and biodistribution of PLGA-PEG in the term-equivalent rat

Table 2-2. PK parameters of PLGA-PEG/F127 and PLGA-PEG/P80 nanoparticles in P10 rat serum after i.p. injection (n=4 per timepoint). T_{max}, time to reach maximum concentration; C_{max}, maximum concentration; V_d, volume of distribution; V_{ss}, volume of distribution at steady state; $T_{1/2}$, half-life; AUC, area under the curve; MRT, mean residence time. T_{max} is the experimental value, and all other PK parameters are reported as mean ± standard deviation.

Formulation	PK parameter	
PLGA-PEG/F127	T_{max} (h)	4
	C_{max} (mg/mL)	2.1 ± 0.4
	V_d (mL)	1.4 ± 0.4
	V_{ss} (mL)	1.2 ± 1.1

	Clearance (mL/h)	0.17 ± 0.03
	$T_{1/2}$ (h)	5.9 ± 2.1
	AUC (h-mg/mL)	23.1 ± 3.8
	MRT (h)	7.2 ± 1.7
PLGA-PEG/P80	T_{max} (h)	4
	C_{max} (mg/mL)	2.3 ± 0.6
	V_d (mL)	0.74 ± 0.3
	V_{ss} (mL)	1.6 ± 1.6
	Clearance (mL/h)	0.31 ± 0.06
	$T_{1/2}$ (h)	1.7 ± 0.7
	AUC (h-mg/mL)	12.4 ± 2.3
	MRT (h)	5.2 ± 1.5

Both PLGA-PEG/F127 and PLGA-PEG/P80 nanoparticles entered systemic circulation within 30 min after i.p. injection, reached the maximum serum concentration around 4 h, and were not detectable at 72 h (Fig 2-2A). At the maximum serum concentration, 54.0% of injected PLGA-PEG/F127 nanoparticles and 54.6% of injected PLGA-PEG/P80 nanoparticles were detected in serum, showing no significant difference between these formulations. However, compared with PLGA-PEG/P80 nanoparticles, PLGA-PEG/F127 nanoparticles had longer half-life, larger volume of distribution, longer mean residence time, and slower clearance rate in systemic circulation (Table 2-2). Maximum serum concentration of PLGA-PEG/F127 nanoparticles was 2.1 mg/mL, which was lower than PLGA-PEG/P80 nanoparticle (2.3 mg/mL), but this difference was not significant. At 8 h post administration, PLGA-PEG/F127 concentration was significantly higher than PLGA-PEG/P80. At 24 h after injection, no PLGA-PEG/P80 nanoparticles were detectable via UV-Vis spectrometry, but PLGA-PEG/F127 nanoparticles remained detectable in some rats, albeit at

relatively low concentrations. No F127- or P80-formulated nanoparticles were detectable 72 h after the i.p. injection.

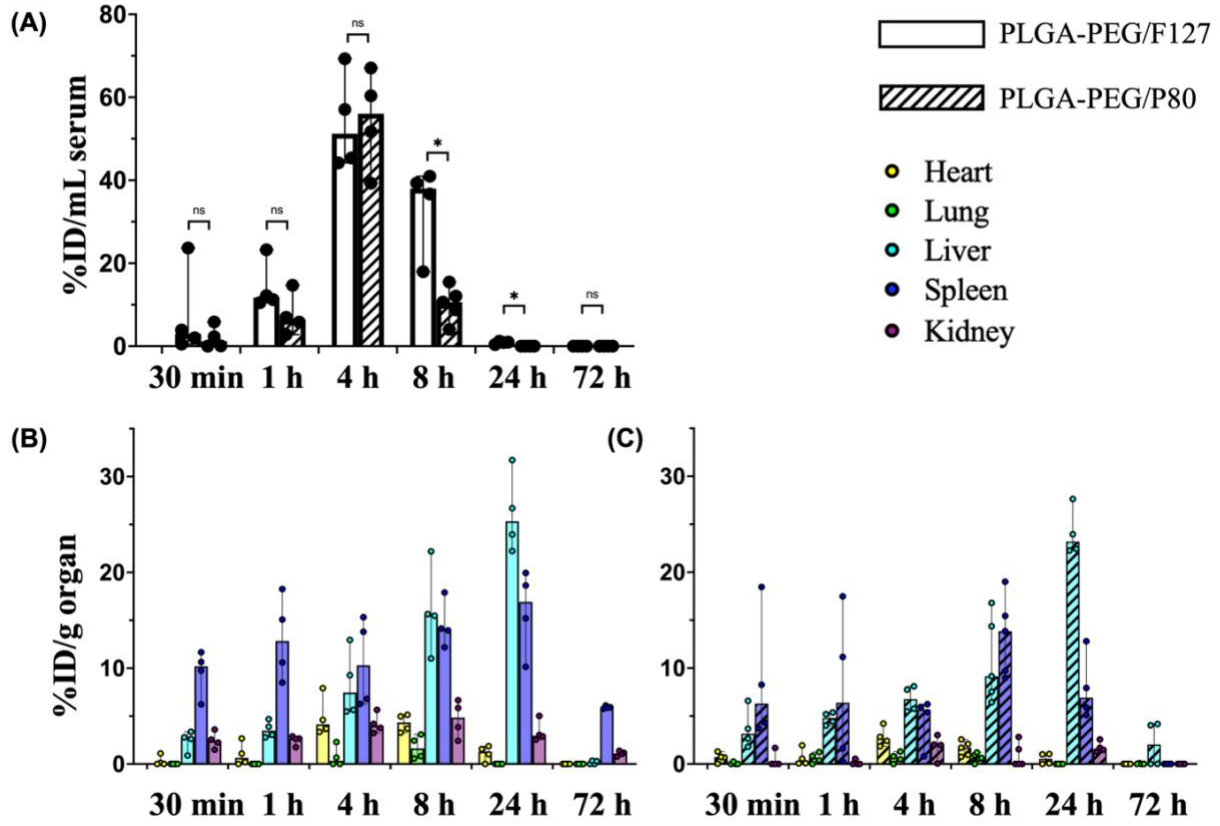

Figure 2-2. Biodistribution of PLGA-PEG/F127 and PLGA-PEG/P80 versus post injection time (30 min, 1 h, 4 h, 8 h, 24 h, and 72 h) in P10 rat (A) serum, and (B, C) organs (heart, lung, liver, spleen, kidney) after i.p. injection (n=4 per timepoint), %ID: percentage of injected dose. Graphs display median ± 95% confidence interval. Group differences were evaluated by Welch's t-test, ns: not significant, *: $p<0.05$.

Table 2-3. PK parameters of PLGA-PEG/F127 and PLGA-PEG/P80 nanoparticles in P10 rat organs (heart, lung, liver, spleen, kidney) after i.p. injection (n=4 per timepoint). T_{max}, time to reach maximum concentration; C_{max}, maximum concentration; V_d, volume of distribution; V_{ss}, volume of distribution at steady state; $T_{1/2}$, half-life; AUC, area under the curve; MRT, mean residence time. T_{max} is the experimental value, and all other PK parameters are reported as mean ± standard deviation.

		Organ				
Formulation	**PK parameter**	**Heart**	**Lung**	**Liver**	**Spleen**	**Kidney**
PLGA-PEG/F127	T_{max} (h)	4	8	24	24	8
	C_{max} (mg/mL)	0.19 ± 0.06	0.069 ± 0.04	1.2 ± 0.1	0.70 ± 0.2	0.19 ± 0.07
	V_d (mL)	13.1 ± 6.9	591.8 ± 531.4	0.77 ± 0.1	5.3 ± 1.2	22.7 ± 6.4
	V_{ss} (mL)	13.0 ± 15.5	33.5 ± 53.0	1.8 ± 1.2	2.9 ± 2.3	10.9 ± 9.7
	Clearance (mL/h)	1.0 ± 0.2	4.6 ± 2.3	0.082 ± 0.07	0.11 ± 0.2	0.47 ± 0.08
	$T_{1/2}$ (h)	9.4 ± 2.4	89.3 ± 21.0	6.5 ± 0.5	33.5 ± 2.9	33.4 ± 6.7
	AUC (h-mg/mL)	4.0 ± 1.0	0.84 ± 0.4	47.0 ± 4.1	34.9 ± 4.8	8.2 ± 1.3
	MRT (h)	13.4 ± 6.3	7.3 ± 5.4	22.0 ± 2.7	26.0 ± 4.9	23.2 ± 5.3
PLGA-PEG/P80	T_{max} (h)	4	8	24	8	24
	C_{max} (mg/mL)	0.12 ± 0.04	0.025 ± 0.01	0.89 ± 0.1	0.53 ± 0.1	0.065 ± 0.02
	V_d (mL)	15.7 ± 12.5	114.8 ± 107.0	2.1 ± 0.6	7.4 ± 2.9	48.1 ± 22.0

V_{ss} (mL)	28.2 ± 41.2	96.8 ± 152.0	2.5 ± 2.3	4.1 ± 4.3	27.3 ± 30.8
Clearance (mL/h)	2.2 ± 0.8	9.9 ± 3.8	0.11 ± 0.01	0.24 ± 0.05	1.4 ± 0.4
$T_{1/2}$ (h)	4.9 ± 2.3	8.0 ± 1.8	13.5 ± 2.4	21.2 ± 4.1	24.0 ± 2.2
AUC (h-mg/mL)	1.7 ± 0.6	0.39 ± 0.2	36.3 ± 4.9	15.8 ± 3.2	2.8 ± 0.7
MRT (h)	12.6 ± 9.0	9.7 ± 8.3	24.1 ± 6.3	17.0 ± 5.7	19.6 ± 7.3

For both PLGA-PEG/F127 and PLGA-PEG/P80 nanoparticles, heart, lung, and liver reached the maximum nanoparticle concentration around 4 h, 8 h, and 24 h (Table 2-3) after i.p. injection, respectively. PLGA-PEG/F127 accumulation in the spleen reached the maximum concentration by 24 h after administration, but PLGA-PEG/P80 had maximum accumulation by 8 h post injection. PLGA-PEG/F127 accumulation reached the peak in the kidney by 8 h after i.p. injection, but the maximum concentration of PLGA-PEG/P80 occurred by 24 h. In the heart, lung, spleen and kidney, PLGA-PEG/F127 had a longer half-life than PLGA-PEG/P80 – the only exception where PLGA-PEG/F127 had a shorter half-life than PLGA-PEG/P80 was in the liver. PLGA-PEG/F127 had shorter mean residence time in lung and liver, PLGA-PEG/P80 had shorter mean residence time in heart, spleen, and kidney.

Collectively, PLGA-PEG/F127 had higher maximum concentration and slower clearance rate, compared with PLGA-PEG/P80. Following i.p. injection, PLGA-PEG/F127 appeared in liver, spleen, and kidney in the first 30 min, appeared in heart in the first 1 h. At 72 h, no to minimal concentrations were detected in the heart, lung, and liver (Fig 2-2B). In lung, PLGA-PEG/F127 was detected only between 4 h to 8 h. PLGA-PEG/P80 was first being detectable in the heart, liver, and spleen approximately 30 min after i.p. injection and became detectable in lung and kidney at 1 h after injection. At 24 h, except in lung, PLGA-PEG/P80 was still detectable in heart, liver, spleen, and kidney, but there were no to minimal concentrations detected at 72 h (Fig 2-2C). Among all organs for both formulations, the liver accumulated the most nanoparticles (26.2% injected PLGA-PEG/F127 at 24 h, 24.1% injected PLGA-PEG/P80 at 24 h), whereas

heart, lung and kidney had relatively low accumulation (less than 5% injected dose), and spleen accumulated intermediate amounts at 16.0% injected dose PLGA-PEG/F127 at 24 h and 13.4% injected dose PLGA-PEG/P80 at 8 h.

2.3.3. Tissue-level biodistribution

To further explore the nanoparticle distribution in the tissue among a single organ, tissues from lung, liver and kidney were cryosectioned and stained, then tissue-level biodistribution was characterized by confocal microscopy at 240× magnification (Fig 2-3). No obvious difference in the biodistribution was noticed between PLGA-PEG/F127 and PLGA-PEG/P80 in lung, liver, and kidney at both 4 h and 24 h after administration. Following i.p. injection, few nanoparticles were observed in P10 rat lung at 4 h, and no nanoparticles were observed at 24 h. As the organ with the highest nanoparticle accumulation, many nanoparticles were observed in the liver at both 4 h and 24 h after the administration. In the kidney tissue, all the nanoparticles were found in blood vessels, and no nanoparticles were observed in the tissue parenchyma. Nanoparticles were not localized within nuclei, as evidenced by lack of co-localization between the DAPI nuclear stain and the particles in any tissue.

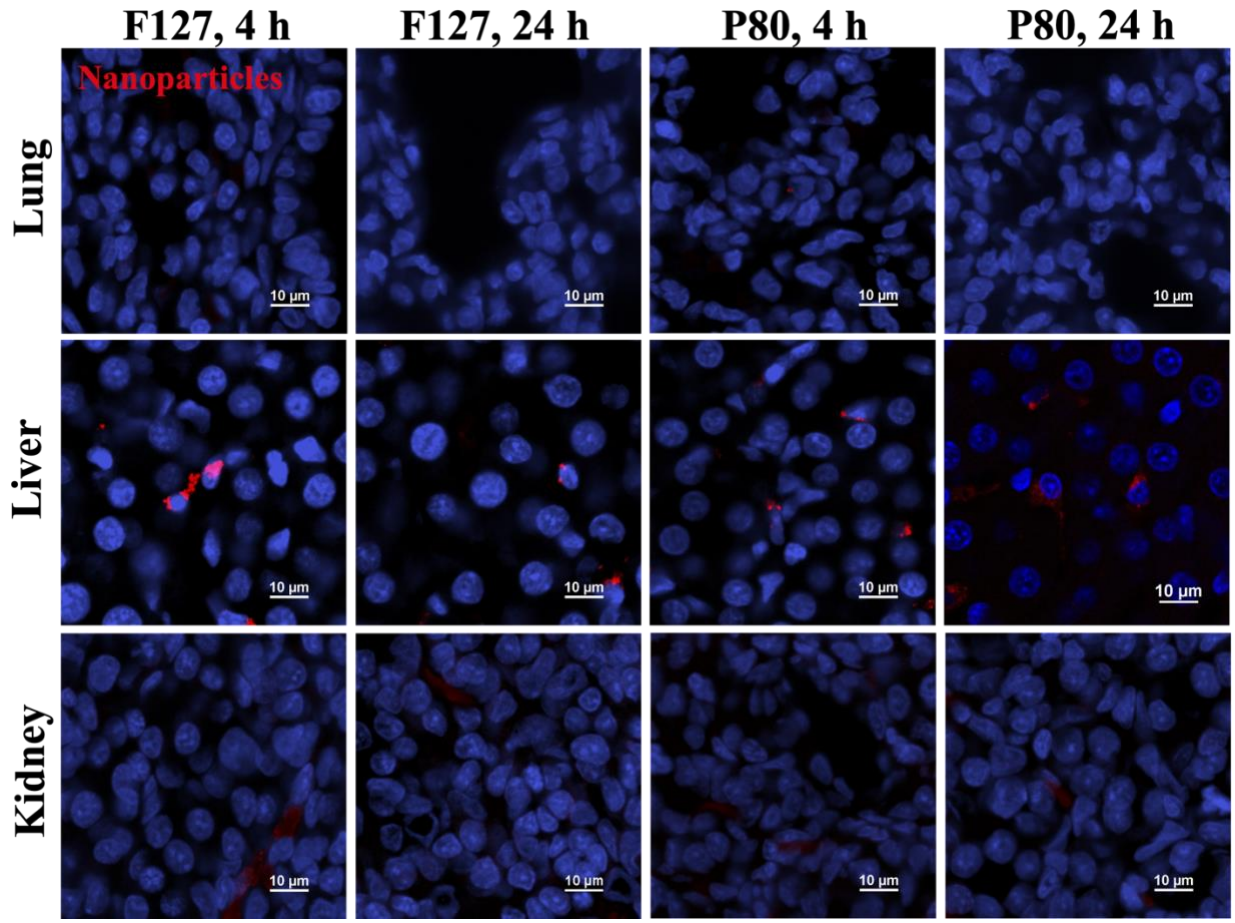

Figure 2-3. Tissue-level biodistribution of PLGA-PEG/F127 (F127) and PLGA-PEG/P80 (P80) nanoparticles (red) in P10 rat lung (first row); liver (second row); kidney (third row) at 4 h (first and third column) and 24 h (second and fourth column) after administration. Blue: DAPI nuclei stain. Scale bars: 10 μm.

2.3.4. PLGA-PEG PK and biodistribution in the term-equivalent brain

There are many neonatal nanotherapeutic applications where the brain is the target organ for nanoparticle delivery, such as hypoxic-ischemic encephalopathy (HIE, occurs in 2 to 4 per 1000 live births in developed countries), acute seizures (the most common neurological emergency in newborn babies, arising in roughly 3 per 1000 term livebirths), and periventricular leukomalacia (PVL, affects 3 to 4% preterm newborns) [121-123]. Neonatal brain injury, regardless of etiology, has no cure, and many brain injuries around birth or early in life have long-term side effects even if clinical treatment is provided. In addition, drug delivery to the brain is an ongoing challenge. Given the promise of prior work with PLGA-PEG nanoparticles for delivery to the injured newborn brain [31, 124], we further explored the brain PK and biodistribution. Herein, PLGA-PEG/F127 nanoparticles in P10 rat brain were not detectable before 1 h and after 72 h, and reached the maximum concentration by 4 h post injection. PLGA-PEG/P80 nanoparticle concentration in the P10 rat brain started increasing at 30 min after injection, reached the maximum brain concentration around 4 h, and was still detectable in some pups at 72 h after i.p. injection (Fig 2-4). At the maximum brain concentration, PLGA-PEG/P80 concentration (0.02 mg/mL) was higher than PLGA-PEG/F127 (0.01 mg/mL), but both formulations had low brain accumulation (less than 1% of injected dose), which is consistent with other literature, especially given these are healthy animals [125, 126]. PLGA-PEG/P80 had a shorter half-life, higher clearance rate, and lower volume of distribution compared with PLGA-PEG/F127 nanoparticles. It is worth noting that PLGA-PEG/P80 nanoparticles had longer mean brain residence time although a shorter brain half-life (Table 2-4).

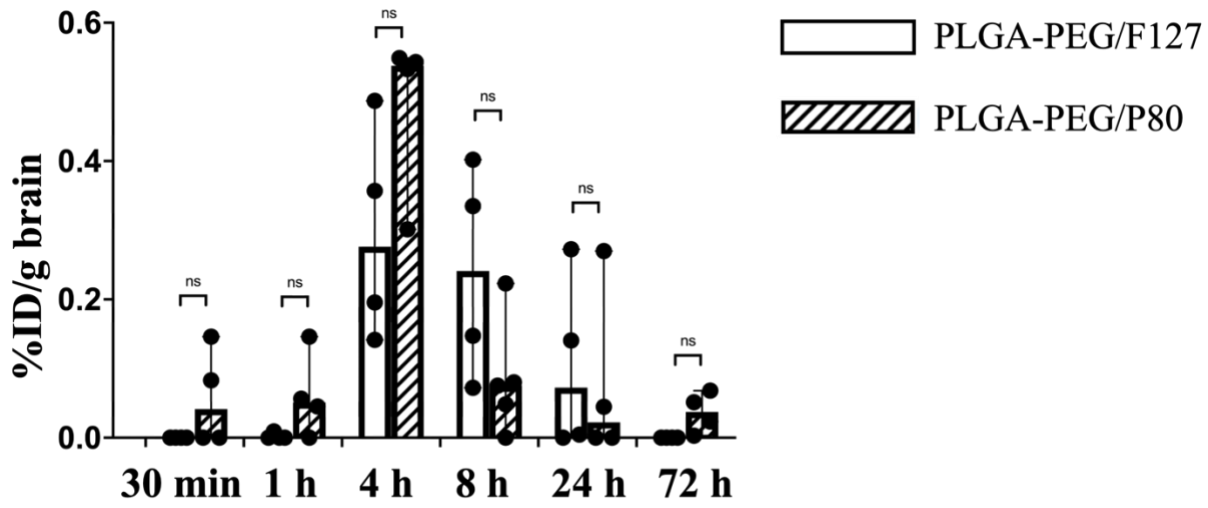

Figure 2-4. Biodistribution of PLGA-PEG/F127 and PLGA-PEG/P80 versus post injection time (30 min, 1 h, 4 h, 8 h, 24 h, and 72 h) in P10 rat brain after i.p. injection (n=4 per timepoint). Graph displays median ± 95% confidence interval. Group differences were evaluated by Welch's t test, ns: not significant.

In the cortex of brain, the localization of PLGA-PEG/F127 and PLGA-PEG/P80 were also different. Small amounts of PLGA-PEG/P80 nanoparticles were observed at both 4 h and 24 h in the extracellular space adjacent to cortical neurons (Fig 2-5C). However, for PLGA-PEG/F127 nanoparticles, at both 4 h and 24 h after i.p. injection, no to minimal PLGA-PEG/F127 nanoparticles were found in the extracellular space (Fig 2-5A and B). No PLGA-PEG/F127 or PLGA-PEG/P80 nanoparticles were observed to be internalized with neurons or microglia in the cortex.

Table 2-4. PK parameters of PLGA-PEG/F127 and PLGA-PEG/P80 nanoparticles in P10 rat brain after i.p. injection (n=4 per timepoint). T_{max}, time to reach maximum concentration; C_{max}, maximum concentration; V_d, volume of distribution; V_{ss}, volume of distribution at steady state; $T_{1/2}$, half-life; AUC, area under the curve; MRT, mean residence time. T_{max} is the experimental value, and all other PK parameters are reported as mean ± standard deviation.

Formulation	PK parameter	
PLGA-PEG/F127	T_{max} (h)	4
	C_{max} (mg/mL)	0.013 ± 0.01

	V_d (mL)	261.5 ± 281.7
	V_{ss} (mL)	208.0 ± 256.4
	Clearance (mL/h)	13.6 ± 7.2
	$T_{1/2}$ (h)	13.3 ± 4.4
	AUC (h-mg/mL)	0.28 ± 0.2
	MRT (h)	15.3 ± 14.4
PLGA-PEG/P80	T_{max} (h)	4
	C_{max} (mg/mL)	0.020 ± 0.01
	V_d (mL)	38.7 ± 38.5
	V_{ss} (mL)	379.2 ± 628.2
	Clearance (mL/h)	16.7 ± 8.8
	$T_{1/2}$ (h)	1.6 ± 0.9
	AUC (h-mg/mL)	0.23 ± 0.1
	MRT (h)	22.7 ± 19.1

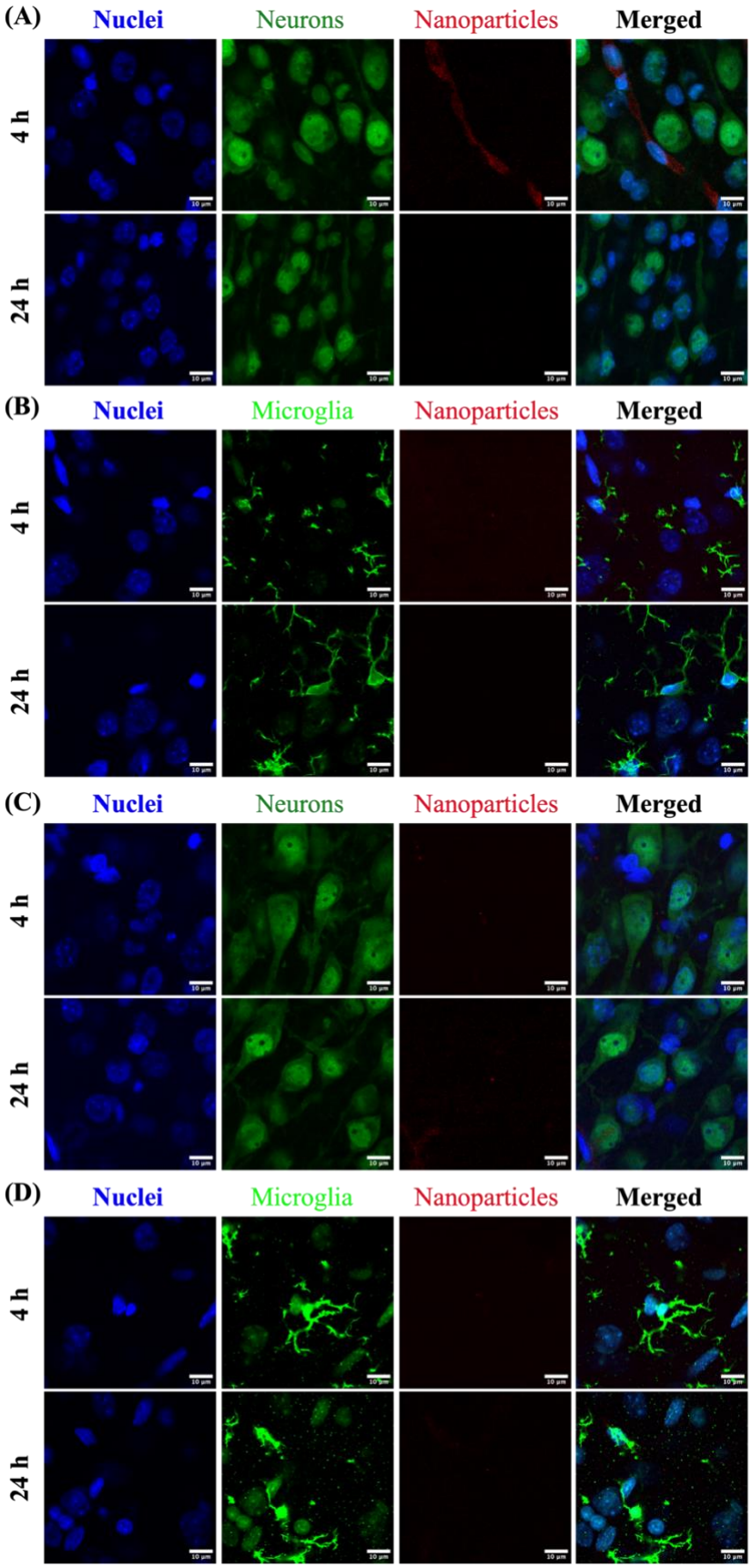
(A)
Nuclei
Neurons
Nanoparticles
Merged
4 h
24 h
(B)
Nuclei
Microglia
Nanoparticles
Merged
4 h
24 h
(C)
Nuclei
Neurons
Nanoparticles
Merged
4 h
24 h
(D)
Nuclei
Microglia
Nanoparticles
Merged
4 h
24 h

Figure 2-5. Localization of PLGA-PEG/F127 and PLGA-PEG/P80 nanoparticles (red) in the cortex of brain of healthy P10 rat at 4 h and 24 h after administration. (A) PLGA-PEG/F127 in cortical neurons, (B) PLGA-PEG/F127 in cortical microglia, (C) PLGA-PEG/P80 in cortical neurons, and (D) PLGA-PEG/P80 in cortical microglia. Blue: DAPI nuclei stain. Scale bars: 10 μm.

2.4. Discussion

PK and biodistribution of nanoparticles depend on the surface functionality, composition, particle size, surface charge, and particle shape [127-129]. It is necessary to control the physicochemical properties of nanoparticles when comparing the effect of surfactant. In this study, both PLGA-PEG/F127 and PLGA-PEG/P80 were formulated to produce particles within a 60 to 70 nm size range, 0.2 PDI, and near neutral zeta potential, which minimized the impact of physicochemical property differences. At 4 h post injection, 54.0% of the injected dose of PLGA-PEG/F127 and 54.6% of the injected dose of PLGA-PEG/P80 were detected in rat serum. PLGA-PEG/F127 and PLGA-PEG/P80 had a similar time delay to enter the systemic circulation, underwent a rapid concentration increase in serum since 1 h, and reached the peak concentration at 4 h. No significant difference was found between these two formulations during the absorption process. Although the biodistribution of a nanoformulation can be impacted by its surface functionality, composition, surface charge, and particle shape, the size of nanoparticles is critical to biodistribution of the nanoparticles. The percentage of injected dose in serum can vary when there is a 20 nm size difference for a nanoparticle [130-132]. Generally, smaller nanoparticles need a shorter time for absorption from the peritoneal cavity to systemic circulation, which results in higher bioavailability but shorter exposure time, compared with larger nanoparticles [133]. The similar size of PLGA-PEG/F127 and PLGA-PEG/P80 may explain the similarity in the absorption process of these two formulations. The systemic half-life of PLGA-PEG/F127 (5.9 h) was significantly longer than PLGA-PEG/P80 (1.7 h), which indicates that PLGA-PEG/F127 had a slower elimination in serum. P80 is reported to have higher affinity for ApoE [114, 116, 134]. Therefore, one potential explanation for the different profiles is the protein composition of the corona adsorbed on the PLGA-PEG/P80 is different from that of PLGA-PEG/F127. Overall, the bioavailability of PLGA-PEG/F127 is higher than PLGA-PEG/P80, this is consistent with their area under the curve (23.1 h-mg/mL for PLGA-PEG/F127 and 12.4 h-mg/mL for PLGA-PEG/P80). From the perspective of serum half-life and bioavailability, compared with PLGA-PEG/P80, PLGA-PEG/F127 can enhance systemic circulation time, which can prolong the dosing interval.

At the organ level, PLGA-PEG/F127 had a longer half-life in heart, lung, spleen, and kidney, which follows the same trend as that of serum. In contrast, PLGA-PEG/P80 had a longer liver half-life. This may also be caused by higher ApoE composition adsorbed on PLGA-PEG/P80 nanoparticles, as both low

density lipoprotein (LDL) and the LDL receptor-related protein (LRP) receptors are highly expressed in liver tissue [115, 118]. For all organs, PLGA-PEG/F127 had higher area under the curve than PLGA-PEG/P80, although the difference was not significant. This biodistribution data can be explained by the shorter systemic half-life and lower bioavailability of PLGA-PEG/P80. For both PLGA-PEG/F127 and PLGA-PEG/P80, nanoparticle accumulation was highest in the liver and spleen of the neonatal rat, which is consistent with prior literature for polymer nanoparticle delivery in adult rodents [128, 132]. Due to the immaturity of their metabolic system, at the same dosage, term neonates are more sensitive than adults to some active agents [135]. Hence, when using PLGA-PEG nanoparticles in 60-70 nm size range for drug delivery in neonatal rats, cytotoxic evaluation should focus on the liver and spleen.

For brain-specific targeting, it is notable that PLGA-PEG/P80 nanoparticles were still detectable 72 h after the administration, but PLGA-PEG/F127 nanoparticles were not observed in brain parenchyma at 24 h (Figure 8). This trend is also supported by the longer mean residence time of PLGA-PEG/P80. The contrast in the half-life, area under the curve, and the mean residence time might be attributed to the different brain biodistribution of these two formulations: most of the PLGA-PEG/F127 nanoparticles were retained in the brain capillaries where they would be cleared with continued blood circulation. Many of the PLGA-PEG/P80 nanoparticles were not vascular-associated and were present in the brain parenchyma. Prior cellular uptake studies using P80 modified PLGA nanoparticles indicates that P80 modified formulation results in greater brain endothelial cell association [118]. This explanation is further supported by the mechanism of ApoE-mediated particle transport. ApoE adsorption to a nanoparticle surface can result in receptor-ligand interaction with LDL receptor and LRP, which mediates transport across brain endothelial cells where LRP receptors are highly expressed in brain tissue [115, 118]. However, no to minimal intracellular uptake in neurons or microglia of PLGA-PEG/P80 nanoparticles were observed. The mechanism of particle translocation from BBB interaction to neuron or microglia uptake remains unknown. In addition, the degree of ApoE enrichment on the nanoparticle surface has an important effect on the distribution [136]. PLGA-PEG/P80 nanoparticles were emulsified in P80 solution rather than conjugated with P80, so the ApoE affinity of these nanoparticles may not be strong enough to impact cellular association with neurons after the particles have crossed the BBB. The animals used in this study were healthy animals with an intact BBB. Levels of ApoE in the term neonate compared to the adult are not well studied, which limits the ability to assess whether ApoE is present in high enough quantity to interact with PLGA-PEG/P80 particles in animals of this age. Even if the P80-modified nanoparticles are injected into carotid artery, which has significantly higher brain uptake compared with jugular vein injection, nanoparticle brain accumulation is still limited [125].

As supported by differences in biodistribution at both the whole-body level and the tissue level, the surface of the PLGA-PEG/F127 and PLGA-PEG/P80 particles are likely different while bulk physicochemical properties are comparable. The different stabilizers on the nanoparticle surface may lead to slightly differences on the surface of the nanoparticle, which could impact absorption of blood proteins such as ApoE and subsequent interaction with vascular endothelium. The kinetics of corona formation and the composition of the corona can be different when the surface composition of a nanoparticle changes [137], which can drive different compositions of protein adsorbed to the nanoparticle that alters biodistribution and half-life of nanoparticles [138, 139]. Further studies will need to provide quantitative analysis of the protein corona formation on PLGA-PEG nanoparticles as a function of surface composition, orientation, and distribution.

Due to lack of availability of an accessible tail vein at this age in rodents, and the higher bioavailability compared to subcutaneous and oral routes, i.p. injection is a commonly used administration route for neonatal laboratory rodents. The main pathway for nanoparticles to enter systemic circulation from the peritoneal cavity is via lymphatic uptake rather than diffusion [133]. Therefore, one critical parameter for the nanoparticle absorption following i.p. injection is particle size, as opposed to the amount of injected dose. We did not observe any significant difference among all the tissues when administering different i.p. doses of PLGA-PEG particles in neonatal rats (Fig S2-2). Additionally, Panagi et al. showed that the blood clearance of PLGA-PEG nanoparticles was independent of dose [140]. However, the physiological status of an individual rat may affect the nanoparticle absorption [141], which could alter uptake into systemic circulation. Lastly, there are prior reports that the time to reach the maximum serum concentration may be influenced by the position of the i.p. injection, where the maximum concentration might vary two-fold between injection position above and below the transverse mesocolon [142]. Therefore, i.p. injection does introduce several challenges and potential limitations for reproducible and high yield systemic nanoparticle delivery, even in the neonate.

To confirm the quantitative measurements of dye were not due to free dye in our tissue samples, we assessed the stability of the dye conjugation to PLGA-PEG. PLGA-PEG nanoparticles do not have electron-dense atoms, limiting the resolution of visualization in tissue samples through standard electron microscopy techniques [120, 143]. Therefore, we used an indirect method to verify the dye-labeling stability of PLGA-PEG nanoparticles after crossing the peritoneal cavity. Compared with the unconjugated CF647 sample, serum extracts from CF647-labeled PLGA-PEG/F127 and PLGA-PEG/P80 injected rats showed no peak for free CF647 with a UV-Vis detector at 650 nm and a fluorescence detector for Ex/Em at 635 nm/665 nm. This indicates that there was no detectable free CF647 in blood after i.p. injection, confirming

the bond between the CF647 and polymer remained intact after partitioning into the lymphatic system and entering systemic circulation.

2.5. Conclusion

PLGA-PEG nanoparticles are promising drug delivery vehicles for the neonatal population. PK data can guide dosage determination for improving biodistribution of nanoparticles in neonates. In this study, we showed PLGA-PEG nanoparticles formulated with different surfactants had different PK parameters and different biodistributions at the whole body and organ level. Compared with PLGA-PEG/P80, PLGA-PEG/F127 had longer systemic circulation time and higher bioavailability, and thus had longer half-life in heart, lung, spleen, kidney, and brain. In the brain, PLGA-PEG/P80 had better distribution in the brain parenchyma, while PLGA-PEG/F127 remained associated with brain capillaries, although both formulations had low brain accumulation. The neonatal population is underrepresented in PK clinical trials resulting in a data gap that is a prominent cause for off-label drug use in neonates. Understanding PK profiles and biodistribution, and associated residence time, of PLGA-PEG and other polymer nanoparticles in neonates will help with the design and implementation of therapeutic nanoparticles with maximum efficiency and minimum toxicity. Neonatal PK data will help improve the speed of clinical translation and drug safety for use of nanomedicines in this underserved population.

Chapter 3: Nano-formulated curcumin uptake and biodistribution in the fetal growth restricted newborn piglet brain

Part of this chapter was published as: Xu, N.; Wixey, J.; Chand, K.; Wong, M.; Nance, E. Nano-formulated curcumin uptake and biodistribution in the fetal growth restricted newborn piglet brain. *Drug Delivery and Translational Research* 2025, 1-15. https://doi.org/10.1007/s13346-025-01830-y

3.1. Introduction

As introduced in Chapter 1.1.1, fetal growth restriction (FGR) is associated with long-term neurological disorders and there is no treatment to protect the FGR newborn brain. Effective therapies for FGR treatment are urgently needed. Inflammation is associated with brain impairment in the FGR newborn and results in sustained activation of pro-inflammatory microglia that persists up to weeks after birth[144, 145]. The increased proinflammatory cytokine markers in the blood of FGR infants are correlated with adverse neurological outcomes at 2 years of age[146]. These clinical data suggest targeting inflammation as a therapeutic approach for FGR-associated brain injury may prevent ongoing neurological damage in FGR infants.

Curcumin is an anti-inflammatory and antioxidant chemical that has been widely used to treat oxidative and inflammatory conditions, metabolic syndrome, arthritis, anxiety, and hyperlipidemia, and has demonstrated neuroprotective effects in neonatal rats[147, 148]. The bioavailability of curcumin is greatly affected by its low solubility, which has led to the use of nanoparticles that can encapsulate curcumin to improve solubility. Poly(lactic-co-glycolic acid) (PLGA)-based polymeric nanoparticles, which are a biocompatible and biodegradable polymer approved by the U.S. Food and Drug Administration (FDA), are one of the most commonly used vehicles for drug delivery. PLGA-based nanoparticles have been successfully used in various applications such as cancer, neurological diseases, pain management, and bacterial infections[149-153]. Functionalization via copolymerization of polyethylene glycol (PEG) can increase systemic circulation time by reducing protein adsorption and can also improve the diffusivity of nanoparticles[51, 154]. However, the encapsulation capacity of curcumin in polymer nanoparticles, including PLGA, is limited and often less than 10% by weight of the drug-polymer formulation[155, 156].

Herein, we used PLGA copolymerized with PEG (PLGA-PEG) to formulate a curcumin-loaded nano-formulation with high drug loading and high drug encapsulation efficiency. To improve the curcumin encapsulation efficiency in PLGA-PEG nanoparticles and enhance the stability and reproducibility of these nanoparticles, we investigated the effects of PLGA length, surfactant concentration, polymer functionalization, and formulation method on curcumin loading. Upon successful optimization of a PLGA-

PEG nanoparticle with high curcumin encapsulation efficiency and curcumin loading, we also sought to assess particle accumulation in the FGR piglet brain to evaluate its potential for FGR treatment.

The newborn pig brain is comparable to the human infant brain in histology, cortical surface area, white to grey matter ratio, myelination, vascularization, and development processes[88, 157, 158]. Therefore, compared to rodent models, which are commonly used for preclinical studies, an FGR piglet model has potential to expedite translation of a therapeutic to clinical use. Additionally, FGR in piglets spontaneously occurs through placental insufficiency and the resulting brain injury mimics human pathophysiological outcomes associated with FGR, including asymmetrical growth restriction with brain sparing[88]. The FGR piglet model can be used as a clinical-trial ready model. Based on the unmet need of an effective neuroprotection strategy for FGR, we quantified the biodistribution and brain localization of curcumin nanoparticles administered via different administration routes to analyze the feasibility of these nanoparticles to target and treat brain inflammation caused by FGR.

Our results provide guidance for polymeric nano-formulation encapsulating small hydrophobic molecules, which can be used to design a tunable, stable, and reproducible nanoparticle with high hydrophobic drug loading. Our findings also reveal the biodistribution and brain localization of curcumin-loaded polymeric nanoparticles in neonatal pigs in a human-like FGR model.

3.2. Materials and Methods

3.2.1. Nanoparticle formulation and optimization

Formulation optimization initiated with a standard nanoprecipitation method[148]. Briefly, 2 mg curcumin (Sigma-Aldrich, St. Louis, MO, USA) 20 mg PLGA-PEG (Methoxy PLGA-PEG-methoxy, 45k:5k, LA:GA = 50:50, Akina, Inc., West Lafayette, IN, USA) polymer were dissolved in 1 mL acetone (Sigma-Aldrich) to prepare the organic solution, and then this solution was added dropwise into 25 mL of 1% (w/v) Pluronic® F127 (F127, Sigma-Aldrich) solution. The nanoparticles formed spontaneously in the surfactant solution. The solution was stirred magnetically at 500 rpm for 3 h, and any remaining organic solvent was removed by rotary evaporation at 4 °C under reduced pressure for 30 min. After that, nanoparticles were collected at 100,000× g for 60 min and washed at 100,000× g for 25 min by centrifugation. Nanoparticles were resuspended in 1× PBS after washing and then stored at 4 °C for future use. PLGA-PEG with 15k, 45k, 75k and 70k-70k PLGA length, F127 with concentration at 0.1% (w/v), 0.5% (w/v), 1% (w/v) and 10% (w/v), and PLGA-PEG with amine functionalization (30k:5k PLGA-PEG-NH_2, Akina, Inc.) were iterated to identify an optimal curcumin formulation via standard nanoprecipitation technique with high drug loading, reproducibility, and long-term stability.

To tune the precipitation rates of curcumin and PLGA-PEG polymer to increase drug loading and encapsulation efficiency, sequential nanoprecipitation was used[159]. PLGA-PEG (45k:5k, LA:GA = 50:50) and curcumin were dissolved in mixed organic solvent (DMSO: DMF: EtOH = 3:3:4). Aqueous solution was added into the organic phase at an organic:aqueous = 1:10 ratio. Organic and aqueous phase were gently mixed by pipetting until the solution was transparent. The particles were washed with aqueous solution 3 times using the above method. Nanoparticles were resuspended in 1× PBS after washing and then stored at 4 °C for short-term storage. 10% (w/w) sucrose was added to the washed nanoparticles, and then the nanoparticles were lyophilized for 24 h. The lyophilized nanoparticles were stored at -20 ℃ for long-term storage. Organic:aqueous = 1:5, 1:10, and 1:20, aqueous solution containing H_2O, F127, and Tween® 80 (P80, Sigma-Aldrich), F127 with concentration at 0.1% (w/v), 0.5% (w/v), and 1% (w/v), and different curcumin and PLGA-PEG concentrations were iterated to characterize the effects of formulation parameters on nanoparticle physicochemical properties. The optimal curcumin formulation was used for further analysis. To help quantify and visualize the *in vivo* biodistribution, PLGA backbone in PLGA-PEG was covalently labeled with fluorescent dye CF555® Succinimidyl Ester (CF555, Biotium, Fremont, CA, USA) and CF647® Succinimidyl Ester (CF647, Biotium) before nanoparticle formulation[160].

3.2.2. Particle physicochemical properties and morphology

The particle size and polydispersity index (PDI) of nanoparticles were measured by dynamic light scattering (DLS), and the zeta potential (ζ-potential) was determined using a zeta potential analyzer (NanoSizer Zeta Series, Malvern Instruments, Malvern, UK). Samples were diluted to appropriate concentrations to obtain accurate measurements in 10 mM sodium chloride (NaCl, Sigma-Aldrich), pH 7.4. Morphologies of optimal curcumin formulation before and after lyophilization were characterized by transmission electron microscopy (TEM).

3.2.3. Drug loading and encapsulation efficiency

To quantify the drug loading and encapsulation efficiency of curcumin-loaded nanoparticles, the lyophilized nanoparticles were measured by ultraviolet–visible light (UV–Vis) spectrometry as compared to a standard calibration curve of curcumin in DMSO. Each sample's absorbance at 430 nm was measured and adjusted by subtracting a blank of unloaded polymer nanoparticles' absorbance in DMSO. The weight of a polymer and drug was the weight of lyophilized nanoparticles. Drug loading and drug encapsulation efficiency are defined as follows:

$$\%\text{Drug loading} = \frac{\text{Weight of drug encapsulated in nanoparticles}}{\text{Weight of polymer and drug in nanoparticles}} \times 100 \quad (3\text{-}1)$$

$$\%\text{Drug encapsulation efficiency} = \frac{\text{Weight of drug encapsulated in nanoparticles}}{\text{Weight of intial drug}} \times 100 \quad (3\text{-}2)$$

3.2.4. In vitro curcumin release profile

Curcumin-loaded PLGA-PEG nanoparticles were resuspended in 1 mL of 1× PBS. Each sample was equally distributed to three dialysis tubes made of cellulose ester (MW cutoff: 300 kDa, Spectrum Laboratories, Inc., Piscataway, NJ, USA). The membranes were submerged in 20 mL of 1× PBS containing 1% of P80 and placed on a shaker at 60 rpm and 37 °C. At designated time points, the membranes were transferred to fresh 20 mL of 1× PBS containing 1% of P80. In the supernatants collected at each time point, curcumin content was determined by UV–Vis compared to a calibration curve of curcumin in the 1× PBS 1% P80 solution. Percent curcumin released from the nanoparticles was defined as the curcumin amount released at a specific time point divided by the total curcumin encapsulated in the nanoparticles.

3.2.5. Long-term stability assay

To assess the long-term stability of curcumin-loaded PLGA-PEG nanoparticles, 5% (w/v) sucrose was added to fresh formulated nanoparticles. Nanoparticles were lyophilized for 24h. Three storage conditions were tested: room temperature, 4 ℃, and -20 ℃. Nanoparticles stored at room temperature were measured on the first day, 30th day, and 180th day after lyophilization. At the indicated timepoint, lyophilized nanoparticles were reconstituted in 1× PBS. Then the nanoparticles were measured by DLS using the same protocol described above.

3.2.6. Nanoparticle administration and tissue extraction

All animal procedures were conducted at The University of Queensland, Brisbane, QLD, Australia and approval for this study was granted by The University of Queensland Animal Ethics Committee (2022/AE000163). A piglet model of growth restriction where FGR occurs spontaneously was used. Newborn FGR (<10th percentile) and normally grown (NG) piglets were collected from a piggery nearby the University of Queensland on the first day of life, defined as postnatal (P) day 1. On P1, NG piglets and FGR piglets (n = 6 per timepoint; 3 FGR, 3 NG per group) received intranasal (i.n.) and intravenous (i.v.) administration of CF555-labeled curcumin-loaded PLGA-PEG and CF647-labeled curcumin-loaded PLGA-PEG nanoparticles at a PLGA-PEG concentration of 15 mg/kg pig in 1× PBS, respectively. Piglets were sacrificed at the indicated time (4 h, 48 h) after injection by an overdose of euthanasia solution (650 mg/kg sodium phenobarbital; Lethabarb, Virbac, Australia) and were transcardially flushed with PBS. For each piglet, the parietal cortex and cerebellum of brain, and the liver, spleen, and kidney were collected and immersion fixed in 4% paraformaldehyde. The parietal cortex and cerebellum were the focal brain regions for tissue collection due to prior literature that shows both regions display pathology in the piglet that is associated with FGR in humans[144, 161]. Blood was collected in a ethylenediaminetetraacetic acid (EDTA)-coated tube, and plasma was separated via 5 min of centrifugation at 3000× g.

3.2.7. Tissue processing for biodistribution analysis

To quantify the nanoparticle biodistribution, a portion of the parietal cortex and cerebellum of the brain, liver, spleen, and kidney were homogenized in 4 × PBS, and the supernatants were collected via centrifugation at 10,000× g for 10 min. The percent injected dose (%ID) of CF555-labeled curcumin-loaded PLGA-PEG and CF647-labeled curcumin-loaded PLGA-PEG nanoparticles in plasma, parietal cortex, cerebellum, liver, spleen, and kidney tissues were calculated from a calibration curve for each tissue using UV-Vis spectrometry. Tissue from piglets not injected with nanoparticles served as baseline measurements.

3.2.8. Immunohistochemistry

To characterize the brain localization of nanoparticles, the parietal cortex and cerebellum of the brain were placed in a formalin-to-30% sucrose gradient and cryosectioned on a Leica cryostat into 30 µm sections [148]. Following cryosection, primary antibodies for microglia (1:250 rabbit anti-Iba1, Wako, Fuji-film, Minato City, Tokyo, Japan) and neurons (1:250 donkey anti-NeuN, Abcam, Cam-bridge, UK) were prepared in 1× PBS containing 1% Triton X-100 (Sigma-Aldrich) and 3% normal goat serum (Sigma-Aldrich). Primary antibody solutions were added to tissue sections for 4–6 h at room temperature in a humified dark chamber. The tissue slices were washed twice in 1× PBS. Secondary antibodies were dissolved in 1× PBS containing 1% Triton X-100 and added to the tissue slices with 2 h incubation. The slices were washed twice in 1× PBS, then stained with 1:10,000 4′,6-diamidino-2-phenylindole (DAPI, Invitrogen, Waltham, MA, USA). The slides were washed and dried for 30 min in the dark. Mounting medium (Dako, Agilent Technologies, Santa Clara, CA, USA) was added to each slide, and a glass coverslip was placed on top. Slides were stored at 4 °C until imaged under an A1 confocal microscope (Nikon, Tokyo, Japan) and at −20 °C for long-term storage.

3.2.9. Statistical analysis

Statistical analysis was performed using the Mann Whitney test. All statistical analyses were carried out using GraphPad Prism (GraphPad Software Inc., Version 10.2.3). A p-value of <0.05 was considered statistically significant.

3.3. Results

3.3.1. Optimization and characterization of curcumin-loaded PLGA-PEG via standard nanoprecipitation

We formulated curcumin-loaded PLGA-PEG nanoparticles based on 10% (w/w) target loading of curcumin using standard nanoprecipitation technique to characterize the effects of different formulation parameters on the nanoparticle physicochemical properties and drug loading. Increasing length of the PLGA chain in

the PLGA-PEG polymer results in increased hydrodynamic diameter (Fig 3-1A). Particles prepared with 45k:5k PLGA-PEG had the highest curcumin loading: curcumin loading increased with the increase of PLGA length before reaching 45k but decreased with the increase of PLGA length after 45k. The concentration of surfactant did not have significant impact on particle size (Fig 3-1B). However, the curcumin loading decreased when surfactant concentration was increased. When using 0.5% (w/v) F127, stable curcumin-loaded PLGA-PEG nanoparticles can be formulated with the highest curcumin loading. The formulation was not stable when F127 concentration was decreased to 0.1% (w/v). We measured hydrodynamic diameter and PDI of curcumin-loaded PLGA-PEG (45k:5k) nanoparticles after lyophilization to assess long-term storage. Cryoprotectants such as sucrose, F68, F127, inulin and trehalose were tested but could not maintain colloidal stability or resulted in significant curcumin release (Table S3-1).

We further analyzed the effects of polymer functionalization on lyophilization stability. With amine-functionalized PLGA-PEG (PLGA-PEG-NH_2) polymer, more stable curcumin particles were formulated – when lyophilizing with 5% trehalose, these curcumin nanoparticles maintained their size and PDI after lyophilization (Fig 3-1C). Curcumin-loaded PLGA-PEG-NH_2 nanoparticles had an average of 7.7% curcumin loading before and after lyophilization.

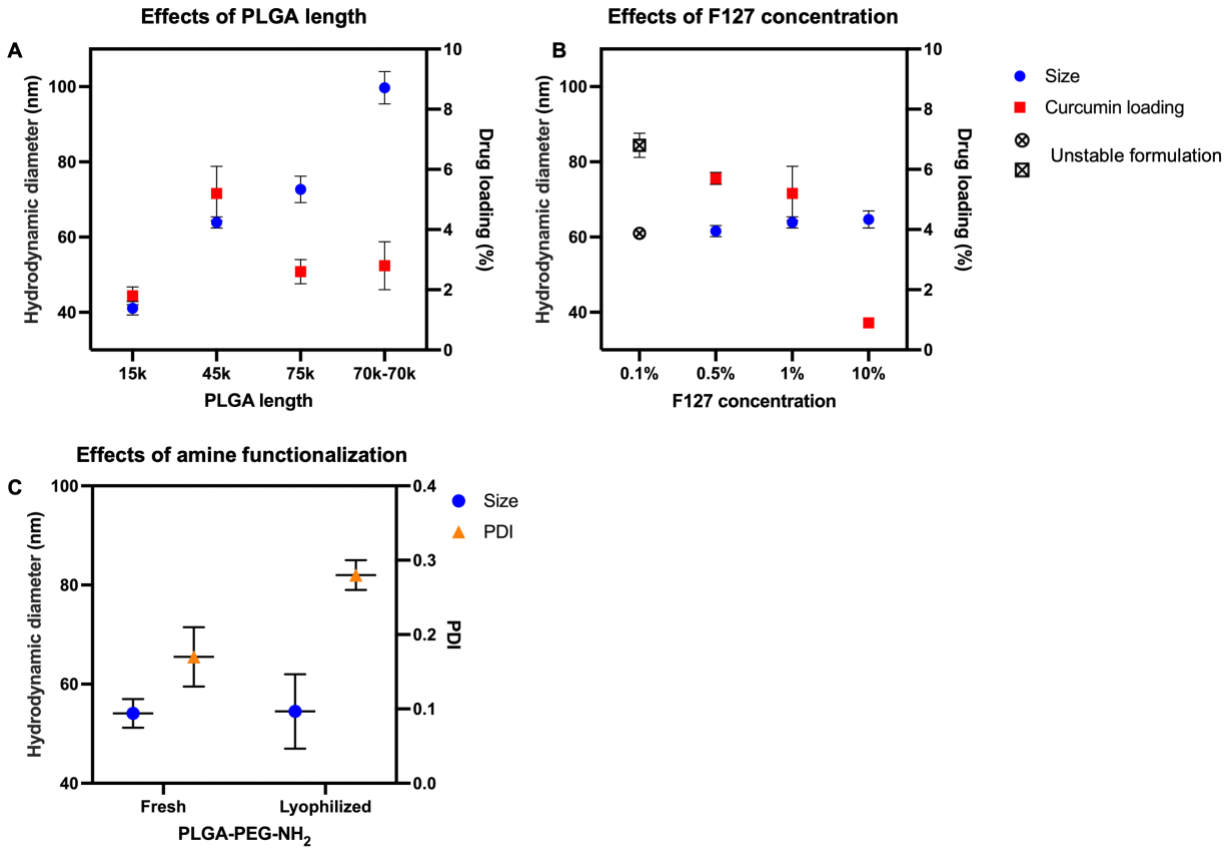

Figure 3-1. Curcumin-loaded PLGA-PEG nanoparticles formulated via standard nanoprecipitation. (A) Size of curcumin-loaded nanoparticles increased with the increase of PLGA length, and nanoparticles formulated using 45kDa PLGA had highest curcumin loading. All polymers had a 5kDa PEG length and 1% F127 was used as the surfactant. (B) Curcumin-loaded particles had minimal size change when changing the concentration of surfactant, whereas curcumin loading had an obvious decrease with the increase of F127 concentration. All nanoparticles were formulated with 45k:5k PLGA-PEG polymer. (C) Hydrodynamic diameter and PDI of 30k:5k PLGA-PEG-NH_2 polymer freshly made and after lyophilization.

3.3.2. Optimization and characterization of curcumin-loaded PLGA-PEG via sequential nanoprecipitation

To overcome the low curcumin loading and loss of stability caused by standard nanoprecipitation, we next tested sequential nanoprecipitation. According to Liu *et al.*, precipitation rates of curcumin and PLGA-PEG can be tailored by a mixed solvent system, where the rates are close when using mixed organic solvent DMSO/DMF/EtOH at the ratio of 3/3/4[159]. Substituting acetone with 3/3/4 DMSO/DMF/EtOH solvent mixture, we varied the organic phase to aqueous phase ratio, surfactant, PLGA chain length, surfactant concentration, PLGA-PEG concentration, and curcumin concentration.

Starting from 3 mg/mL curcumin and 45k:5k PLGA-PEG formulated without surfactant, three organic:aqueous ratios were tested. The reproducibility of the formulation was impaired by the high organic ratio, but there was an obvious PDI increase with highest aqueous ratio. Among 1:5, 1:10, and 1:20 organic:aqueous, the 1:10 organic to aqueous ratio showed the best reproducibility across three formulations and the lowest PDI (Fig 3-2A). To explore the tunability of the formulation, the surfactants F127 and P80 were introduced (Fig 3-2B). F127 has been shown to increase the circulation half-life of nanoparticles[160], while P80 has demonstrated cell-specific targeting of PLGA nanoparticles in the brain[162]. Both F127 and P80 surfactant decreased size and increased PDI of the nanoparticles. P80-formulated nanoparticles could not maintain a < 0.3 PDI, which undermined possible *in vivo* applications. Particle size decreased with the increased F127 concentration, and the PDI increased with the increase of F127 concentration (Fig 3-2C). At 0.1% F127 (w/v), the curcumin formulation was most stable and reproducible. Additionally, both the starting curcumin concentration and PLGA-PEG concentration had effects on the particle size: a higher concentration led to larger particle size (Fig 3-2D-E). The lowest PLGA-PEG/curcumin ratio to maintain the lyophilization stability was 3:2 (Fig 3-2G-H, Table S3-2).

The optimized curcumin formulation had an average hydrodynamic diameter of 54.5 ± 3.4 nm, a PDI of 0.18 ± 0.01, an average zeta-potential of -4.6 ± 0.5 mV, and greater than 39% curcumin loading and higher than 95% curcumin encapsulation efficiency. When 5% sucrose was used as the cryoprotectant, particle size, PDI, surface charge, drug loading, and morphology could be maintained after lyophilization (Table 3-1, Fig 3-2G-H). In pH = 7.4 $1 \times$ PBS solution, this optimized formulation showed sustained

curcumin release over one-week (Fig 3-2F). After 192 h, 60% curcumin was released; the remaining 40% curcumin could be fully released via NaOH degradation of the PLGA-PEG nanoparticle.

Meanwhile, the shelf-life stability of curcumin-loaded PLGA-PEG nanoparticles at room temperature, 4 ℃, and -20 ℃ were characterized. At room temperature, the nanoparticles maintained their size and PDI in the first 30 days after the lyophilization, then the size and PDI increased due to the particle aggregation (Fig 3-3A). 180 days after lyophilization, nanoparticles stored at 4 ℃ or -20 ℃ were still comparable to the freshly made nanoparticles, although the nanoparticles stored at room temperature lost their colloidal stability due to aggregation (Fig 3-3B).

Due to its reproducibility, tunability, lyophilization stability, long-term stability, and sustained release profile compared to curcumin-loaded nanoparticles formulated via standard nanoprecipitation method (Table S3-3), curcumin-loaded PLGA-PEG nanoparticles (20 mg/mL PLGA-PEG and 13.3 mg/mL curcumin) formulated with 0.1% F127 (w/v) were administered to newborn pigs to further analyze their biodistribution and brain uptake.

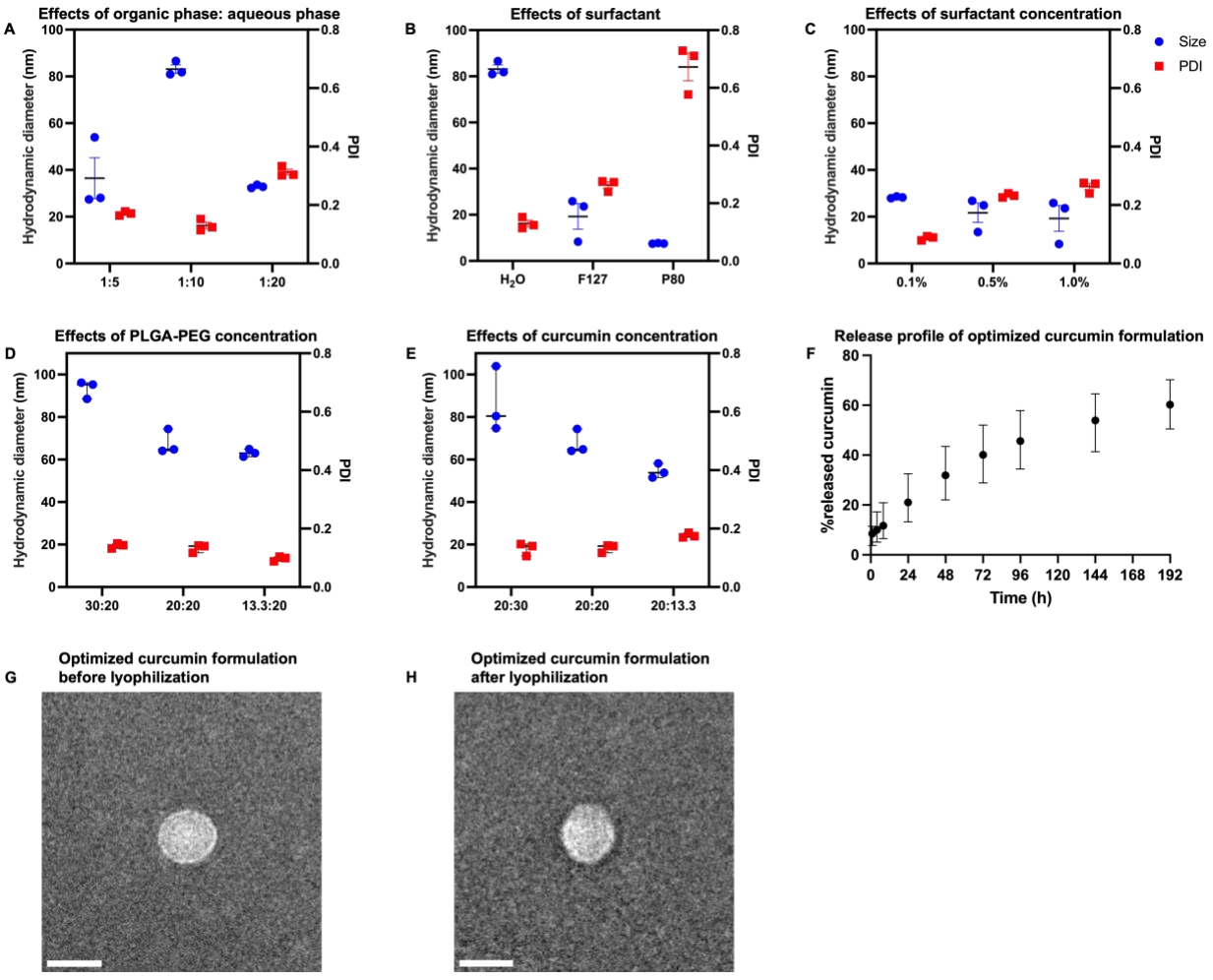

Figure 3-2. Curcumin-loaded PLGA-PEG nanoparticles formulated via sequential nanoprecipitation. (A) Effects of organic phase to aqueous phase ratio on size and PDI; the curcumin and PLGA-PEG concentration were 3 mg/mL, and no surfactant was used. (B) Effect of surfactants on size and PDI; the curcumin and PLGA-PEG concentrations were 3 mg/mL and the organic phase to aqueous phase ratio was 1:10. (C) Effect of surfactant (F127) concentration (w/v) on size and PDI; the curcumin and PLGA-PEG concentration were 3 mg/mL and the organic phase to aqueous phase ratio was 1:10. (D) Effect of PLGA-PEG concentration on size and PDI. The organic phase to aqueous phase ratio was 1:10 and a 0.1% F127 surfactant concentration was used. For the 13.3:20 formulation: 13.3 mg/mL PLGA-PEG: 20 mg/mL curcumin. (E) Effect of curcumin concentration on size and PDI. The organic phase to aqueous phase ratio was 1:10; 20:30: 20 mg/mL PLGA-PEG: 30 mg/mL curcumin; 20:20: 20 mg/mL PLGA-PEG: 20 mg/mL curcumin; 20:13.3: 20 mg/mL PLGA-PEG: 13.3 mg/mL curcumin. (F) Curcumin-loaded PLGA-PEG formulated with 0.1% F127 had a sustained curcumin release profile over a one-week period. (G) TEM image of freshly made curcumin-loaded PLGA-PEG, scale bar: 50 nm. (H) TEM image of curcumin-loaded PLGA-PEG lyophilized with 5% sucrose, scale bar: 50 nm.

Table 3-1. Physicochemical properties, drug loading, and drug encapsulation efficiency of optimized curcumin-loaded PLGA-PEG nanoparticles. Initial concentration of curcumin: 13.3 mg/mL, initial concentration of PLGA-PEG: 20 mg/mL; organic solution: aqueous solution = 1: 10; 0.1% F127 was used as aqueous solution. All values are reported as mean ± standard error of the mean (SEM) (n = 3).

Curcumin-loaded PLGA-PEG	Size ± SEM (nm)	PDI ± SEM	Zeta potential ± SEM (mV)	Drug loading ± SEM (%)	Drug encapsulation efficiency ± SEM (%)
Before lyophilization	54.5 ± 3.4	0.18 ± 0.01	-4.6 ± 0.5	39.2 ± 1.1	98.1 ± 2.7
Lyophilized with 5% sucrose	70.6 ± 4.1	0.18 ± 0.01	-4.7 ± 0.2	39.5 ± 0.9	98.8 ± 2.3

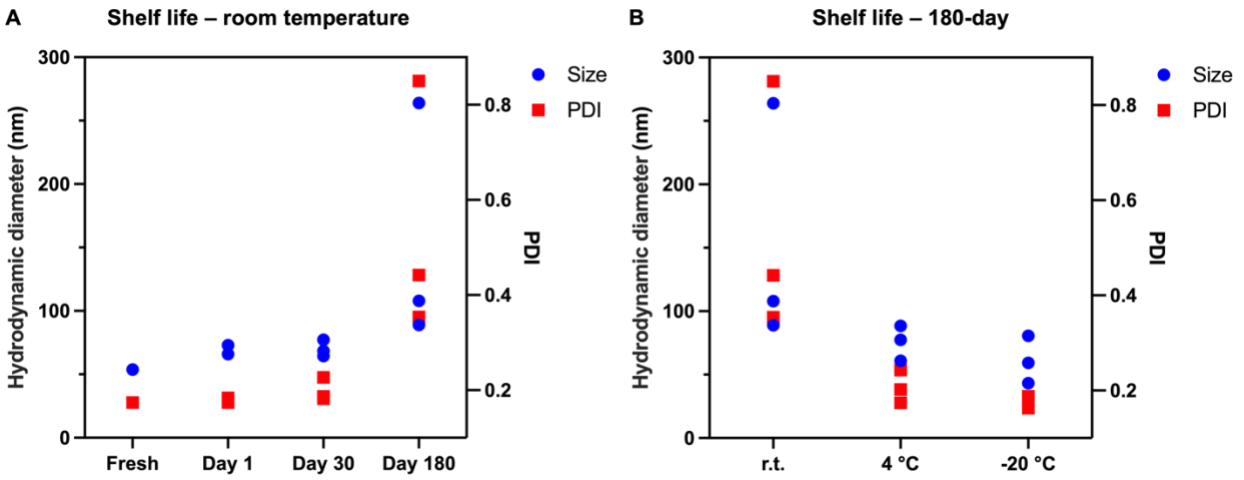

Figure 3-3. Shelf-life stability of lyophilized curcumin-loaded PLGA-PEG nanoparticles. (A) Shelf-life stability at room temperature, and (B) shelf-life stability after a 180-day storage at room temperature, 4 ℃, and -20 ℃. r.t.: room temperature.

3.3.3. Biodistribution of curcumin-loaded PLGA-PEG nanoparticles

Establishing the biodistribution of nanoparticles can inform off-target accumulation, any associated potential toxicity, and an optimized dosing schema. In addition, there is limited biodistribution data for nanoparticles in neonatal animals, particularly large animal models such as pigs. To evaluate the biodistribution of curcumin-loaded PLGA-PEG nanoparticles, PLGA-PEG polymer was labeled with fluorescent dye CF555 and CF647 prior to formulation. Nanoparticles labeled with fluorescent dye (Table S3-4) were administered intravenously (CF555-labeled PLGA-PEG) and intranasally (CF647-labaled PLGA-PEG) to FGR and NG pigs at P1. At 4 h following i.v. administration, a large % of the injected dose (ID) of curcumin particles was detected in plasma, with small %ID in the liver, spleen and kidney (Fig 3-4A). No to minimal amount of PLGA-PEG was detectable in the parietal cortex and cerebellum of the piglet brain 4 h after i.v. administration. Following i.n administration, 5.7% ID of PLGA-PEG was detected in the parietal cortex and 9.7% ID of PLGA-PEG was detected in cerebellum of brain at 4 h - particle accumulation via i.n. administration was at least 5-fold higher compared to i.v. administered particles (Fig 3-4B). The difference in accumulation between the parietal cortex and cerebellum following i.n. administration was not significant.

Nanoparticles also accumulated in liver, spleen, and kidney 4 h after i.n. administration. Less than 10% ID of nanoparticles were in systemic circulation 4 h after i.n. administration. At 48 h, for both i.v. and

i.n. administration, no-to-minimal amount of nanoparticles could be detected in tissue or plasma. We did not observe a significant difference in biodistribution between FGR and NG piglets at these time points.

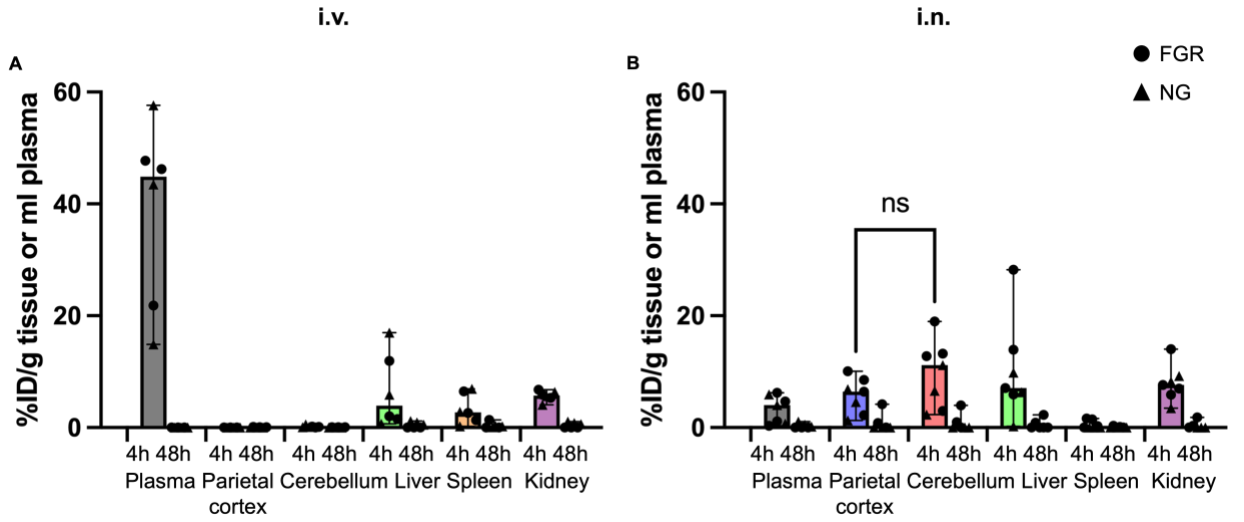

Figure 3-4. Curcumin-loaded PLGA-PEG nanoparticle accumulation in the FGR (circle) and NG (triangle) plasma, brain (parietal cortex and cerebellum), liver, spleen, and kidney after (A) i.v. administration and (B) i.n. administration at 4 h and 48 h. %ID: percent of injected dose. Graphs display median ± 95% confidence interval. Group differences were evaluated using Mann Whitney test, ns: not significant.

3.3.4. Brain localization of curcumin-loaded PLGA-PEG nanoparticles

Polymeric nanoparticles are promising as effective neuroprotective therapeutics to mitigate adverse neurodevelopmental outcomes in neonates[124, 148, 163, 164]. In FGR brain injury, microglia are therapeutic targets of interest to mitigate ongoing inflammation[12, 14, 144, 165]. Therefore, we evaluated if i.v. or i.n. administration resulted in microglial localization of PLGA-PEG in the P1 pig brain. To characterize the localization of curcumin-loaded PLGA-PEG nanoparticles in the newborn pig brain, cryosectioned parietal cortex and cerebellum tissues were imaged using confocal microscopy. At 4 h after administration, a significant amount of i.n. administered nanoparticles were visualized in both parietal cortex and cerebellum, whereas i.v. injected nanoparticles were not observed in either the parietal cortex or cerebellum. Nanoparticle localization was cellular and co-localized in Iba-1+ microglia (Fig 3-5A, Fig S3-1), which was further confirmed by higher resolution, volume-rendered images (Fig 3-5B).

Although the amount of nanoparticles in the parietal cortex and cerebellum was not quantifiable at 48 h after administration, i.n. administered nanoparticles were visualized in the brain and co-localized in microglia at this timepoint (Fig 3-6A-B). Similar to the 4 h timepoint, no to minimal nanoparticles were observed in the extracellular space or in neurons at 48 h (Fig. S3-2). At both 4 h and 48 h, no significant

difference in nanoparticle localization between the parietal cortex and cerebellum was visualized. Additionally, no difference in cellular nanoparticle localization was found between NG and FGR piglets.

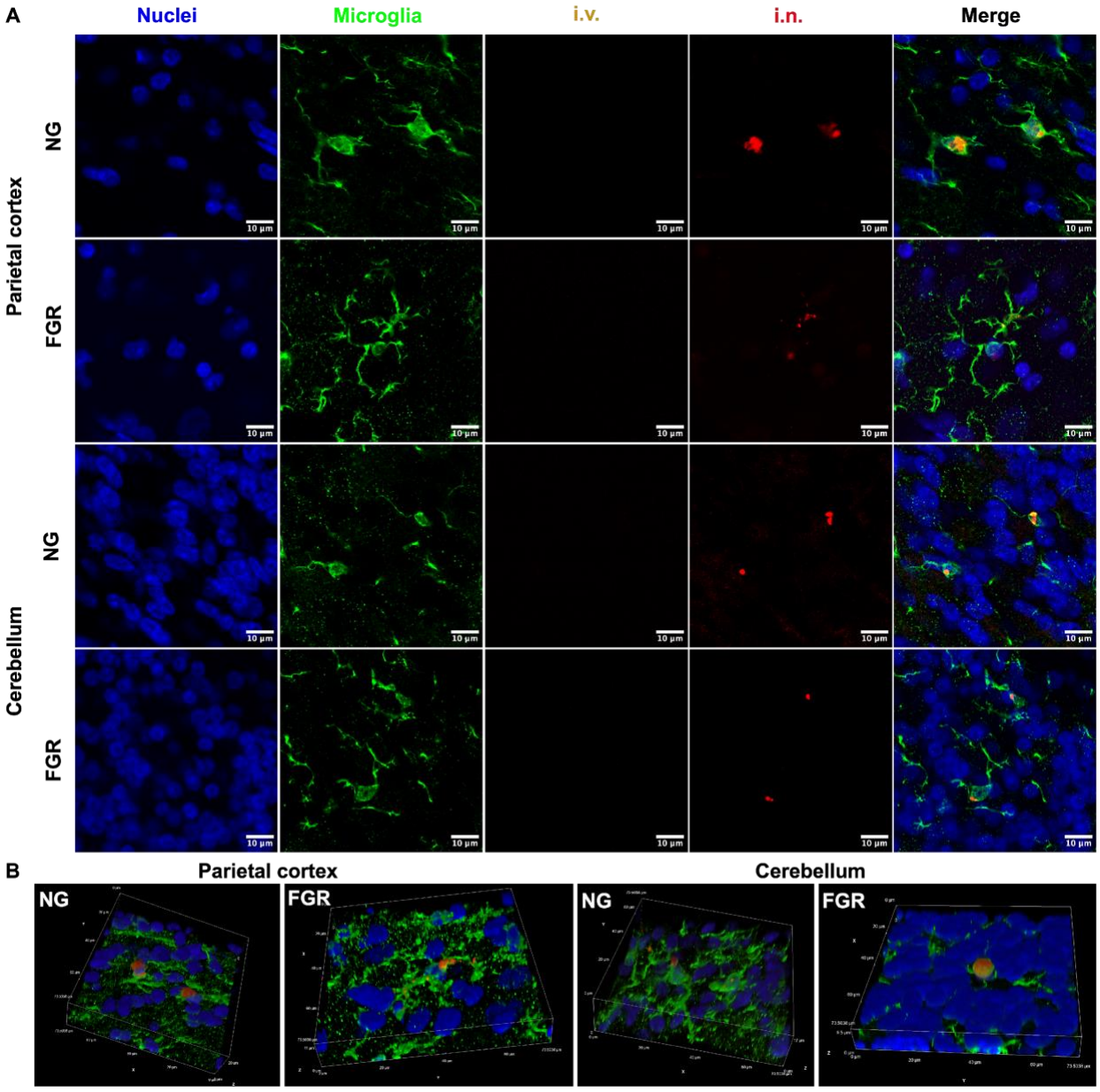

Figure 3-5. Curcumin-loaded PLGA-PEG accumulation in the parietal cortex and cerebellum at 4 h after i.v. (orange) and i.n. (red) administration. (A) Particle localization in NG and FGR piglet brains. Scale bars: 10 μm. (B) Representative z-stack images showing 3D particle co-localization in microglia. Blue: DAPI nuclei stain. Green: Iba-1+ microglia stain.

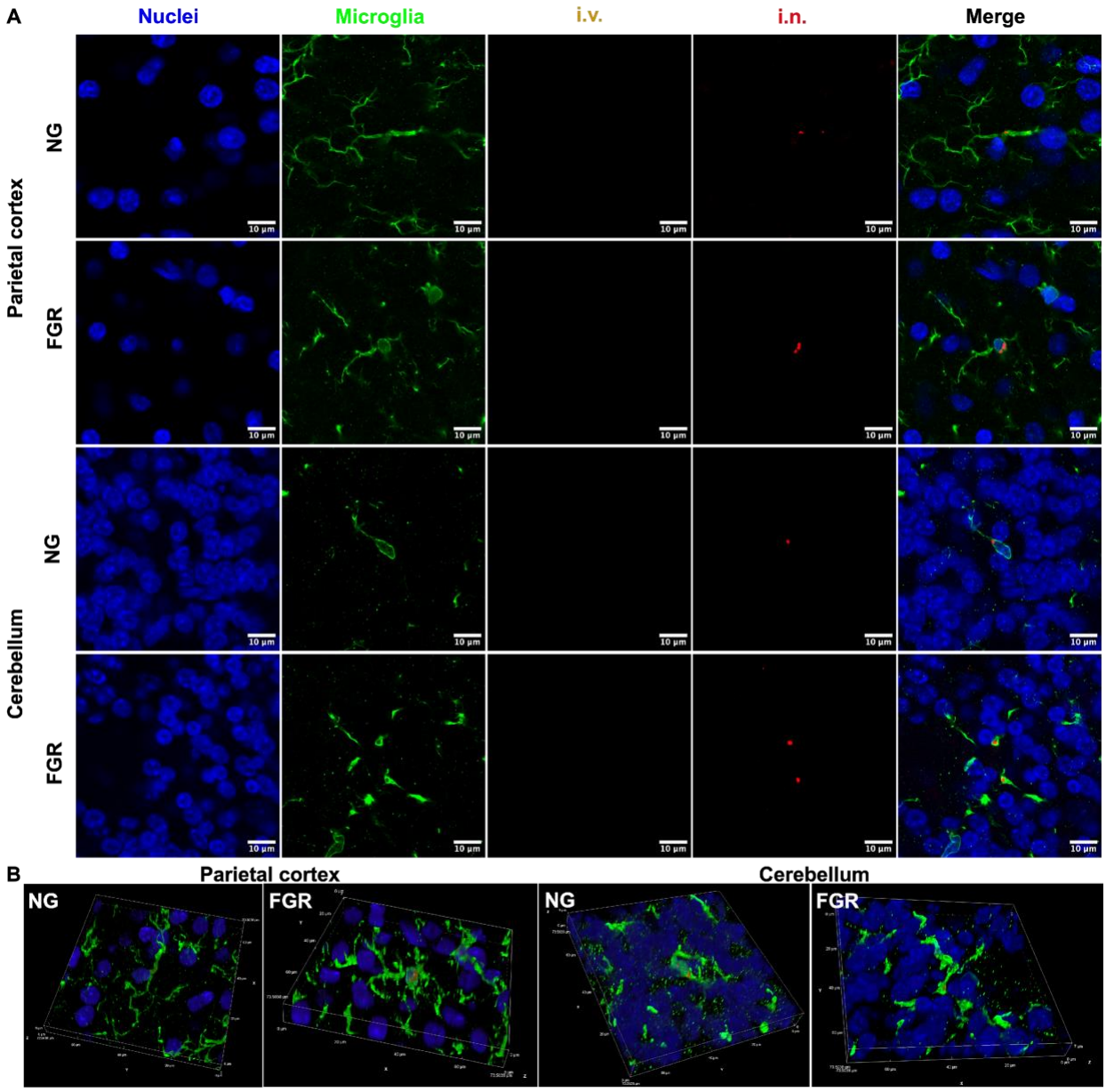

Figure 3-6. Curcumin-loaded PLGA-PEG accumulation in the parietal cortex and cerebellum at 48 h after i.v. (orange) and i.n. (red) administration. (A) Particle localization in NG and FGR piglet brains. Scale bars: 10 μm. (B) Representative z-stack images showing 3D particle co-localization in microglia. Blue: DAPI nuclei stain. Green: Iba-1+ microglia stain.

3.4. Discussion

This work optimizes incorporation of curcumin in PLGA-PEG nanoparticles to achieve high curcumin loading and high encapsulation efficiency in a stable, sub-100nm nanoparticle for cellular delivery in the

neonatal brain. In a large animal model, we show that i.n. administration outperforms i.v. administration in neonatal pigs, resulting in a significant amount of curcumin-loaded nanoparticles in microglia as early as 4 h after administration.

The standard nanoprecipitation method is commonly used for encapsulating hydrophobic drugs into polymer nanoparticles but is limited in tuning process parameters to maximize hydrophobic drug incorporation. For example, in formulating curcumin-loaded PLGA-PEG particles via standard nanoprecipitation, the particle size and the colloidal stability of the nano-formulation are difficult to effectively control by tuning parameters such as the initial polymer or drug concentration, spinning speed, and time. PLGA chain length is one of the few variables that can be leveraged since the concentration of the surfactant has minimal impact on particle size. Increasing PLGA chain length drives larger particle core size due to the longer polymeric chain and higher inherent viscosities[166]. The effects of PLGA length on curcumin loading demonstrates that both the PLGA length and associated % w/w of PLGA in the formulation play critical roles in controlling the drug loading: a longer PLGA length will form a larger hydrophobic core and can incorporate more curcumin molecules[166, 167]. However, the different PLGA ratio may alter the precipitation rate of PLGA-PEG polymer and drive curcumin diffusion from the polymer matrix, which can also affect the curcumin loading[167]. Both the PLGA length and PLGA ratio are vital factors to improve curcumin loading, particle size, and drug loading when using standard nanoprecipitation technique. Although only one end-functional group was explored in this study, alternative PLGA or PEG end-group functionalization may also help improve the stability and loading capacity of PLGA-PEG formulation[168].

The most significant issue caused by standard nanoprecipitation is low hydrophobic molecule loading. To maximize drug loading, the key parameter to control when encapsulating a hydrophobic drug such as curcumin into polymeric nanoparticles is the precipitation rate of drug and polymer. Due to the difference in solubility of cargo and polymer in a single organic solvent, the cargo and polymer will have different precipitation rates when added to aqueous solution. Hence, hydrophobic cargoes will recrystallize in the aqueous phase if they cannot be encapsulated right after they precipitate in the solution[159]. These recrystallized hydrophobic molecules decrease the drug loading and undermine the colloidal stability of the formulation. To avoid the recrystallization of the hydrophobic molecules, the initial drug concentration must be controlled at a low value. For example, based on our results in this study, the initial curcumin concentration should not exceed 2 mg/mL. The limit on the initial concentration further reduces the drug loading capacity and tunability of the nano-formulation. These observations indicate that tuning the precipitation rates of drug and polymer is a key variable to improve drug loading, long-term stability, and the tunability of the nano-formulation.

Sequential nanoprecipitation provides a solution for narrowing the gap between the different precipitation rates of drug and polymer[159]. Using sequential nanoprecipitation, we saw an increase of the curcumin loading from less than 10% to greater than 39%. This is a significant improvement compared with most polymer nanoparticles formulated via standard nanoprecipitation methods, where drug loading is usually limited to 5-10%[169, 170]. Formulated via standard nanoprecipitation, curcumin-loaded PLGA-PEG nanoparticles have a hydrophobic PLGA core and a hydrophilic PEG shell, where curcumin molecules are incorporated in the PLGA matrix that forms the core. Through sequential nanoprecipitation, curcumin nanoparticles may form a curcumin core and a PLGA-PEG shell. By adjusting the precipitation rates of curcumin and PLGA-PEG, curcumin will form a hydrophobic core that is encapsulated spontaneously and simultaneously by PLGA-PEG shell, and the encapsulation efficiency is largely increased because it is no longer confined by the loading capacity of the PLGA core. Figure 3-7 provides a schematic representation of the proposed distribution of curcumin, PLGA-PEG, and F127 for sequential compared to standard nanoprecipitation. The significant increase in drug loading is important for translational use in patients: the increased mass amount of drug to polymer greatly reduces the amount of polymer needed for formulation, which can decrease the total mass needed to deliver an equivalent amount of drug in patients and improve the safety of the formulation.

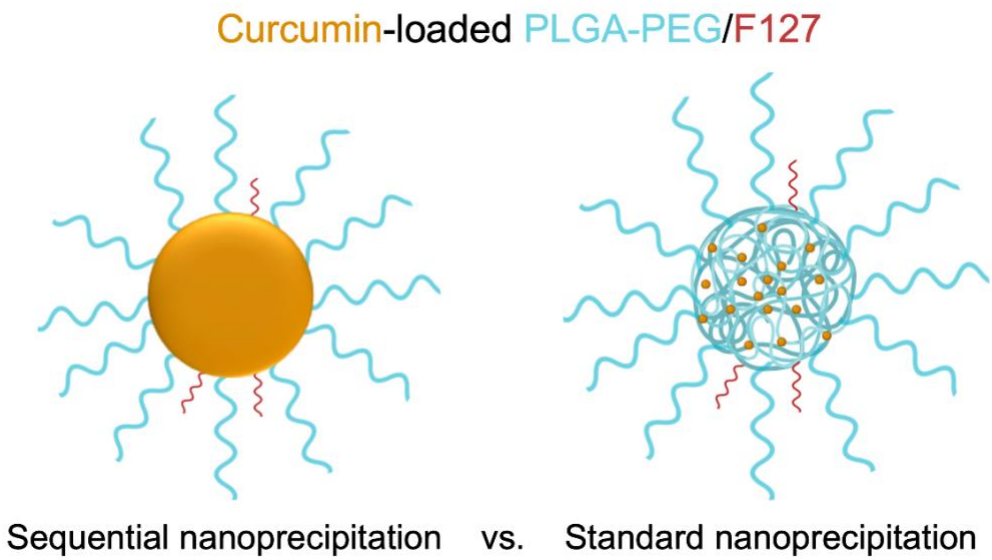

Figure 3-7. Structure and curcumin encapsulation mechanism of curcumin-loaded PLGA-PEG nanoparticles formulated via sequential nanoprecipitation (left) and standard nanoprecipitation (right).

Sequential nanoprecipitation also improves the formulation tunability and reproducibility. Particle size can be adjusted by varying the drug or polymer concentration, where the higher concentration of curcumin and/or PLGA-PEG creates a larger particle size, increasing the design space for controlling

biodistribution based on size and for loading a wider range of active agents[171]. In contrast to standard nanoprecipitation, particles made with more diluted surfactant tended to have lower PDI. One explanation for this inverted trend is the PLGA-PEG nanoparticle prepared via sequential nanoprecipitation has a stable structure. PLGA-PEG polymer is an amphiphilic polymer with a hydrophobic PLGA monomer and hydrophilic PEG monomer. Therefore, the PLGA-PEG shell can diminish interfacial tension between the hydrophobic curcumin core and the aqueous phase[172]. The addition of surfactant changes the precipitation rate of curcumin and thus leads to less uniform nanoparticles. Nonetheless, the inclusion of a surfactant is not a redundancy in this formulation because surfactants have been shown to increase particle diffusivity in brain parenchyma and may be able to increase specific cellular uptake[50, 173, 174]. The curcumin core- polymer shell structure also results in a more sustained release curcumin profile compared to formulations prepared via standard nanoprecipitation (Fig S3-3). Sustained release is the foundation for the successful application of a nano-formulation, however, other properties such as targeting, toxicity, and therapeutic efficacy are vital as well. Tunability of PLGA-PEG size can be leveraged to direct particle biodistribution, given that size is one key physical property that can impact the fate of nanoparticles, including in the brain and dependent on the administration route[51, 175].

During storage, PLGA-based particles can be subjected to several degradation pathways mediated by light, oxygen, heat and water, which can lead to lower potency or even toxicity of the formulation. It has been shown that hydrolytic degradation of PLGA-based nanoparticles in aqueous media can take place as early as 15 days depending on the PLGA molecular weight, LA:GA ratio and particle morphology etc. [108, 176, 177]. Therefore, an efficient technique to remove water content from the PLGA-based nano-formulations can enhance their shelf-life stability, as well as to facilitate handling, reduce storage space and transportation costs [108]. In this respect, lyophilization is one of the most commonly used techniques to improve the stability of nano-formulations. Our sequential nanoprecipitation formulated curcumin-loaded PLGA-PEG nanoparticles showed storage stability at room temperature for at least 30 days and at 4 ℃ for at least 6 months after lyophilization, which provides a solid foundation for the storage and transportation of PLGA-based nanoparticles.

Compared to i.v. injected PLGA-PEG made via sequential nanoprecipitation, which had no to minimal brain accumulation, 50 nm PLGA-PEG administered via the i.n. route had significantly higher brain accumulation. For i.n. administered nanoparticles, the nanoparticle needs to have less than 200 nm size in order to pass through tight junctions in the olfactory route[178-180]. Nanoparticle size also plays a vital role for transport across the nasal mucus layer. The resistance to crossing the nasal mucus layer is more significant when nanoparticles are smaller than 100 nm. Albarki *et al.* quantified the size effect on PLGA nanoparticle uptake in nasal mucosa and found that 125 nm PLGA nanoparticles had at least 2-fold

higher nasal mucosa uptake than 60 nm PLGA nanoparticles[181]. Nanoparticles administered via the i.v. route should be controlled within the size range of 10 to 100 nm, where generally, particles below 10 nm are rapidly cleared by renal filtration[182]. In systemic circulation, nanoparticles larger than 100 nm have shorter systemic half-life due to higher clearance by macrophage phagocytosis in the liver and spleen[183, 184]. For example, Ohta *et al.* demonstrated that with i.v. injection, 15 nm gold nanoparticles had the highest brain delivery efficiency compared with 3 nm and 120 nm gold nanoparticles[185]. In general, the optimal size of a brain targeting nanoparticle may need to be designed based on the intended administration route. In addition, the near neutral surface charge of the PLGA-PEG platform used in this study is favorable for brain penetration and distribution, as well as longer circulation half-life[48, 50, 129].

The greater accumulation of PLGA-PEG following i.n. administration suggests that i.n. administration can directly deliver nanoparticles to the brain rather than relying on navigating the blood-brain barrier through systemic circulation and aligns with prior i.n. nanoparticle delivery strategies[186-188]. The low particle concentration in plasma 4 h after i.n. administration in our study also supports this. The mechanism of accumulation was not explored in this study; however, there is literature evidence to suggest that the PLGA-PEG particles may enter the piglet brain directly through the extracellular pathway of the olfactory and trigeminal routes[188]. Both olfactory and trigeminal routes have intracellular and extracellular pathways[179, 189]. The intracellular pathway of the olfactory route relies on neuronal endocytosis and originates from olfactory neuron internalization and terminates in cerebral neuron exocytosis, where molecules are transported in endocytic vesicles between neurons. The trigeminal route is similar to the olfactory route but instead depends on trigeminal nerves instead of olfactory nerves. The transportation mechanism for the intracellular pathway makes it a slow process and is unlikely to be the primary nose-to-brain delivery mechanism since i.n. delivered molecules can rapidly accumulate in brain within 2 hours[190]. Molecules transported via the extracellular pathway will cross the nasal epithelia, navigate tight junctions, and pass through lamina propria to enter the brain. Transport via the extracellular pathway is mainly passive and is a faster pathway to reach the brain and widely believed to be the primary transport mechanism for many i.n. administered molecules[178, 191-193]. In our study, no neuronal uptake of particles was observed in piglet brains, which could indicate that the transport of these nanoparticles involved minimal intracellular transport. The rapid particle accumulation in the newborn pig brain indicates a more rapid transport process is taking place, which does not align with the slow axonal transport rate via the intracellular pathway[189, 194]. The extracellular transport via passive diffusion can also explain the even particle biodistribution between parietal cortex and cerebellum. Future studies assessing accumulation and transport of nanoparticles in the neonatal nasal cavity can elucidate these mechanisms.

We did observe that the biodistribution of curcumin-loaded PLGA-PEG was not affected by the disease conditions for both i.n. and i.v. administration routes. Misan *et al.* showed that FGR could change the integrity of the blood-brain barrier (BBB)[195]; our previous study on P4 FGR piglets also indicated that there existed subtle BBB impairment in the parietal cortex[13]. However, curcumin-loaded PLGA-PEG did not accumulate in the FGR brain following i.v. administration and little to no accumulation was present in both NG and FGR piglets. There are two possible reasons for this: firstly, the relationship between the timing of BBB impairment and administration in FGR brain injury is unknown, so the timing of particle administration may not overlap with maximal or substantial BBB impairment. Additionally, only slight BBB impairment was observed in this model, so it is possible that the BBB impairment in these FGR piglets was not sufficient to facilitate passive particle transport across the BBB. Compared to i.n. administration, i.v. administration may not be a favorable route to deliver PLGA-PEG nanoparticles to the piglet brain without confirmation of significant BBB permeability, or additional particle modifications to alter surface functionalization that can enhance the receptor binding or permeability of nanoparticles to further promote their brain uptake[196, 197].

Less than 10% of injected nanoparticles were found accumulated in off-site organs such as liver, spleen, and kidney 4 h after administration. No to minimal nanoparticles were detectable 48 h after administration, suggesting the accumulation peak of nanoparticles is between 4 h and 48 h. Based on our previous pharmacokinetic and biodistribution study in term-equivalent rats, PLGA-PEG nanoparticles do not cause toxicity or adverse effects for a polymer dose range of 150 mg/kg to 450 mg/kg[160]. Due to the low polymer dose administered and that we observed no toxic effects in the piglets, this study supports the feasibility of safely using PLGA-PEG in a large-scale animal model and for neonatal brain injury. In addition, the off-site accumulation of nanoparticles in liver and kidney might be beneficial, as the liver and kidney are also impaired in the hypoxic conditions common in many neonates born with brain injury, including FGR infants[198, 199]. Hence, low-dose curcumin delivered to liver and kidney could mitigate systemic and other organ-associated inflammation.

Most brain-accumulated nanoparticles were colocalized in microglia in both the parietal cortex and cerebellum. A recent analysis of nanoparticle fate in vivo by Gu *et al.* showed that almost 80% of microglia were involved in paravascular transport of PEG-polylactic acid (PLA) nanoparticles and PEG-PLA nanoparticles had an approximate 4 h brain half-life in mice[200]. The rapid brain clearance of organic nanoparticles could account for our results showing undetectable amounts of PLGA-PEG nanoparticles by 48 h after the administration. Nonetheless, for particles that accumulated in microglia in the brain, we still captured PLGA-PEG colocalized in microglia at the 48 h timepoint. Further research is needed to explore the particle accumulation in other brain regions not collected in this study. Considering our drug release

occurs over a time-course of a week, nanoparticle retention in microglia could be beneficial to sustained therapeutic delivery of curcumin to mediate ongoing inflammatory process associated with the activated microglia in the newborn brains. Therefore, our curcumin-loaded nano-formulation could further prevent or mitigate the adverse outcomes following inflammation. Future studies could explore alternative polymers to tune the brain retention time of polymeric nanoparticles[129].

3.5. Conclusions

We formulated a PLGA-PEG nano-platform via sequential nanoprecipitation that can incorporate curcumin with high drug loading, reproducibility, tunability, and storage stability. The physicochemical properties and biodistribution of these polymeric nanoparticles are tunable via adjusting the drug or polymer concentration and polymer composition. We showed PLGA-PEG with 39% (w/w) curcumin loading can accumulate in the newborn piglet brain following i.n. administration, which was a more favorable route compared to i.v. administration. PLGA-PEG nanoparticles accumulated in the parietal cortex and cerebellum of the piglet brain within 4 h after administration and by 48 h after administration, off-site accumulation was minimal. Brain accumulation of these nanoparticles was comparable for NG and FGR piglets and nanoparticle accumulation was observed in microglia. These results support the use of PLGA-PEG in a human-like model of newborn brain injury. There is additional benefit in that the optimized PLGA-PEG platform has high drug loading that can reduce total mass dose, sustained release of curcumin that can lead to less frequent dosing, and microglial accumulation that can mitigate ongoing inflammation.

Chapter 4: Developmental age specific neuroprotective nano-therapies for perinatal brain injury

4.1. Introduction

Developmental changes in utero and from birth to two years old are rapid. Maturation of organ function and alterations in enzymatic composition critical to drug distribution and metabolism can impact PK parameters such as the drug circulation half-life, drug breakdown, and clearance[201]. For example, neonatal calves between 1 and 42 days of age see a decrease in the elimination half-life of i.v. injected sulfadiazine from 5.7 to 3.6 hours, and total body clearance increased from 1.43 to 1.88 ml/min/kg[202]. The change in PK parameters can affect the therapeutic efficacy and therapeutic window of drugs at different developmental stages[202, 203]. Therefore, in determining the therapeutic dosage of drug to maximize safety and minimize toxicity in newborns and children and different developmental stages, especially for drugs with narrow therapeutic windows, it is necessary to tailor the dose based on physiological parameters at each developmental age rather than adjusting the dose only by age or body weight[203, 204].

Assessing the effect of developmental age on therapeutic outcome is particularly important for supporting the success of therapeutic translation into the clinic for newborns with brain injury. Term HIE can impact babies born anywhere from 36 weeks to 42 weeks. All babies born in this time frame are considered term, and therefore would receive the same treatment intervention. However, the effects of developmental age on treatment outcomes using the same treatment have not been studied and are unknown. Importantly, there is clinical evidence that supports the standard of care for babies with HIE is not effective for a preterm infant although it has been approve for term HIE treatment: preterm infants with HIE did not benefit from TH treatment[205]. Due to this knowledge gap and the clinical evidence, we sought to characterize the therapeutic efficacy of drugs in neonatal rats with HI brain injury onset from late preterm to late term to determine if the same treatment is equally effective at different developmental stages.

Using the Vannucci rat model of HI brain injury, we evaluated the therapeutic efficacy of curcumin-loaded PLGA-PEG nanoparticles (developed in Chapter 3) in rats with HI brain injury at postnatal day (P) 7, P10, and P13. Compared with humans, a P7 rat is late preterm-equivalent to a 34-36 gestational week human, a P10 rat is term-equivalent to a human, and a P13 rat is late-term equivalent to a 42-44 postnatal week human (Fig 4-1). Prior work from our lab in the Vannucci rat model showed a therapeutic benefit of curcumin-loaded PLGA-PEG nanoparticles for HI in P7 rats, and catalase-loaded PLGA-PEG nanoparticles for mild HI injury in P10 rats[31, 124]. In this study, we control the injury severity of P7, P10, and P13 rats to normalize the severity of injury in the HI rat at each developmental stage and dose with a single systemic treatment of our optimized PLGA-PEG curcumin formulation.

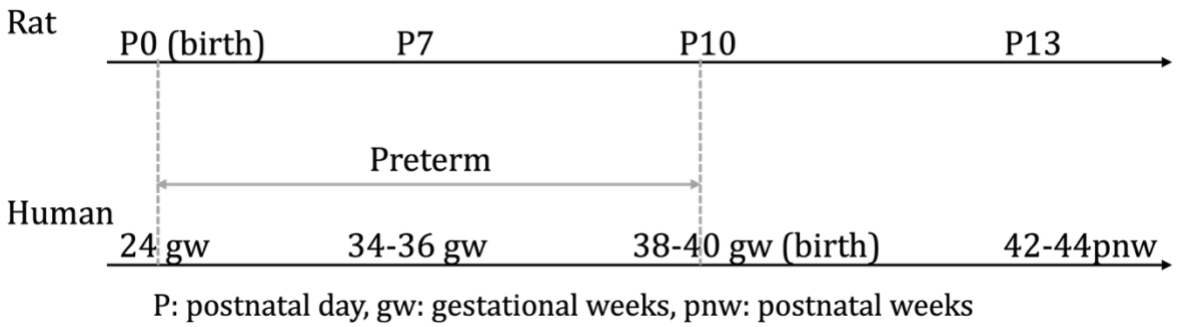

Figure 4-1. Rat age versus human age. P: postnatal day, gw: gestational weeks, pnw: postnatal weeks.

In this chapter, curcumin is chosen as the model drug to explore the developmental age specific neuroprotective effects on perinatal brain injury due to 1) natural fluorescence of curcumin[206], which is favorable for the efficacy evaluation and quantification study; 2) we successfully developed a curcumin-loaded PLGA-PEG formulation with reproducibility, tunability, extended shelf-life stability, high curcumin loading, and sustained curcumin release, which targeted microglia in the piglet brain following i.n. administration (Chapter 3); and 3) some curcumin containing nano-formulations, such as Lipocurc, Imx-110, SinaCurcumin, TheraCurmin, Mervia, Norflo Oro, and CurcuPhyt, etc., have reached clinical trials[207], providing support for the translational potential of curcumin-containing formulations. In this study, we quantify the brain area loss at 3 days and 7 days after the treatment of curcumin-loaded nanoparticles. With these results, the potential optimal therapeutic dosage and dosing schedule for neonatal brain injury at different developmental stages can be identified, which can accelerate the translation of our polymeric nano-platform. Our results also provide reference for the pediatric application of other neuroprotective nano-therapies, which can potentially reduce the number of animals needed in future preclinical studies exploring nanotherapeutic options.

4.2. Materials and methods

4.2.1. Nanoparticle formulation and characterization

Nanoparticles were prepared using the sequential nanoprecipitation method, as described previously[208]. Briefly, PLGA-PEG (45k:5k, LA:GA = 50:50, Akina, Inc., West Lafayette, IN, USA) and curcumin (Sigma-Aldrich) were dissolved in mixed organic solvent (DMSO:DMF:EtOH = 3:3:4) at 20 mg/mL and 13.3 mg/mL concentration. 0.1% (w/w) F127 (pH = 6) solution were added into the organic phase at an organic:aqueous = 1:10 ratio. Organic and aqueous phase were gently mixed by pipetting until the solution was transparent. The particles were washed with 0.1% F127 solution for 3 times. Fresh nanoparticles were stored at 4 ℃ for short-term use. For long-term storage, 5% (w/w) sucrose was added to the washed

nanoparticles, and then the nanoparticles were lyophilized for 24h. The lyophilized nanoparticles were stored at -20 ℃ for future use.

The particle size and polydispersity index (PDI) of nanoparticles were measured by dynamic light scattering (DLS), and the zeta potential (ζ-potential) was determined using a zeta potential analyzer (NanoSizer Zeta Series, Malvern Instruments, Malvern, UK). Samples were diluted to appropriate concentrations to obtain accurate measurements in 10 mM sodium chloride (NaCl, Sigma-Aldrich), pH 7.4.

To quantify the drug loading of curcumin-loaded nanoparticles, the lyophilized nanoparticles were measured by ultraviolet–visible light (UV–Vis) spectrometry as compared to a standard calibration curve of curcumin in DMSO. Each sample's absorbance at 430 nm was measured and adjusted by subtracting a blank of unloaded polymer nanoparticles' absorbance in DMSO. The weight of a polymer and drug was the weight of lyophilized nanoparticles. Drug loading is defined as follow:

$$\%Drug\ loading = \frac{Weight\ of\ drug\ encapsulated\ in\ nanoparticles}{Weight\ of\ polymer\ and\ drug\ in\ nanoparticles} \times 100 \quad (4\text{-}1)$$

$$\%Drug\ encapsulation\ efficiency = \frac{Weight\ of\ drug\ encapsulated\ in\ nanoparticles}{Weight\ of\ intial\ drug} \times 100 \quad (4\text{-}2)$$

4.2.2. Animal Care and Ethics Statement

This study was performed in accordance with the guide for the care and use of laboratory animals of the National Institutes of Health (NIH). All animals were handled according to approved Institutional Animal Care and Use Committee (IACUC) protocols of the University of Washington, Seattle, WA. Time-mated pregnant female Sprague–Dawley rats (virus antibody-free CD® (SD) IGS, Charles River Laboratories, Raleigh, NC, USA) were purchased and arrived on postnatal day 5 (P5) with a litter of 12 sex-balanced pups. Dams were housed individually with their litter and allowed to acclimate to their environment. Before and after the experiment, each dam and her pups were housed under standard conditions with an automatic 12 h light/dark cycle, a temperature range of 20 - 26 °C, and access to standard chow and autoclaved tap water *ad libitum*. The pups were checked for health daily.

4.2.3. Vannucci model of unilateral HI injury in neonatal rats

On indicated age (P7, P10, or P13), pups were separated from their dams, weighed and sexed, and randomized to experimental groups. Anesthesia with isoflurane (3-5%) was given in 100% O_2 via a nose cone, under a dissecting microscope. The left carotid artery was identified and ligated. Pups were maintained in a temperature-controlled water bath before and after undergoing unilateral ligation of the left carotid artery. After all the animals are recovered from anesthesia, they were returned to the dams for a

minimum of 30 min before placement in a hypoxic chamber in a temperature-controlled water bath. Once rectal temperature in a sentinel animal was stable at 36°C for 5 min, the chamber was sealed and 8% O_2 (92% N_2) administered at a rate of 2.5 L/min. Once the oxygen concentration within the chamber reaches 8%, for P7, P10, and P13 rats, hypoxia was maintained for 150 min, 120 min, and 90 min, respectively. The end of hypoxia marked the end of the insult (i.e. 0 h timepoint).

4.2.4. Nanoparticle administration

At 30 min after injury, treatments were i.p. administered. For 72h therapeutic efficacy evaluation: three ages, P7, P10, P13, were used for treatment evaluations. For each age, there were 2 separate treatment groups: saline, and curcumin-loaded PLGA-PEG nanoparticles. At least 20 animals (10 males, 10 females) were used for each treatment group, each age. For 7-day endpoint neuroprotection evaluation, P7 animals were used. There were 4 separate treatment groups: saline, free curcumin, blank PLGA-PEG nanoparticles, and curcumin-loaded PLGA-PEG nanoparticles. At least 20 animals (10 males, 10 females) were used for each treatment group, each age. Curcumin-loaded nanoparticles were dosed at 25 mg curcumin/kg rat.

4.2.5. Gross brain injury

At indicated endpoint (72 h, or 7 days after injury), animals were injected with an overdose of pentobarbital before transcardiac perfusion with 0.9% saline. Immediately following brain extraction, a photo of each whole brain was taken for gross injury scoring. Gross injury scoring was conducted by two independent individuals who are blinded to group allocation. Gross brain injury in the hemisphere ipsilateral to ligation was assessed on a five-point ordinal scale (0 to 4) as follows: 0 = no injury, 1 = mild injury with < 25% lesion of ipsilateral hemisphere, 2 = 25–50% lesion, 3 = 51–75%, and 4 = ≥75% injury, as previously described[209].

4.2.6. Area loss assessment

For 72h neuroprotection efficacy evaluation, immediately after brain extraction, brains were cut into 1-mm sections, and stained with 2,3,5-triphenyltetrazolium chloride (TTC). Four 1-mm sections from the slices best representing the cortex, hippocampus, basal ganglia, and thalamus were selected. The area loss was the average percentage area loss from the four sections.

For 7-day neuroprotection efficacy evaluation, whole brains were post-fixed in 10% neutral-buffered formalin for at least 48 h. Following the fixation, blocks of brain were obtained. Using external landmarks, brains were cut at approximately the level of the striatum (block 1) and at the level of the hippocampus and thalamus (block 2). The tissue samples were paraffin embedded, cut into 5-µm sections, and stained with hematoxylin and eosin (H&E). Slides were scanned in bright field with a 20× objective using a Nanozoomer Digital Pathology slide scanner (Hamamatsu, Bridgewater, NJ, USA). Area loss

scoring was conducted by two independent individuals who were blinded to group allocation. Area loss analysis was performed as previously described [210]. Briefly, two 5-μm sections from the slices best representing the cortex, hippocampus, basal ganglia, and thalamus were selected. Virtual slides were exported as 600 dpi images. The optical density and hemispheric area of each section were analyzed in the ImageJ software (National Institutes of Health, Bethesda, MD, USA) by another blinded individual. The area loss was the average percentage area loss from the two sections (one at the level of the frontal cortex and the other at the midhippocampal level).

Area loss of each section was quantified by measuring the area of healthy tissue in the ipsilateral hemisphere normalized to the contralateral hemisphere, according to the following equation:

$$\%\ Area\ Loss = \frac{1-ipsilateral\ area}{contralateral\ area} \times 100 \quad (4\text{-}3)$$

4.2.7. Gene expression fold-change quantification

Changes in inflammation, cell death, oxidative stress, and hypoxia and vascular damage gene expression profiles following nanoparticle treatment were quantified using RT-qPCR. At the indicated endpoint (72 h, or 7 days after injury), ipsilateral and contralateral hemispheres were collected and homogenized. The RNA from homogenized brains was extracted with TRIzol reagent, pelleted at 15,000× g, washed several times with ultrapure DEPC water (Fisher Scientific) and 70% ethanol, and the RNA final concentration was measured using a NanoDrop. RNA was transcribed into cDNA using Applied Biosystems™ High-Capacity RNA-to-cDNA™ kit (Fisher Scientific). cDNA was diluted to 20 ng/μL with ultrapure RNA-free water. RT-qPCR was performed using the transcribed cDNA and iTaq Universal SYBR Green Supermix (Bio-Rad, Hercules, CA, USA) that binds to double-stranded DNA to quantitatively track the progress of DNA amplification in real-time. Gene expression change was quantified for inflammation (interleukin-1beta (IL-1β), IL-4, IL-6, IL-10, interferon gamma (INFG), tumor necrosis factor alpha (TNF-α), and nuclear factor kappa B (NF-κB)), cell death (inducible nitric oxide synthase (iNOS) and caspase-3 (Casp-3)), oxidative stress (PTGES2, GPx4, SLC7A11, and GCLM), and hypoxia and vascular damage (HIF1α and aquaporin-4 (AQP4)) (Table 4-1)[211, 212]. Glyceraldehyde-3-phosphate dehydrogenase (GAPDH) was used as housekeeping gene. The qPCR was run at 95 ℃ for 30 s, 95 ℃ for 5 s, and then 60 ℃ for 30 s for 40 cycles. The gene expression changes in treatment groups were normalized to healthy controls to quantify gene expression fold-changes.

Table 4-1. mRNA primer design for qPCR.

Gene	Forward Primer	Reverse Primer

GAPDH	ACTCCCATTCTTCCACCTTTG	CCCTGTTGCTGTAGCCATATT
IL-1b	CTATGGCAACTGTCCCTGAA	GGCTTGGAAGCAATCCTTAATC
IL-6	GAAGTTAGAGTCACAGAAGGAGTG	GTTTGCCGAGTAGACCTCATAG
TNF-a	CCCAATCTGTGTCCTTCTAACT	CAGCGTCTCGTGTGTTTCT
NF-kB	GGTTACGGGAGATGTGAAGATG	GTGGATGATGGCTAAGTGTAGG
IL-4	GTCACTGACTGTAGAGAGCTATTG	CTGTCGTTACATCCGTGGATAC
IL-10	AGTGGAGCAGGTGAAGAATG	GAGTGTCACGTAGGCTTCTATG
INFG	CGAATCGCACCTGATCACTAA	TGGATCTGTGGGTTGTTCAC
Casp3	CCACGGAATTTGAGTCCTTCT	CCACTCCCAGTCATTCCTTTAG
iNOS	TGGAGCGAGTTGTGGATTG	CCTCTTGTCTTTGACCCAGTAG
PTGES2	CCTCCTTATTTCCTGCCTCTTC	ACATAGGAGGGTCTCGACTG
GPx4	GGCCTGGAAGTGGAGTTAATAG	CACTTCGTTCCTCTAACCACTG
SLC7A11	GTGACCATCCACCTCTGTATTT	AATATCAACCAACCAGACCCTC
GCLM	GAACAAGCAGAAGACCAGTAAGA	TTTACTGTGTTGCCCTGGAG
HIF1a	CGGTATCTTTGCTCTCTCCTTT	CTAAACCAGAGCCAGAGAGTTC
AQP4	CTTGTCTGGGCTCTGGATATG	CTAATCTCATCCCTGTTGGGTC

4.2.8. Statistical analysis

Injury data and gene expression fold-change will be summarized as a median (95% CI). Gross injury scores, area loss, and gene expression fold-change were statistically analyzed using the Mann Whitney test. All statistical analyses were carried out using GraphPad Prism (GraphPad Software Inc., Version 10.4.2). A p-value of <0.05 was considered statistically significant.

4.3. Results

4.3.1. Curcumin-loaded PLGA-PEG nanoparticles

Curcumin-loaded PLGA-PEG nanoparticles (NanoCurc) and blank PLGA-PEG nanoparticles used for administration had comparable hydrodynamic size, PDI, and zeta potential (Table 4-2). Curcumin-loaded PLGA-PEG nanoparticles (NanoCurc) had 39.2% curcumin loading, 98.1% curcumin encapsulation efficiency, and sustained curcumin release profile (Chapter 3.3.2), which made it possible to have long-term neuroprotective effects with a single dose of administration.

Table 4-2. Physicochemical properties of optimized curcumin-loaded PLGA-PEG nanoparticles (NanoCurc) and blank PLGA-PEG nanoparticles (PLGA-PEG). All values are reported as mean ± standard error of the mean (SEM) (n = 3).

Formulation	Size ± SEM (nm)	PDI ± SEM	Zeta potential ± SEM (mV)	Drug loading ± SEM (%)	Drug encapsulation efficiency ± SEM (%)
NanoCurc	54.5 ± 3.4	0.18 ± 0.01	-4.6 ± 0.5	39.2 ± 1.1	98.1 ± 2.7
PLGA-PEG	57.3 ± 0.9	0.14 ± 0.01	-3.8 ± 0.7	N/A	N/A

4.3.2. Short-term neuroprotection efficacy in different developmental ages

To evaluate the relationship between neuroprotection effects of NanoCurc and developmental age at onset of injury, Nanocurc was administered following HI at P7, P10, and P13. At the indicated endpoint (72h), gross injury score and percent area loss of all the brains were assessed. TTC was used as a marker for percent area loss after HI brain injury because it is rapid, cost-efficient, and provides clear visualization of injury [206]. The penumbra of the tissue has the potential to recover from the injury, so the percent area loss was quantified via two methods: excluding the penumbra and including the penumbra (Fig 4-2A). In late preterm-equivalent (P7) rats with HI, gross injury score of the NanoCurc treatment group was lower than the saline group (Fig 4-2B). Percent brain area loss of the NanoCurc treatment group excluding or including penumbra was significantly lower than the saline group (Fig 4-2C-D). In term-equivalent (P10) rats with HI, gross injury score and percent brain area of the NanoCurc treatment group showed no difference compared to saline group (Fig 4-2F-H). In late-term equivalent (P13) rats with HI, similar to P10, both the gross injury score and the percent brain area of the NanoCurc treatment group showed no difference compared to the saline group (Fig 4-2J-L). Due to more than a half of P13 animals losing 20% or more of their bodyweight 48h after the injury, all the P13 animals were humanely euthanized at 48h. In all three developmental ages, the penumbra areas of the NanoCurc treatment group and saline group were comparable (Fig 4-2E, I, and M). To compare the percent neuroprotection in all three developmental ages, the medians of the controls (saline groups) were taken to normalize the percent area loss (Fig 4-2N): a single dose of NanoCurc had neuroprotective effects on preterm-equivalent HI brains, but no therapeutic effects were found on term-equivalent or late-term equivalent HI brains.

Many brain injuries and diseases have sex differences in outcomes and responses[213-215]. Therefore, biological sex should be taken into consideration when analyzing the neuroprotection effects on HI rat brains. In all the treatment groups, at least 10 animals of each sex were used. In three different developmental ages, P7, P10, and P13, we found no sex-dependent differences in outcomes (Fig 4-2O-Q).

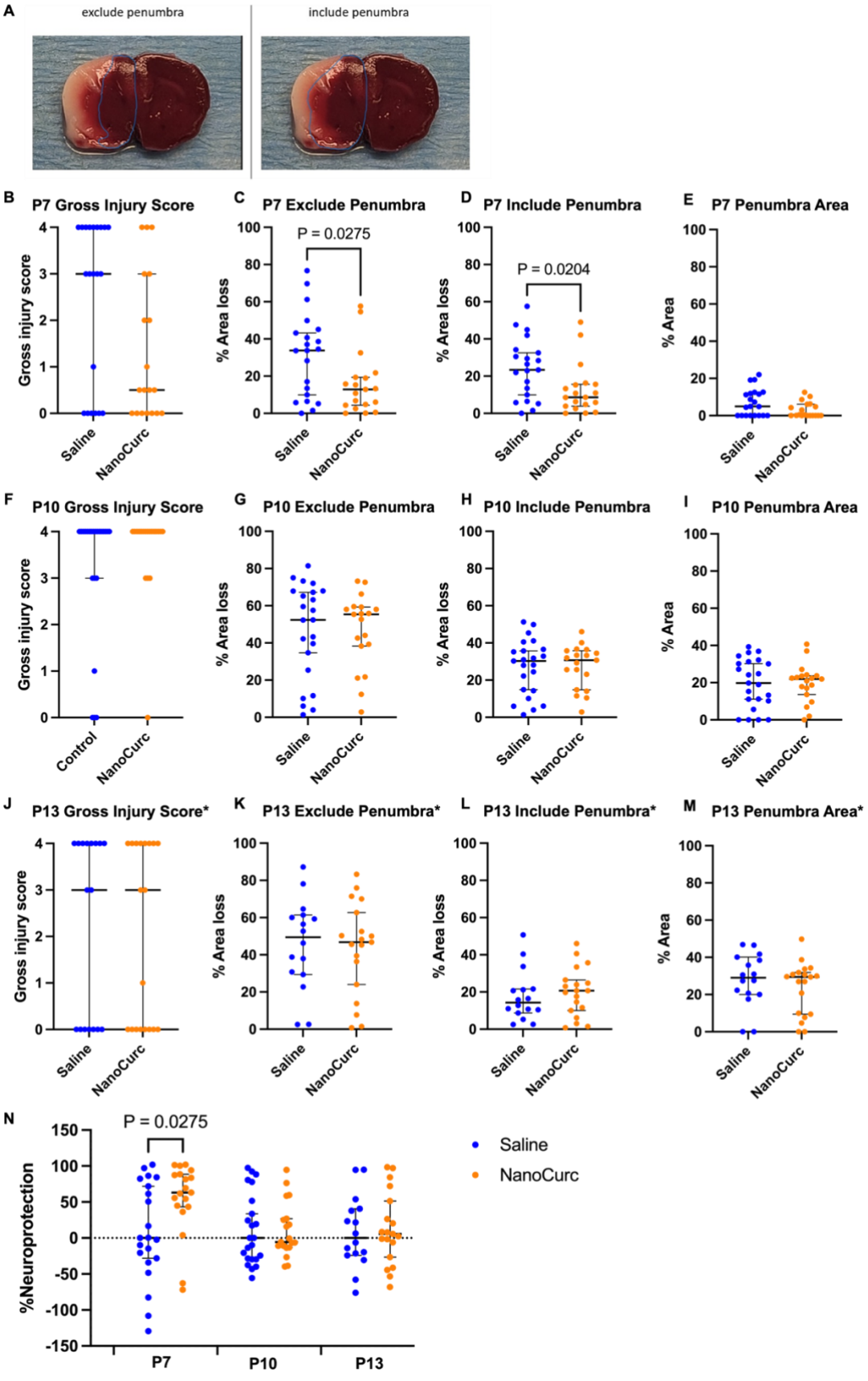
A
exclude penumbra
include penumbra
B
P7 Gross Injury Score
Gross injury score
Saline
NanoCurc
C
P7 Exclude Penumbra
P = 0.0275
% Area loss
D
P7 Include Penumbra
P = 0.0204
% Area loss
E
P7 Penumbra Area
% Area
F
P10 Gross Injury Score
Gross injury score
Control
NanoCurc
G
P10 Exclude Penumbra
% Area loss
H
P10 Include Penumbra
% Area loss
I
P10 Penumbra Area
% Area
J
P13 Gross Injury Score*
Gross injury score
K
P13 Exclude Penumbra*
% Area loss
L
P13 Include Penumbra*
% Area loss
M
P13 Penumbra Area*
% Area
N
P = 0.0275
%Neuroprotection
P7
P10
P13
Saline
NanoCurc

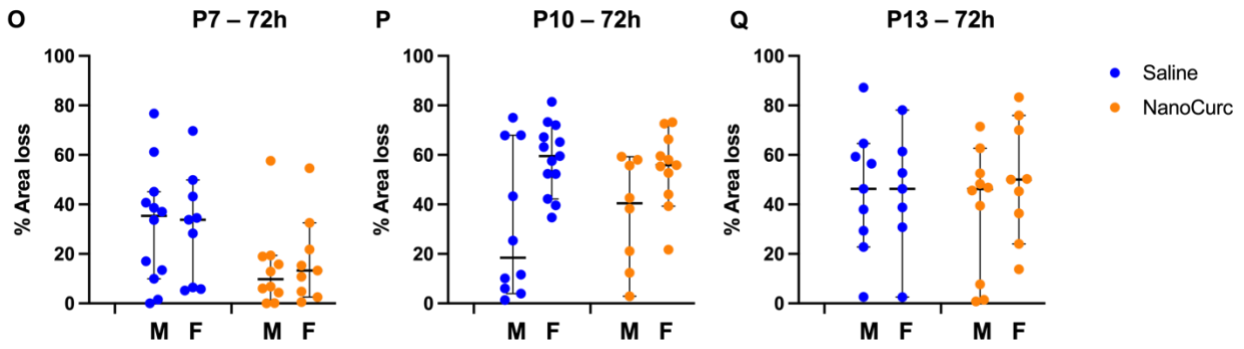

Figure 4-2. Neuroprotective efficacy at 72h endpoint after administering a single dose of NanoCurc. (A) Representative TTC image shows two different area loss quantification methods: exclude penumbra (left) and include penumbra (right). (B) Gross injury score of P7 rats. (C) Brain area loss percent of P7 rats exclude penumbra. (D) Brain area loss percent of P7 rats include penumbra. (E) Penumbra area percent of P7 rats. (F) Gross injury score of P10 rats. (G) Brain area loss percent of P10 rats exclude penumbra. (H) Brain area loss percent of P10 rats include penumbra. (I) Penumbra area percent of P10 rats. (J) Gross injury score of P13 rats. (K) Brain area loss percent of P13 rats exclude penumbra. (L) Brain area loss percent of P13 rats include penumbra. (M) Penumbra area percent of P13 rats. (N) Percent neuroprotection of NanoCurc in P7, P10, and P13 rats after normalization to saline treatment group. (O) Neuroprotective efficacy in P7 rats with different sexes. (P) Neuroprotective efficacy in P10 rats with different sexes. (Q) Neuroprotective efficacy in P13 rats with different sexes. *P13 animals were humanely euthanized at 48h due to they lost 20% or more bodyweight. M: male rats, F: female rats. Graphs display median ± 95% confidence interval. Group differences were evaluated using Mann Whitney test.

4.3.3. Neuroprotection efficacy at 1 week after injury in preterm-equivalent HI brains

Although NanoCurc had neuroprotective effects on preterm-equivalent HI brains after a single dose of administration in an acute period, its neuroprotection efficacy beyond the acute phase remained unclear. To explore the neuroprotection effects of NanoCurc in rats with HI, injury severity was assessed 1 week after HI. According to the gross injury score, no neuroprotection efficacy was observed after the administration of a single dose of NanoCurc (Fig 4-3A) at 1 week after HI. Both of the percent area loss and the percent neuroprotection suggested that a single dose of NanoCurc did not have sustained neuroprotection beyond the acute period after HI (Fig 4-3B-C). Focusing on preterm-equivalent rats with HI, we saw no sex-dependent differences in outcome at 1 week after HI (Fig 4-3D).

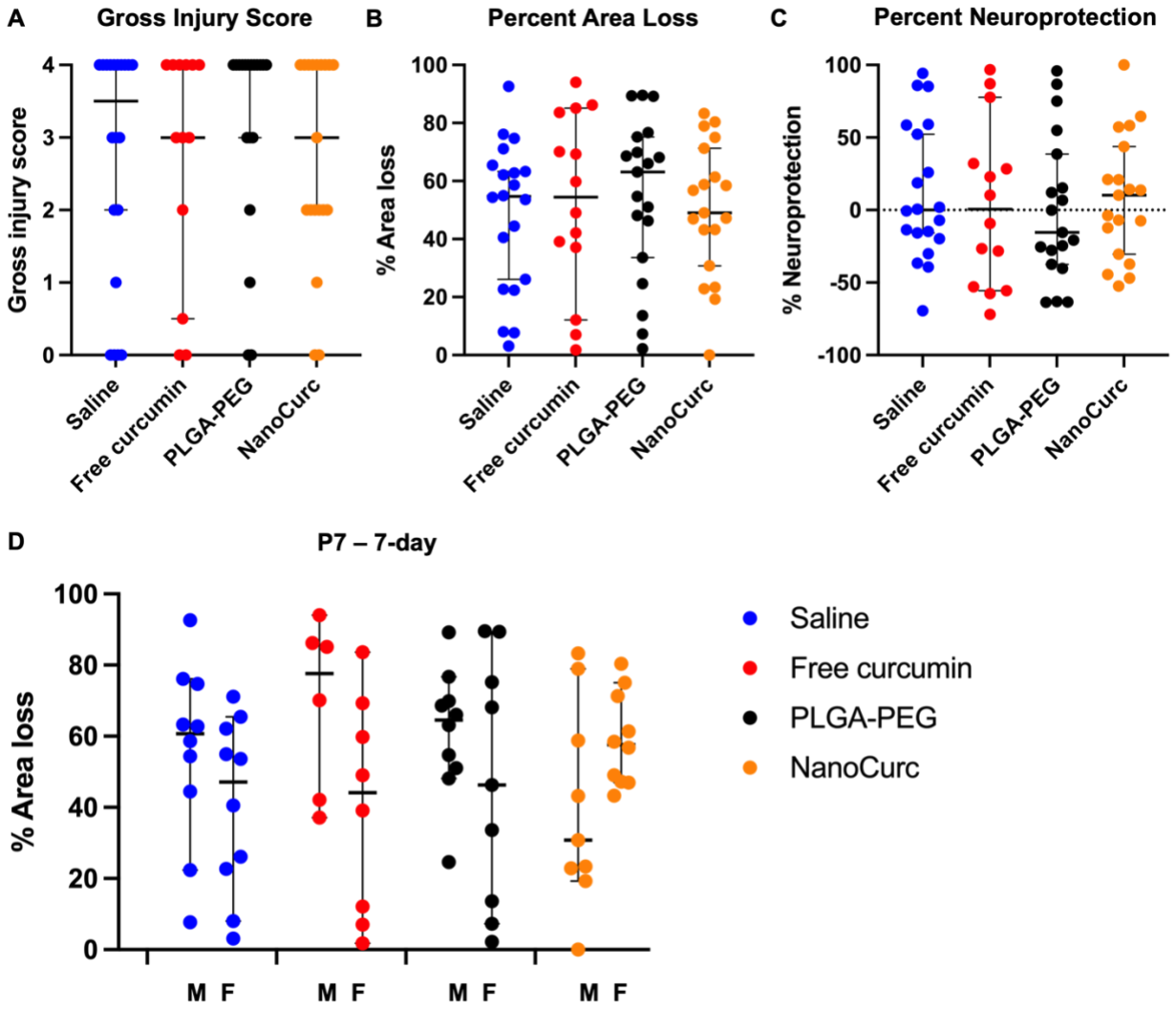

Figure 4-3. Neuroprotective efficacy in P7 rats with Hi at 7-day endpoint after administering a single dose of NanoCurc. (A) Gross injury score. (B) Brain area loss percent. (C) Percent neuroprotection of different treatment groups (Free curcumin, PLGA-PEG, and NanoCurc) after normalization to saline treatment group. (D) Neuroprotective efficacy in P7 rats with different biological sexes. Graphs display median ± 95% confidence interval. Group differences were evaluated using Mann Whitney test.

4.3.4. Analysis of gene expression in response to NanoCurc treatment

HIE is usually associated with inflammation, cell death, oxidative stress, and hypoxia and vascular damage[216, 217]. Therefore, to further reveal the therapeutic effects of a single dose of NanoCurc, gene expression fold-change among all these three developmental ages was quantified for inflammation, cell death, oxidative stress, and hypoxia and vascular damage. In P7 rats with HI, IL-6 in the ipsilateral hemisphere was upregulated significantly with the treatment of NanoCurc. Other cytokines such as IL-1β

and IL-4 also had a trend of upregulation after NanoCurc administration (Fig 4-4A). In P10 rats with HI, no significance in cytokine gene expression fold-change was found with the treatment of NanoCurc (Fig 4-4B). There was no significant difference in cytokine gene expression fold-change after the administration of NanoCurc in P13 rats with HI as well, but the cell death genes were upregulated in P13 ipsilateral hemispheres compared to the contralateral hemisphere (Fig 4-4C).

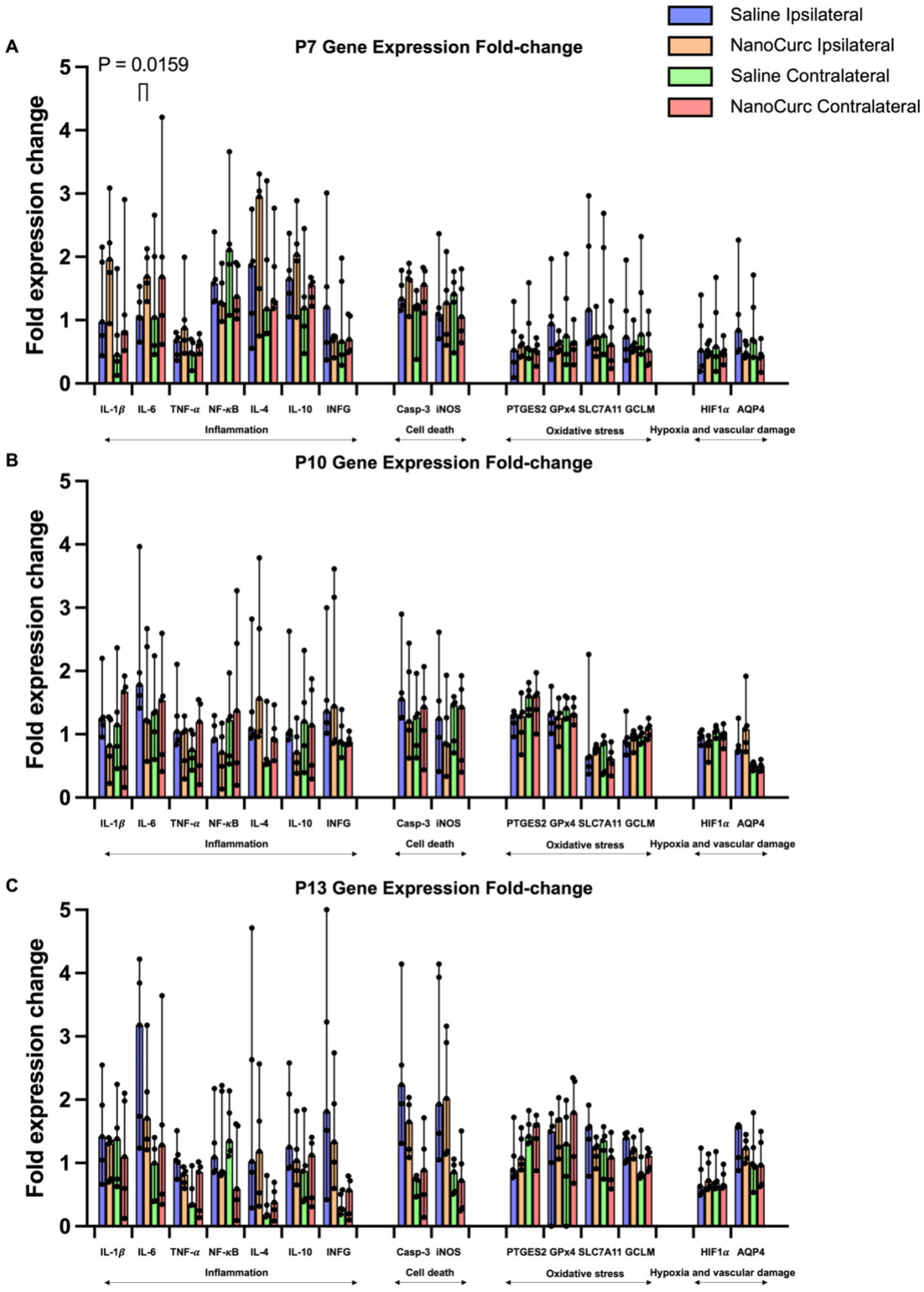
Saline Ipsilateral
NanoCurc Ipsilateral
Saline Contralateral
NanoCurc Contralateral
A
P7 Gene Expression Fold-change
P = 0.0159
Fold expression change
IL-1β IL-6 TNF-α NF-κB IL-4 IL-10 INFG Casp-3 iNOS PTGES2 GPx4 SLC7A11 GCLM HIF1α AQP4
Inflammation
Cell death
Oxidative stress
Hypoxia and vascular damage
B
P10 Gene Expression Fold-change
Fold expression change
IL-1β IL-6 TNF-α NF-κB IL-4 IL-10 INFG Casp-3 iNOS PTGES2 GPx4 SLC7A11 GCLM HIF1α AQP4
Inflammation
Cell death
Oxidative stress
Hypoxia and vascular damage
C
P13 Gene Expression Fold-change
Fold expression change
IL-1β IL-6 TNF-α NF-κB IL-4 IL-10 INFG Casp-3 iNOS PTGES2 GPx4 SLC7A11 GCLM HIF1α AQP4
Inflammation
Cell death
Oxidative stress
Hypoxia and vascular damage

Figure 4-4. Gene expression fold-change of different developmental ages at a 72h endpoint. (A) Gene expression fold-change in P7 rats. (B) Gene expression fold-change in P10 rats. (C) Gene expression fold-change in P13 rats. Graphs display median ± 95% confidence interval. Group differences were evaluated using Mann Whitney test.

4.4. Discussion

In this chapter, we assessed the effects of developmental age at injury onset on the neuroprotective capacity of NanoCurc using a single, systemic treatment immediately after HI. With a single dose of NanoCurc, we observed neuroprotective effects in the acute period for the late preterm rats with HI, but this effect was not sustained, and genetic expression levels were not altered. We saw no neuroprotective effect in term equivalent and late-term equivalent rats with HI.

Barriers to deliver nanoparticles to the brain may be impacted differently in response to injury at different developmental stages. The integrity of the blood-brain barrier (BBB) is affected by HI injury and subsequent inflammation, which will lead to increased BBB permeability[218]. However, to the best of our knowledge, no direct comparison of BBB permeability and dysfunction has been performed for rats across the late preterm to late term age range. Fernández-López et al. compared the BBB permeability of P7 rats and adult rats after acute focal stroke: the BBB is more integrated in acutely injured neonatal brain than adult brain, which demonstrates that P7 rats may be more resistant to permeability changes following ischemic injury compared to adults[219]. This difference could be attributed to the different expression of brain endothelial tight junction proteins such as occludin and claudin-5 during the developing ages - from P7, P14, P17 to adulthood, the expression of claudin-5 and PDGFRβ are gradually increasing while the occludin expression is decreasing[219]. Therefore, the BBB permeability after the insult at different developmental ages could be different. We have shown that nanoparticle uptake can be correlated to degree of BBB permeability[220]. Therefore, if BBB permeability is more significant following HI insults in late preterm-equivalent rats, then a greater proportion of curcumin-loaded nanoparticles may have accessed the brain parenchyma compared to term-equivalent and late-term equivalent brains. In short, NanoCurc only had neuroprotective effects on late preterm-equivalent rats.

Microglia are resident immune cells present of the central nervous system (CNS) starting in the prenatal period[221]. Microglia have a specific role in the early postnatal period. In rodents, microglia number increases rapidly since birth, reaching the peak between P7 and P14, especially in parietal cortex and hippocampus. Microglia number decreases via apoptosis and stabilize to adult levels after P15[222, 223]. In the neonatal brains, microglia produce more pro-inflammatory cytokines than other ages[224].

Thus, they are especially sensitive to external signals such as hypoxia and the microglia activation usually has long-term neurological effects[225]. Due to the anti-inflammatory property of curcumin and microglia uptake of curcumin-loaded nanoparticles based on our previous studies, future analysis should characterize the number and morphology changes of microglia after the NanoCurc treatment in rats with HI at different developmental ages.

Preterm brains are more susceptible to oxidative stress than term brains because of the imbalance between the oxidant and antioxidant systems[226]. However, P7 rats have the highest capacity to respond to oxidative stress by dramatically elevating their glutathione and free thiol levels compared to P10 and P13 rats[227]. At P14, reactive oxygen and nitrogen species (ROS and RNS) production reaches the peak. The capacity to respond to oxidative stress is more limited at this age, even if the antioxidative enzymes are continuing developing[228]. As an antioxidant, NanoCurc could reduce the oxidative stress to some extent. However, its effectiveness may be related to the oxidative capacity of the brain at the specific developmental stage. This may account for the different neuroprotective effects of NanoCurc on rats with HI at different developmental ages.

It is notable that the sustained release of curcumin from nanoparticles did not lead to prolonged neuroprotection following a single systemic injection. There are several potential explanations. First, nanoparticles might be cleared out after initial accumulation in the brain. As our previous PK study showed (Chapter 2), PLGA-PEG nanoparticles formulated using 1% F127 have a 5.9 h systemic half-life following i.p. administration, so most of the nanoparticles not accumulated in the brain by 6 h would be cleared in 24 h. However, this explanation has two limitations: these curcumin nanoparticles were made with 0.1% F127, and the previous particle circulation half-life was characterized in healthy term-equivalent rats. Also, organic nanoparticles do not have long brain retention even if they transport into the brain parenchyma. Both our previous brain uptake study in term pigs and the PEG-PLA half-life in mouse brain quantified by Gu et al.[200] suggest that most of nanoparticles are cleared by microglia within 24-48 hours. Additionally, the brain uptake amount of i.p. administrated nanoparticles might have an upper limit, although more detailed PK data are needed to support this. Based on our previous PK data and the lack of therapeutic effect with a single dose in this study, future studies will explore dosing every 24-48 hours after HI to determine if curcumin nanoparticles provide neuroprotective at longer time points at these developmental stages. Meanwhile, more detailed PK data including brain-based curcumin PK and brain-based nanoparticle PK in HI rats at the different developmental stages need to be quantified to provide clearer guidance for the dose schedule determination.

In clinical pediatric drug use, term infants receive the same therapies, and the difference in PK between 37 weeks to the first month of life is often overlooked. However, there can be significant impact

of specific age-related effects on PK of drugs. For example, for oral administered formulations, absorption can be greatly affected by the gastric pH and stomach empty time in the pediatric population – the gastric acid production doubles in the first two months after birth[229]. The stomach empty time is longer in preterm newborns: gastric half emptying time is 83 min and 72 min in preterm newborns of 28-32 weeks and full term newborns[230]. For systemically accumulated formulations, developmental ages have significant effects on plasma protein concentration. In neonatal calves, concentrations of total proteins, β_2- and γ-globulins increased significantly one day after colostrum intake and then significantly decreased gradually till the end of the first month of age[231]. Body water of neonates decreases from approximately 80% at birth to 60% at 1 year of age. Conversely, body fat increases with age, from 1% to 2% in a preterm neonate to 10% to 15% in a term neonate[201]. Different plasma protein concentrations, and body water to fat ratios can lead to different drug distributions in newborns. Metabolic processes are often immature at birth, which can cause reduced clearance and a prolonged half-life for some of the drugs. Cytochrome P450 enzymes are a super family of multiple hemeproteins relevant to drug metabolism, and their maturation is thought to be complete after 1 year with significant increases in the first month of life[232]. Renal excretion increases sharply after birth and during the first 2 weeks of life in neonates due to the rapid development of glomerular filtration, tubular secretion, and reabsorption[201, 233]. These changes in physiological parameters alter the drug PK which can affect the therapeutic efficacy and therapeutic window of drugs. Although 25 mg/kg of NanoCurc is an effective drug concentration for preterm-equivalent rats, it may not be sufficient to hit the therapeutic window for term-equivalent or late-term equivalent rats. Our result in rats of different developmental ages suggests that physiological parameters that may vary at different developmental stages should be taken into consideration when developing the dose schedule for developing newborns.

In our gene expression analysis, IL-6 was upregulated 3 days after NanoCurc administration in our P7 rats with HI. However, IL-6 is associated with adverse outcomes after HIE in human infants where upregulation indicates the exacerbation of the inflammation[234]. Orrock et al. characterized the cytokine response during TH in newborns with moderate to severe HIE: cytokines IL-1β, IL-2, IL-6, IL-8, IL-10, and IL-13 were significantly elevated at 24 hours of TH in infants with adverse outcomes compared to those with favorable outcomes. After 72 hours of TH, only IL-6 remained significantly elevated in the adverse outcome group[235]. Similarly, in our study, we saw IL-6 had significant upregulation in the late preterm-equivalent brains, which may be a signal of adverse outcomes and could explain why no neuroprotective effects were observed after 1 week. To further clarify the outcomes after HI and the responses to the therapy, BBB function needs to be assessed as well. Tight junction proteins including occludin and claudin-5 are potential biomarkers for BBB permeability indication[219, 236]. In addition, plasma cytokine levels will be quantified in the future study both at 24 hours and endpoints to characterize the gene expression change.

For HIE clinically and HI preclinically, there are some sex differences in pathophysiology, neurological outcomes, and responses to therapies: apoptotic cell death after HI proceeds predominantly via poly (ADP-ribose) polymerase (PARP-1) activation and apoptosis inducing factor (AIF)-dependent pathway in males versus a cytochrome c- and caspase-3-dependent pathway in female[237-239]. Clinically, male infants are more vulnerable to ischemic insults, show stronger inflammatory response, and suffer more long-term deficits than females[240, 241]. Also, some evidence suggests that females may benefit more from therapies such as TH and caspase-3 inhibitor[239, 242, 243]. However, in this study, the effects of biological sex were not obvious. It is possible that sex differences are age specific. Adult brain injury is sexually dimorphic has been widely reported, but the role of sex in perinatal brain injury is far less clear[244]. For example, estradiol and progesterone are believed to support improved neurological outcomes in females[245], but testosterone might exacerbate neuronal injury in males[246]. Nevertheless, this factor is not relevant to prepubertal animals. To tease out sex-based differences, if any, longer term assessments may be needed. Mirza et al. analyzed the histological damage in P10 mice after HI. They found that male and female exhibited equivalent histological changes in the brain one day after HI. However, males had significantly larger infarct in the ipsilateral hemisphere compared to females 3 days after HI[240]. These indicate that the sex specific differences may not occur immediately after the insult, and the endpoint of our study might be too early to capture sex differences. Additionally, standard practice in the field is to power the studies at 20 animals per sex per group to detect sex-based differences, therefore increased group sizes may be needed to verify the sex-based outcomes.

4.5. Conclusions

We characterized the neuroprotective effects of curcumin loaded polymeric nanoparticles in rats with HI at different developmental ages. With a single systemic dose of NanoCurc, a neuroprotective effect was only observed in the late preterm-equivalent rat with HI within 3 days after HI. We did not observe a neuroprotective effect in term-equivalent or late-term equivalent rats with HI or a sustained neuroprotective effect in late preterm-equivalent HI brains at 1 week after injury. We also observed no significant difference in outcomes based on biological sex. Lastly, we identified that a single dose of Nanocurc did not significantly alter gene expression levels of inflammatory, oxidative stress, cell death, or hypoxia and vascular damage markers in rats with HI. Collectively, these data lead to several needed areas of future study to determine if NanoCurc is a promising neuroprotective treatment strategy for the full developmental range of infants with HIE. Therefore, our ongoing and future work will aim to characterize BBB permeability and microglia response in P7, P10, and P13 rat withs HI. In addition, the therapeutic

effectiveness of repeat doses of NanoCurc in the P7 rat using the optimized NanoCurc platform will be evaluated.

Chapter 5 Conclusions and future directions

In this thesis, we firstly quantify the PK and biodistribution of different surfactants formulated PLGA-PEG nanoparticles in term-equivalent rats. We find that F127 formulated PLGA-PEG nanoparticles has a 5.9 h systemic half-life, which is significantly higher than P80 formulated PLGA-PEG nanoparticles ($t_{1/2}$ = 1.7 h). Therefore, F127 is a more favorable surfactant for polymeric nano-formulations due to the improved bioavailability of F127 formulated PLGA-PEG nanoparticles. To identify the mechanism underlying the differences in the *in vivo* PK profiles and biodistribution of nanoparticles formulated with different surfactants, our future work will quantify the protein composition of the protein corona adsorbed outside these nanoparticles. This could potentially reveal the ADME process of our surfactant formulated nanoparticles.

Using F127 as the stabilizer, we further optimize our previous curcumin-contained nano-formulation to maximize drug loading and shelf-life stability so that we can increase the success rate of its translation. By tuning the precipitation rates of curcumin and PLGA-PEG using a mixture of organic solvent, a curcumin-loaded nanoparticle with the curcumin core and a PLGA-PEG shell is formulated. This formulation has high curcumin loading (40% by weight) and encapsulation efficiency (>95%), reproducibility, tunability, and shelf-life stability, and thus has the potential to effectively deliver neuroprotective molecules to treat neonatal neurological disorders. Using the optimized nano-formulated curcumin, we assess the potential of this polymeric nano-formulation to be used for brain delivery in a FGR piglet model. Administered via i.n. administration, most of curcumin-loaded nanoparticles can rapidly enter the brain parenchyma and be internalized by microglia 4 hours after the administration. We found i.n. administration outperformed i.v. administration by showing greater brain uptake and longer residence time. This presents the potential of the PLGA-PEG nano-platform to treat perinatal brain injury in a human-like model.

With the biodistribution and brain uptake results, we will next characterize the neuroprotective effects of curcumin-loaded nanoparticles in piglet model of FGR. Curcumin nanoparticles will be administered intranasally on P1, P3, P5. At P10, we will examine neuronal injury, neuronal cell death and cellular proliferation to assess neuroprotection following treatment using immunohistochemistry methods to assess the neuroprotective effects. Biomarkers include NeuN, Iba, and GFAP will be used to stain neurons, microglia, and astrocytes. Meanwhile, we will examine whether curcumin nanoparticles reduce inflammation in the blood of FGR piglets using multiplex ELISA at P10. Cytokines and chemokines in the inflammatory panel will include IL-1β, IL-4, IL-6, IL-8, IL-10, IFN-α, IFN-γ, TNF-α. This therapeutic efficacy study may advance the clinical application our curcumin-contained nano-formulation in FGR infants.

Due to the potential of P80 formulated nanoparticles to passage through the BBB and target neurons and microglia after systemic administration. We will use the combined surfactants of P80 and F127 to explore whether we can incorporate both P80 and F127 in one PLGA-PEG nano-formulation to increase its BBB penetration. If we can successfully formulate a curcumin loaded PLGA-PEG nanoparticle with both of high drug loading and enhanced BBB permeability using the combined surfactants, the neuroprotection and inflammatory responses following the treatment of this nano-therapy will be further characterized in FGR piglets.

To better tailor the therapeutic schedule for neonatal brain injury treatment, we evaluate the neuroprotective effects of curcumin-loaded nanoparticles on rats of HI in different developmental ages. At the same dosage, we only observe neuroprotective effects in preterm rats of HI in the first three days after injury, and did not observe gene expression change in inflammatory, oxidative stress, or cell death markers. Hence, the neuroprotective effects for the same nano-therapy are developmental age specific. With a single dose administration, neuroprotective effects of curcumin nanoparticles are not sustained, and the genetic expression levels are not altered. Our ongoing work is focused on evaluating multiple doses of curcumin nanoparticles in preterm rats of HI: we will administer 3 doses of curcumin-loaded nanoparticles at a 48h dosing interval to align with clinically relevant dosing schemes and based on our PK data generated in these animals. At 7 days after HI, we will extract the brains to assess the neuroprotective effects and gene expression fold-change and compare these data to our single dose treatment outcomes.

We are still unsure about the therapeutic window of the curcumin nano-formulation at different developmental stages. To help determine the dose and dosing schedule for our future therapeutic efficacy evaluation, detailed PK profiles for curcumin and nanoparticles in rats with HI at different developmental stages will be quantified. Additionally, the relationship of the BBB permeability and brain dysfunction, the change of BBB permeability after the injury, and the time when brain impairment reaches the maximum are uncleared. To address these remaining questions, the BBB permeability of rats with HI at different developmental ages need to be characterized. Using tight junction proteins such as occludin and claudin-5 as the biomarkers, their expression levels will be quantified. With the BBB permeability assessment in rats at different developmental ages after HI, we can further disclose the mechanism under the neuroprotection of drug loaded polymeric nanoparticles.

With the quantification results including protein corona composition, detailed PK profiles of curcumin and nanoparticles, and the BBB permeability after injury at different developmental ages, we will be able to precisely tailor the therapeutic dose, frequency, administration timing, and administration routes of our curcumin-loaded polymeric nanoparticles for perinatal brain injury treatment. The efficacy evaluation of curcumin nanoparticles in FGR piglets and rats with HI at different developmental ages will

elevate their predictability and thus help accelerate their clinical translation. These robust formulation design and preclinical efficacy results will provide the possibility for the curcumin-loaded neuroprotective nano-therapy to be used in clinical perinatal neuroprotection. These results will also guide the formulation design of other hydrophobic molecule encapsulated nanoparticles and preclinical studies of neonatal neuroprotective nano-therapies.

Chapter 6 Research Summary

6.1. Data management schema design for effective nanoparticle formulation for neurotherapeutics

Hawley Helmbrecht, **Nuo Xu**, Rick Liao, Elizabeth Nance*. AIChE Journal (2021) 67:12, e17459.

Translation of nanotherapeutics from preclinical research to clinical application is difficult due to the complex and dynamic interaction space between the nanotherapeutic and the brain environment. To improve translation, increased insight into nanoformulation-brain interactions in preclinical research is necessary. We developed a nanoformulation-brain database and wrote queries to connect the complex physical, chemical, and biological features of neurotherapeutics based on experimental data. We queried the database to select nanoformulations based on specific physical characteristics that enable effective penetration within the brain, including size, polydispersity index, and zeta potential. Additionally, we demonstrate the ability to query the database to return select nanoformulation characteristics, including nanoformulation methodology or methodological variables such as surfactant, polymer, drug loading, and sonication times. Finally, we show the capacity of our database to produce correlations relating nanoparticle formulation parameters to biological outcomes, including nanotherapeutic impact on cell viability in cultured brain slices.

6.2. Surfactants influence polymer nanoparticle fate within the brain

Andrea Joseph, Georges Motchoffo Simo, Torahito Gao, Norah Alhindi, **Nuo Xu**, Daniel Graham, Lara Gamble, Elizabeth Nance*. *Biomaterials* 2021, Vol. 277 Pages 121086.

Drug delivery to the brain is limited by poor penetration of pharmaceutical agents across the blood-brain barrier (BBB), within the brain parenchyma, and into specific cells of interest. Nanotechnology can overcome these barriers, but its ability to do so is dependent on nanoparticle physicochemical properties including surface chemistry. Surface chemistry can be determined by a number of factors, including by the presence of stabilizing surfactant molecules introduced during the formulation process. Nanoparticles coated with poloxamer 188 (F68), poloxamer 407 (F127), and polysorbate 80 (P80) have demonstrated uptake in BBB endothelial cells and enhanced accumulation within the brain. However, the impact of surfactants on nanoparticle fate, and specifically on brain extracellular diffusion or intracellular targeting, must be better understood to design nanotherapeutics to efficiently overcome drug delivery barriers in the brain. Here, we evaluated the effect of the biocompatible and commonly used surfactants cholic acid (CHA), F68, F127, P80, and poly(vinyl alcohol) (PVA) on poly(lactic-*co*-glycolic acid)-poly(ethylene glycol) (PLGA-PEG) nanoparticle transport to and within the brain. The inclusion of these surfactant molecules decreases *ex vivo* microglial uptake and diffusive ability, reflecting the surfactant's role in encouraging cellular interaction at short length scales while reducing nonspecific cellular uptake at longer scales. After *in vivo* administration, PLGA-PEG/P80 nanoparticles demonstrated enhanced penetration across the BBB and subsequent internalization within neurons and microglia. Surfactants incorporated into the formulation of PLGA-PEG nanoparticles therefore represent an important design parameter for controlling nanoparticle fate within the brain.

6.3. Neonatal Pharmacokinetics and Biodistribution of Polymeric Nanoparticles and Effect of Surfactant

Nuo Xu, Megan Wong, Gabrielle Balistreri, Elizabeth Nance*. *Pharmaceutics* 2023, 15, 1176.

The development of therapeutics for pediatric use has advanced in the last few decades, yet the off-label use of adult medications in pediatrics remains a significant clinical problem. Nano-based medicines are important drug delivery systems that can improve the bioavailability of a range of therapeutics. However, the use of nano-based medicines for application in pediatric populations is challenged by the lack of pharmacokinetic (PK) data in this population. To address this data gap, we investigated the PK of polymer-based nanoparticles in term-equivalent neonatal rats. We used poly(lactic-co-glycolic acid)-poly(ethylene glycol) (PLGA-PEG) nanoparticles, which are polymer nanoparticles that have been extensively studied in adult populations but less commonly applied in neonates and pediatrics. We quantified the PK parameters and biodistribution of PLGA-PEG nanoparticles in term-equivalent healthy rats and revealed the PK and biodistribution of polymeric nanoparticles in neonatal rats. We further explored the effects of surfactant used to stabilize PLGA-PEG particles on PK and biodistribution. We showed that 4 h post intraperitoneal injection, nanoparticles had the highest accumulation in serum, at 54.0% of the injected dose for particles with Pluronic® F127 (F127) as the stabilizer and at 54.6% of the injected dose for particles with Poloxamer 188 (P80) as the stabilizer. The half-life of the F127-formulated PLGA-PEG particles was 5.9 h, which was significantly longer than the 1.7 h half-life of P80-formulated PLGA-PEG particles. Among all organs, the liver had the highest nanoparticle accumulation. At 24 h after administration, the accumulation of F127-formulated PLGA-PEG particles was at 26.2% of the injected dose, and the accumulation of P80-formulated particles was at 24.1% of the injected dose. Less than 1% of the injected nanoparticles was observed in healthy rat brain for both F127- and P80-formulated particles. These PK data inform the use of polymer nanoparticle applications in the neonate and provide a foundation for the translation of polymer nanoparticles for drug delivery in pediatric populations.

6.4. Nano-formulated curcumin uptake and biodistribution in the fetal growth restricted newborn piglet brain

Nuo Xu, Julie Wixey, Kirat Chand, Megan Wong, Elizabeth Nance*. *Drug Delivery and Translational Research* 2025, 1-15.

Fetal growth restriction (FGR) affects 5% to 10% of all pregnancies in developed countries and is the second most leading cause of perinatal mortality and morbidity. Life-long consequences of FGR range from learning and behavioral issues to cerebral palsy. To support the newborn brain following FGR, timely and accessible neuroprotection strategies are needed. Curcumin-loaded polymeric nanoparticles, which have been widely explored for the treatment of cancer, neurological disorders, and bacterial infections, have the potential to prevent and mitigate pathogenic inflammatory processes in the FGR brain. Curcumin is a hydrophobic molecule with poor aqueous solubility and therefore has been incorporated into nanoparticles to improve solubility and delivery. However, curcumin loading in many nanoparticles can be limited to 10% by weight or lower. Here, we first optimize the formulation process of curcumin-loaded polymeric nanoparticles to find a tunable, reproducible, and stable formulation with high curcumin loading and encapsulation efficiency. We establish a curcumin formulation with 39% curcumin loading and > 95% curcumin encapsulation efficiency. Using this formulation, we assessed the biodistribution of polymeric nanoparticles in FGR piglets and normally grown (NG) piglets following different administration routes and evaluated brain cellular uptake. We show a significant amount of nanoparticle accumulation in the brain parenchyma of neonatal piglets as early as 4 h after intranasal administration. Nanoparticles colocalized in microglia, a therapeutic target of interest in FGR brain injury. This study demonstrates the potential of curcumin-loaded nanoparticles to treat neuroinflammation associated with FGR in the newborn.

6.5. From Bench to Bedside: Overcoming Translational Hurdles in Nanoparticle Research with Pharmacokinetic Modeling

Madison Parrot, **Nuo Xu**, Md Adnan, Joseph Cave, Hamid Ghandehari, Elizabeth Nance, Venkata Yellepeddi*. Manuscript submitted.

Nanoparticles represent a pivotal advancement in active agent delivery systems, offering enhanced stability, solubility, and targeted therapeutic delivery with minimized non-specific toxicity. Despite promising preclinical research highlighting innovative therapeutic possibilities, only a few nanoparticles transition successfully from lab exploration to clinical application. We review the state of nanoparticles in various phases of preclinical and clinical trials. Lack of adequate pharmacokinetic (PK) data, missing long-term studies, off-target effects, and manufacturing complications of nanoparticles are responsible for these translational issues. Bridging the gap between preclinical potential and clinical implementation demands PK data acquisition. Emphasizing the pivotal role of PK in this development process is essential for harnessing the full therapeutic potential of nanoparticle applications in clinical practice, and PK modeling can assist in this translation. Physiologically-based pharmacokinetic (PBPK) models simulate the absorption, distribution, metabolism, and elimination (ADME) of nanoparticles within the body, incorporating physiological parameters to predict their PK behavior. Population-based PK (PopPK) models utilize population variability to characterize nanoparticle PK across diverse patient groups, optimizing dosing strategies and personalized medicine approaches. Mechanistic models elucidate the intricate interactions between nanoparticles and biological systems, integrating cellular pathways and disease mechanisms to predict therapeutic outcomes and guide nanoparticle design. Current PBPK and PopPK models of nanoparticles are summarized. Emphasizing these modeling approaches enhances our understanding of nanoparticle PK, fosters innovation in active agent delivery systems, and accelerates their translation from research to clinical applications.

References

1. Hansson, E. and E. Skioldebrand, *Anti-inflammatory effects induced by ultralow concentrations of bupivacaine in combination with ultralow concentrations of sildenafil (Viagra) and vitamin D3 on inflammatory reactive brain astrocytes.* PLoS One, 2019. **14**(10): p. e0223648.
2. Rees, S. and T. Inder, *Fetal and neonatal origins of altered brain development.* Early Hum Dev, 2005. **81**(9): p. 753-61.
3. Allen, K.A. and D.H. Brandon, *Hypoxic Ischemic Encephalopathy: Pathophysiology and Experimental Treatments.* Newborn Infant Nurs Rev, 2011. **11**(3): p. 125-133.
4. Babiker, M.O.E., A.A. Abdalla, and M.M. Kabiraj, *Neurological Disorders in the Neonate.*
5. Zhou, K.Q., et al., *Treating Seizures after Hypoxic-Ischemic Encephalopathy-Current Controversies and Future Directions.* Int J Mol Sci, 2021. **22**(13).
6. Malhotra, A., et al., *Neonatal Morbidities of Fetal Growth Restriction: Pathophysiology and Impact.* Front Endocrinol (Lausanne), 2019. **10**: p. 55.
7. Nardozza, L.M., et al., *Fetal growth restriction: current knowledge.* Arch Gynecol Obstet, 2017. **295**(5): p. 1061-1077.
8. Lee, A.C., et al., *National and regional estimates of term and preterm babies born small for gestational age in 138 low-income and middle-income countries in 2010.* Lancet Glob Health, 2013. **1**(1): p. e26-36.
9. Heinonen, K., et al., *Behavioural symptoms of attention deficit/hyperactivity disorder in preterm and term children born small and appropriate for gestational age: a longitudinal study.* BMC Pediatr, 2010. **10**: p. 91.
10. Blair, E.M. and K.B. Nelson, *Fetal growth restriction and risk of cerebral palsy in singletons born after at least 35 weeks' gestation.* Am J Obstet Gynecol, 2015. **212**(4): p. 520.e1-7.
11. Jacobsson, B., et al., *Cerebral palsy and restricted growth status at birth: population-based case-control study.* Bjog, 2008. **115**(10): p. 1250-5.
12. Wixey, J.A., et al., *Ibuprofen Treatment Reduces the Neuroinflammatory Response and Associated Neuronal and White Matter Impairment in the Growth Restricted Newborn.* Front Physiol, 2019. **10**: p. 541.
13. Chand, K.K., et al., *Neurovascular Unit Alterations in the Growth-Restricted Newborn Are Improved Following Ibuprofen Treatment.* Molecular Neurobiology, 2022. **59**(2): p. 1018-1040.
14. Chand, K.K., et al., *Combination of human endothelial colony-forming cells and mesenchymal stromal cells exert neuroprotective effects in the growth-restricted newborn.* NPJ Regen Med, 2021. **6**(1): p. 75.
15. Victor, S., et al., *New possibilities for neuroprotection in neonatal hypoxic-ischemic encephalopathy.* Eur J Pediatr, 2022. **181**(3): p. 875-887.
16. Dilenge, M.E., A. Majnemer, and M.I. Shevell, *Long-term developmental outcome of asphyxiated term neonates.* J Child Neurol, 2001. **16**(11): p. 781-92.
17. Liu, L., et al., *Global, regional, and national causes of child mortality: an updated systematic analysis for 2010 with time trends since 2000.* Lancet, 2012. **379**(9832): p. 2151-61.
18. Mwaniki, M.K., et al., *Long-term neurodevelopmental outcomes after intrauterine and neonatal insults: a systematic review.* Lancet, 2012. **379**(9814): p. 445-52.
19. Robertson, C.M. and M. Perlman, *Follow-up of the term infant after hypoxic-ischemic encephalopathy.* Paediatr Child Health, 2006. **11**(5): p. 278-82.
20. Groenendaal, F., *Time to start hypothermia after perinatal asphyxia: does it matter?* BMJ Paediatr Open, 2019. **3**(1): p. e000494.
21. Larsen, M.L., et al., *The effect of gestational age on major neurodevelopmental disorders in preterm infants.* Pediatr Res, 2022. **91**(7): p. 1906-1912.
22. Raghavan, R., et al., *Preterm birth subtypes, placental pathology findings, and risk of neurodevelopmental disabilities during childhood.* Placenta, 2019. **83**: p. 17-25.
23. Walani, S.R., *Global burden of preterm birth.* Int J Gynaecol Obstet, 2020. **150**(1): p. 31-33.

24. Mullin, A.P., et al., *Neurodevelopmental disorders: mechanisms and boundary definitions from genomes, interactomes and proteomes.* Transl Psychiatry, 2013. **3**(12): p. e329.
25. Kostovic, I. and N. Jovanov-Milosevic, *The development of cerebral connections during the first 20-45 weeks' gestation.* Semin Fetal Neonatal Med, 2006. **11**(6): p. 415-22.
26. Kostovic, I. and M. Judas, *The development of the subplate and thalamocortical connections in the human foetal brain.* Acta Paediatr, 2010. **99**(8): p. 1119-27.
27. Vanes, L.D., R.M. Murray, and C. Nosarti, *Adult outcome of preterm birth: Implications for neurodevelopmental theories of psychosis.* Schizophr Res, 2022. **247**: p. 41-54.
28. Chollat, C., L. Sentilhes, and S. Marret, *Protection of brain development by antenatal magnesium sulphate for infants born preterm.* Dev Med Child Neurol, 2019. **61**(1): p. 25-30.
29. Bachnas, M.A., et al., *The role of magnesium sulfate (MgSO(4)) in fetal neuroprotection.* J Matern Fetal Neonatal Med, 2021. **34**(6): p. 966-978.
30. Molloy, E.J., et al., *Neuroprotective therapies in the NICU in preterm infants: present and future (Neonatal Neurocritical Care Series).* Pediatr Res, 2024. **95**(5): p. 1224-1236.
31. Joseph, A., et al., *Curcumin-loaded polymeric nanoparticles for neuro-protection in neonatal rats with hypoxic-ischemic encephalopathy.* Nano Research, 2018. **11**(10): p. 5670-5688.
32. Pressler, R.M., et al., *The ILAE classification of seizures and the epilepsies: Modification for seizures in the neonate. Position paper by the ILAE Task Force on Neonatal Seizures.* Epilepsia, 2021. **62**(3): p. 615-628.
33. Uria-Avellanal, C., N. Marlow, and J.M. Rennie, *Outcome following neonatal seizures.* Semin Fetal Neonatal Med, 2013. **18**(4): p. 224-32.
34. Pavel, A.M., et al., *Neonatal Seizure Management: Is the Timing of Treatment Critical?* J Pediatr, 2022. **243**: p. 61-68 e2.
35. Valentine, A.Z., et al., *A systematic review evaluating the implementation of technologies to assess, monitor and treat neurodevelopmental disorders: A map of the current evidence.* Clin Psychol Rev, 2020. **80**: p. 101870.
36. Choi, J., et al., *Nanoparticulated docetaxel exerts enhanced anticancer efficacy and overcomes existing limitations of traditional drugs.* Int J Nanomedicine, 2015. **10**: p. 6121-32.
37. Manzoor, A.A., et al., *Overcoming limitations in nanoparticle drug delivery: triggered, intravascular release to improve drug penetration into tumors.* Cancer Res, 2012. **72**(21): p. 5566-75.
38. Anderluzzi, G., et al., *Scalable Manufacturing Processes for Solid Lipid Nanoparticles.* Pharm Nanotechnol, 2019. **7**(6): p. 444-459.
39. Shegokar, R., K.K. Singh, and R.H. Muller, *Production & stability of stavudine solid lipid nanoparticles--from lab to industrial scale.* Int J Pharm, 2011. **416**(2): p. 461-70.
40. Becker Peres, L., et al., *Solid lipid nanoparticles for encapsulation of hydrophilic drugs by an organic solvent free double emulsion technique.* Colloids Surf B Biointerfaces, 2016. **140**: p. 317-323.
41. Tenchov, R., et al., *Lipid Nanoparticles ─From Liposomes to mRNA Vaccine Delivery, a Landscape of Research Diversity and Advancement.* ACS Nano, 2021. **15**(11): p. 16982-17015.
42. Viegas, C., F. Seck, and P. Fonte, *An insight on lipid nanoparticles for therapeutic proteins delivery.* Journal of Drug Delivery Science and Technology, 2022. **77**: p. 103839.
43. Zielińska, A., et al., *Polymeric Nanoparticles: Production, Characterization, Toxicology and Ecotoxicology.* Molecules, 2020. **25**(16).
44. Zielinska, A., et al., *Polymeric Nanoparticles: Production, Characterization, Toxicology and Ecotoxicology.* Molecules, 2020. **25**(16).
45. Kahraman, E., S. Güngör, and Y. Ozsoy, *Potential Enhancement and Targeting Strategies of Polymeric and lipid-based Nanocarriers in Dermal Drug Delivery.* Therapeutic Delivery, 2017. **8**: p. 967-985.

46. Sivadasan, D., et al., *Polymeric Lipid Hybrid Nanoparticles (PLNs) as Emerging Drug Delivery Platform-A Comprehensive Review of Their Properties, Preparation Methods, and Therapeutic Applications.* Pharmaceutics, 2021. **13**(8).
47. Tamarov, K., et al., *Approaches to improve the biocompatibility and systemic circulation of inorganic porous nanoparticles.* J Mater Chem B, 2018. **6**(22): p. 3632-3649.
48. Nance, E.A., et al., *A dense poly(ethylene glycol) coating improves penetration of large polymeric nanoparticles within brain tissue.* Sci Transl Med, 2012. **4**(149): p. 149ra119.
49. Annu, et al., *An Insight to Brain Targeting Utilizing Polymeric Nanoparticles: Effective Treatment Modalities for Neurological Disorders and Brain Tumor.* Frontiers in Bioengineering and Biotechnology, 2022. **10**.
50. Joseph, A., et al., *Surfactants influence polymer nanoparticle fate within the brain.* Biomaterials, 2021. **277**: p. 121086.
51. Nance, E., et al., *Brain-penetrating nanoparticles improve paclitaxel efficacy in malignant glioma following local administration.* ACS Nano, 2014. **8**(10): p. 10655-64.
52. Boswell, G.W., D. Buell, and I. Bekersky, *AmBisome (liposomal amphotericin B): a comparative review.* J Clin Pharmacol, 1998. **38**(7): p. 583-92.
53. Bulbake, U., et al., *Liposomal Formulations in Clinical Use: An Updated Review.* Pharmaceutics, 2017. **9**(2).
54. Barenholz, Y., *Doxil(R)--the first FDA-approved nano-drug: lessons learned.* J Control Release, 2012. **160**(2): p. 117-34.
55. Jones, E. and M. Goldman, *Lipid formulations of amphotericin B.* Cleve Clin J Med, 1998. **65**(8): p. 423-7.
56. Dadpour, S., et al., *The role of size in PEGylated liposomal doxorubicin biodistribution and anti-tumour activity.* IET Nanobiotechnol, 2022. **16**(7-8): p. 259-272.
57. Mousseau, F., et al., *Revealing the pulmonary surfactant corona on silica nanoparticles by cryo-transmission electron microscopy.* Nanoscale Adv, 2020. **2**(2): p. 642-647.
58. Batist, G., et al., *Myocet (liposome-encapsulated doxorubicin citrate): a new approach in breast cancer therapy.* Expert Opin Pharmacother, 2002. **3**(12): p. 1739-51.
59. Jia, Y., et al., *Approved Nanomedicine against Diseases.* Pharmaceutics, 2023. **15**(3).
60. Silverman, J.A. and S.R. Deitcher, *Marqibo(R) (vincristine sulfate liposome injection) improves the pharmacokinetics and pharmacodynamics of vincristine.* Cancer Chemother Pharmacol, 2013. **71**(3): p. 555-64.
61. Burade, V., et al., *Lipodox(R) (generic doxorubicin hydrochloride liposome injection): in vivo efficacy and bioequivalence versus Caelyx(R) (doxorubicin hydrochloride liposome injection) in human mammary carcinoma (MX-1) xenograft and syngeneic fibrosarcoma (WEHI 164) mouse models.* BMC Cancer, 2017. **17**(1): p. 405.
62. Zhou, H., et al., *Population Pharmacokinetics and Exposure-Safety Relationship of Paclitaxel Liposome in Patients With Non-small Cell Lung Cancer.* Front Oncol, 2020. **10**: p. 1731.
63. Anselmo, A.C. and S. Mitragotri, *Nanoparticles in the clinic: An update.* Bioeng Transl Med, 2019. **4**(3): p. e10143.
64. Luan, N., et al., *LNP-CpG ODN-adjuvanted varicella-zoster virus glycoprotein E induced comparable levels of immunity with Shingrix in VZV-primed mice.* Virol Sin, 2022. **37**(5): p. 731-739.
65. Hermosilla, J., et al., *Analysing the In-Use Stability of mRNA-LNP COVID-19 Vaccines Comirnaty (Pfizer) and Spikevax (Moderna): A Comparative Study of the Particulate.* Vaccines (Basel), 2023. **11**(11).
66. Fulton, M.D. and W. Najahi-Missaoui, *Liposomes in Cancer Therapy: How Did We Start and Where Are We Now.* Int J Mol Sci, 2023. **24**(7).
67. Chu, Y., et al., *Physicochemical Characterization and Pharmacological Evaluation of Novel Propofol Micelles with Low-Lipid and Low-Free Propofol.* Pharmaceutics, 2022. **14**(2).

68. Song, J.Y., et al., *Glatiramer acetate persists at the injection site and draining lymph nodes via electrostatically-induced aggregation.* J Control Release, 2019. **293**: p. 36-47.
69. Rosenbaum, D.P., et al., *Effect of RenaGel, a non-absorbable, cross-linked, polymeric phosphate binder, on urinary phosphorus excretion in rats.* Nephrol Dial Transplant, 1997. **12**(5): p. 961-4.
70. DiMemmo, L.M., et al., *Real-time observation of protein aggregates in pharmaceutical formulations using liquid cell electron microscopy.* Lab Chip, 2017. **17**(2): p. 315-322.
71. Moosavi, S., et al., *PF-06881894, a Proposed Biosimilar to Pegfilgrastim, Versus US-Licensed and EU-Approved Pegfilgrastim Reference Products (Neulasta((R))): Pharmacodynamics, Pharmacokinetics, Immunogenicity, and Safety of Single or Multiple Subcutaneous Doses in Healthy Volunteers.* Adv Ther, 2020. **37**(7): p. 3370-3391.
72. Werner, M.E., et al., *Preclinical evaluation of Genexol-PM, a nanoparticle formulation of paclitaxel, as a novel radiosensitizer for the treatment of non-small cell lung cancer.* Int J Radiat Oncol Biol Phys, 2013. **86**(3): p. 463-468.
73. Paik, J., S.T. Duggan, and S.J. Keam, *Triamcinolone Acetonide Extended-Release: A Review in Osteoarthritis Pain of the Knee.* Drugs, 2019. **79**(4): p. 455-462.
74. Ma, P. and R.J. Mumper, *Paclitaxel Nano-Delivery Systems: A Comprehensive Review.* J Nanomed Nanotechnol, 2013. **4**(2): p. 1000164.
75. Jain, D., et al., *Impact of differential particle size of fenofibrate nanosuspensions on biopharmaceutical performance using physiologically based absorption modeling in rats.* Journal of Drug Delivery Science and Technology, 2020. **60**: p. 102040.
76. D'Mello, S.R., et al., *The evolving landscape of drug products containing nanomaterials in the United States.* Nature Nanotechnology, 2017. **12**(6): p. 523-529.
77. Anselmo, A.C. and S. Mitragotri, *A Review of Clinical Translation of Inorganic Nanoparticles.* AAPS J, 2015. **17**(5): p. 1041-54.
78. Sun, D., et al., *Comparative Evaluation of U.S. Brand and Generic Intravenous Sodium Ferric Gluconate Complex in Sucrose Injection: Physicochemical Characterization.* Nanomaterials (Basel), 2018. **8**(1).
79. Dalzon, B., et al., *Influences of Nanoparticles Characteristics on the Cellular Responses: The Example of Iron Oxide and Macrophages.* Nanomaterials (Basel), 2020. **10**(2).
80. Metselaar, J.M. and T. Lammers, *Challenges in nanomedicine clinical translation.* Drug Deliv Transl Res, 2020. **10**(3): p. 721-725.
81. Kimmelman, J. and C. Federico, *Consider drug efficacy before first-in-human trials.* Nature, 2017. **542**(7639): p. 25-27.
82. Hare, J.I., et al., *Challenges and strategies in anti-cancer nanomedicine development: An industry perspective.* Adv Drug Deliv Rev, 2017. **108**: p. 25-38.
83. He, H., et al., *Survey of Clinical Translation of Cancer Nanomedicines-Lessons Learned from Successes and Failures.* Acc Chem Res, 2019. **52**(9): p. 2445-2461.
84. Ragelle, H., et al., *Nanoparticle-based drug delivery systems: a commercial and regulatory outlook as the field matures.* Expert Opin Drug Deliv, 2017. **14**(7): p. 851-864.
85. Szebeni, J., et al., *Roadmap and strategy for overcoming infusion reactions to nanomedicines.* Nat Nanotechnol, 2018. **13**(12): p. 1100-1108.
86. Vannucci, R.C. and S.J. Vannucci, *Perinatal hypoxic-ischemic brain damage: evolution of an animal model.* Dev Neurosci, 2005. **27**(2-4): p. 81-6.
87. Vannucci, R.C. and S.J. Vannucci, *A model of perinatal hypoxic-ischemic brain damage.* Ann N Y Acad Sci, 1997. **835**: p. 234-49.
88. Chand, K.K., et al., *Brain Outcomes in Runted Piglets: A Translational Model of Fetal Growth Restriction.* Dev Neurosci, 2022. **44**(4-5): p. 194-204.
89. Musco, H. and J.A. Wixey, *Understanding the timing of brain injury in fetal growth restriction: lessons from a model of spontaneous growth restriction in piglets.* Neural Regen Res, 2023. **18**(2): p. 322-323.

90. FDA, *Pediatric study plans: content of and process for Submitting initial pediatric study plans and amended initial pediatric study plans.* 2020.
91. Giacoia, G.P., P. Taylor-Zapata, and A. Zajicek, *Eunice Kennedy Shriver National Institute of Child Health and Human Development Pediatrics Formulation Initiative: proceedings from the Second Workshop on Pediatric Formulations.* Clin Ther, 2012. **34**(11): p. S1-10.
92. Nieto Gonzalez, N., et al., *Polymeric and Lipid Nanoparticles: Which Applications in Pediatrics?* Pharmaceutics, 2021. **13**(5).
93. Penkov, D., et al., *Pediatric Medicine Development: An Overview and Comparison of Regulatory Processes in the European Union and United States.* Ther Innov Regul Sci, 2017. **51**(3): p. 360-371.
94. Kim, B.Y., J.T. Rutka, and W.C. Chan, *Nanomedicine.* N Engl J Med, 2010. **363**(25): p. 2434-43.
95. Freitas, R.A., Jr., *What is nanomedicine?* Nanomedicine, 2005. **1**(1): p. 2-9.
96. Krishnan, V., et al., *Dexamethasone-loaded block copolymer nanoparticles induce leukemia cell death and enhance therapeutic efficacy: a novel application in pediatric nanomedicine.* Mol Pharm, 2013. **10**(6): p. 2199-210.
97. Chiappetta, D.A., et al., *Efavirenz-loaded polymeric micelles for pediatric anti-HIV pharmacotherapy with significantly higher oral bioavailability [corrected].* Nanomedicine (Lond), 2010. **5**(1): p. 11-23.
98. Choi, J., et al., *Nonviral polymeric nanoparticles for gene therapy in pediatric CNS malignancies.* Nanomedicine, 2020. **23**: p. 102115.
99. Belayneh, A., E. Tadese, and F. Molla, *Safety and Biopharmaceutical Challenges of Excipients in Off-Label Pediatric Formulations.* Int J Gen Med, 2020. **13**: p. 1051-1066.
100. Yellepeddi, V.K., A. Joseph, and E. Nance, *Pharmacokinetics of nanotechnology-based formulations in pediatric populations.* Adv Drug Deliv Rev, 2019. **151-152**: p. 44-55.
101. Frattarelli, D.A., et al., *Off-label use of drugs in children.* Pediatrics, 2014. **133**(3): p. 563-7.
102. Shah, S.S., et al., *Off-label drug use in hospitalized children.* Arch Pediatr Adolesc Med, 2007. **161**(3): p. 282-90.
103. Pratico, A.D., et al., *Off-Label Use of Drugs and Adverse Drug Reactions in Pediatric Units: A Prospective, Multicenter Study.* Curr Drug Saf, 2018. **13**(3): p. 200-207.
104. Allen, H.C., et al., *Off-Label Medication use in Children, More Common than We Think: A Systematic Review of the Literature.* J Okla State Med Assoc, 2018. **111**(8): p. 776-783.
105. Amin, F.U., et al., *Anthocyanins encapsulated by PLGA@PEG nanoparticles potentially improved its free radical scavenging capabilities via p38/JNK pathway against Abeta1-42-induced oxidative stress.* J Nanobiotechnology, 2017. **15**(1): p. 12.
106. Saneja, A., et al., *Gemcitabine and betulinic acid co-encapsulated PLGA-PEG polymer nanoparticles for improved efficacy of cancer chemotherapy.* Mater Sci Eng C Mater Biol Appl, 2019. **98**: p. 764-771.
107. Khalil, N.M., et al., *Pharmacokinetics of curcumin-loaded PLGA and PLGA-PEG blend nanoparticles after oral administration in rats.* Colloids Surf B Biointerfaces, 2013. **101**: p. 353-60.
108. Operti, M.C., et al., *PLGA-based nanomedicines manufacturing: Technologies overview and challenges in industrial scale-up.* Int J Pharm, 2021. **605**: p. 120807.
109. *Available online: https://clinicaltrials.gov (NCT05456022; accessed on 6 April 2023).*
110. Araujo, L., R. Lobenberg, and J. Kreuter, *Influence of the surfactant concentration on the body distribution of nanoparticles.* J Drug Target, 1999. **6**(5): p. 373-85.
111. Troster, S.D., U. Muller, and J. Kreuter, *Modification of the Body Distribution of Poly(Methyl Methacrylate) Nanoparticles in Rats by Coating with Surfactants.* International Journal of Pharmaceutics, 1990. **61**(1-2): p. 85-100.
112. Miyazawa, T., et al., *A Critical Review of the Use of Surfactant-Coated Nanoparticles in Nanomedicine and Food Nanotechnology.* Int J Nanomedicine, 2021. **16**: p. 3937-3999.

113. Cortes, H., et al., *Non-Ionic Surfactants for Stabilization of Polymeric Nanoparticles for Biomedical Uses.* Materials (Basel), 2021. **14**(12).
114. Kreuter, J., et al., *Apolipoprotein-mediated transport of nanoparticle-bound drugs across the blood-brain barrier.* J Drug Target, 2002. **10**(4): p. 317-25.
115. Wunsch, A., D. Mulac, and K. Langer, *Lipoprotein imitating nanoparticles: Lecithin coating binds ApoE and mediates non-lysosomal uptake leading to transcytosis over the blood-brain barrier.* Int J Pharm, 2020. **589**: p. 119821.
116. Li, Y., et al., *Mechanisms of enhanced antiglioma efficacy of polysorbate 80-modified paclitaxel-loaded PLGA nanoparticles by focused ultrasound.* J Cell Mol Med, 2018. **22**(9): p. 4171-4182.
117. Portioli, C., et al., *Novel functionalization strategies of polymeric nanoparticles as carriers for brain medications.* J Biomed Mater Res A, 2017. **105**(3): p. 847-858.
118. Wagner, S., et al., *Uptake mechanism of ApoE-modified nanoparticles on brain capillary endothelial cells as a blood-brain barrier model.* PLoS One, 2012. **7**(3): p. e32568.
119. Rafiei, P. and A. Haddadi, *Docetaxel-loaded PLGA and PLGA-PEG nanoparticles for intravenous application: pharmacokinetics and biodistribution profile.* Int J Nanomedicine, 2017. **12**: p. 935-947.
120. Malatesta, M., *Transmission Electron Microscopy as a Powerful Tool to Investigate the Interaction of Nanoparticles with Subcellular Structures.* Int J Mol Sci, 2021. **22**(23).
121. Douglas-Escobar, M. and M.D. Weiss, *Hypoxic-ischemic encephalopathy: a review for the clinician.* JAMA Pediatr, 2015. **169**(4): p. 397-403.
122. Pressler, R.M., et al., *Bumetanide for the treatment of seizures in newborn babies with hypoxic ischaemic encephalopathy (NEMO): an open-label, dose finding, and feasibility phase 1/2 trial.* Lancet Neurol, 2015. **14**(5): p. 469-77.
123. Volpe, J.J., *Neurobiology of periventricular leukomalacia in the premature infant.* Pediatr Res, 2001. **50**(5): p. 553-62.
124. Joseph, A., et al., *Formulation and Efficacy of Catalase-Loaded Nanoparticles for the Treatment of Neonatal Hypoxic-Ischemic Encephalopathy.* Pharmaceutics, 2021. **13**(8).
125. Tahara, K., et al., *Brain targeting with surface-modified poly(D,L-lactic-co-glycolic acid) nanoparticles delivered via carotid artery administration.* Eur J Pharm Biopharm, 2011. **77**(1): p. 84-8.
126. Bhawana, et al., *Curcumin nanoparticles: preparation, characterization, and antimicrobial study.* J Agric Food Chem, 2011. **59**(5): p. 2056-61.
127. Li, S.D. and L. Huang, *Pharmacokinetics and biodistribution of nanoparticles.* Mol Pharm, 2008. **5**(4): p. 496-504.
128. Liu, D., A. Mori, and L. Huang, *Role of liposome size and RES blockade in controlling biodistribution and tumor uptake of GM1-containing liposomes.* Biochim Biophys Acta, 1992. **1104**(1): p. 95-101.
129. Alexis, F., et al., *Factors affecting the clearance and biodistribution of polymeric nanoparticles.* Mol Pharm, 2008. **5**(4): p. 505-15.
130. He, C., et al., *Effects of particle size and surface charge on cellular uptake and biodistribution of polymeric nanoparticles.* Biomaterials, 2010. **31**(13): p. 3657-66.
131. Moghaddam, S.P.H., R. Mohammadpour, and H. Ghandehari, *In vitro and in vivo evaluation of degradation, toxicity, biodistribution, and clearance of silica nanoparticles as a function of size, porosity, density, and composition.* Journal of Controlled Release, 2019. **311**: p. 1-15.
132. Li, X.M., et al., *The systematic evaluation of size-dependent toxicity and multi-time biodistribution of gold nanoparticles.* Colloids and Surfaces B-Biointerfaces, 2018. **167**: p. 260-266.
133. Al Shoyaib, A., S.R. Archie, and V.T. Karamyan, *Intraperitoneal Route of Drug Administration: Should it Be Used in Experimental Animal Studies?* Pharm Res, 2019. **37**(1): p. 12.
134. Tao, X., et al., *Brain-Targeted Polysorbate 80-Emulsified Donepezil Drug-Loaded Nanoparticles for Neuroprotection.* Nanoscale Res Lett, 2021. **16**(1): p. 132.

135. Scheuplein, R., G. Charnley, and M. Dourson, *Differential sensitivity of children and adults to chemical toxicity. I. Biological basis.* Regul Toxicol Pharmacol, 2002. **35**(3): p. 429-47.
136. Zhang, Z.A., et al., *Novel brain-targeted nanomicelles for anti-glioma therapy mediated by the ApoE-enriched protein corona in vivo.* J Nanobiotechnology, 2021. **19**(1): p. 453.
137. Pinals, R.L., et al., *Quantitative Protein Corona Composition and Dynamics on Carbon Nanotubes in Biological Environments.* Angew Chem Int Ed Engl, 2020. **59**(52): p. 23668-23677.
138. Tekie, F.S.M., et al., *Controlling evolution of protein corona: a prosperous approach to improve chitosan-based nanoparticle biodistribution and half-life.* Sci Rep, 2020. **10**(1): p. 9664.
139. Bertrand, N., et al., *Mechanistic understanding of in vivo protein corona formation on polymeric nanoparticles and impact on pharmacokinetics.* Nat Commun, 2017. **8**(1): p. 777.
140. Panagi, Z., et al., *Effect of dose on the biodistribution and pharmacokinetics of PLGA and PLGA-mPEG nanoparticles.* Int J Pharm, 2001. **221**(1-2): p. 143-52.
141. Martinez, M.N. and G.L. Amidon, *A mechanistic approach to understanding the factors affecting drug absorption: a review of fundamentals.* J Clin Pharmacol, 2002. **42**(6): p. 620-43.
142. Micossi, P., et al., *Free-insulin profiles after intraperitoneal, intramuscular, and subcutaneous insulin administration.* Diabetes Care, 1986. **9**(6): p. 575-8.
143. Costanzo, M., et al., *Fluorescence and electron microscopy to visualize the intracellular fate of nanoparticles for drug delivery.* Eur J Histochem, 2016. **60**(2): p. 2640.
144. Wixey, J.A., et al., *Neuropathology in intrauterine growth restricted newborn piglets is associated with glial activation and proinflammatory status in the brain.* J Neuroinflammation, 2019. **16**(1): p. 5.
145. McElrath, T.F., et al., *Perinatal systemic inflammatory responses of growth-restricted preterm newborns.* Acta Paediatr, 2013. **102**(10): p. e439-42.
146. Leviton, A., et al., *Two-hit model of brain damage in the very preterm newborn: small for gestational age and postnatal systemic inflammation.* Pediatr Res, 2013. **73**(3): p. 362-70.
147. Sharma, R.A., A.J. Gescher, and W.P. Steward, *Curcumin: The story so far.* European Journal of Cancer, 2005. **41**(13): p. 1955-1968.
148. Joseph, A., et al., *Curcumin-loaded polymeric nanoparticles for neuroprotection in neonatal rats with hypoxic-ischemic encephalopathy.* Nano Research, 2018. **11**(10): p. 5670-5688.
149. Yadav, B., et al., *RGD-decorated PLGA nanoparticles improved effectiveness and safety of cisplatin for lung cancer therapy.* International Journal of Pharmaceutics, 2023. **633**: p. 122587.
150. Hernando, S., et al., *Targeting the central nervous system: From synthetic nanoparticles to extracellular vesicles—Focus on Alzheimer's and Parkinson's disease.* WIREs Nanomedicine and Nanobiotechnology, 2023. **15**(5): p. e1898.
151. Li, B., et al., *Formulation and Evaluation of PLGA Nanoparticulate-Based Microneedle System for Potential Treatment of Neurological Diseases.* International Journal of Nanomedicine, 2023. **18**(null): p. 3745-3760.
152. Wu, X., et al., *Red Blood Cell Membrane-Camouflaged Tedizolid Phosphate-Loaded PLGA Nanoparticles for Bacterial-Infection Therapy.* Pharmaceutics, 2021. **13**(1): p. 99.
153. Nigam, K., et al., *In vitro & in vivo evaluations of PLGA nanoparticle based combinatorial drug therapy for baclofen and lamotrigine for neuropathic pain management.* Journal of Microencapsulation, 2022. **39**(2): p. 95-109.
154. Harris, J.M., N.E. Martin, and M. Modi, *Pegylation.* Clinical Pharmacokinetics, 2001. **40**(7): p. 539-551.
155. Lim, J.M., et al., *Drug loading augmentation in polymeric nanoparticles using a coaxial turbulent jet mixer: Yong investigator perspective.* J Colloid Interface Sci, 2019. **538**: p. 45-50.
156. Xia, X.-X., et al., *Hydrophobic Drug-Triggered Self-Assembly of Nanoparticles from Silk-Elastin-Like Protein Polymers for Drug Delivery.* Biomacromolecules, 2014. **15**(3): p. 908-914.
157. Pond, W.G., et al., *Perinatal ontogeny of brain growth in the domestic pig.* Proc Soc Exp Biol Med, 2000. **223**(1): p. 102-8.

158. Lind, N.M., et al., *The use of pigs in neuroscience: modeling brain disorders.* Neurosci Biobehav Rev, 2007. **31**(5): p. 728-51.
159. Liu, Y., et al., *Stable Polymer Nanoparticles with Exceptionally High Drug Loading by Sequential Nanoprecipitation.* Angewandte Chemie International Edition, 2020. **59**(12): p. 4720-4728.
160. Xu, N., et al., *Neonatal Pharmacokinetics and Biodistribution of Polymeric Nanoparticles and Effect of Surfactant.* Pharmaceutics, 2023. **15**(4): p. 1176.
161. Yawno, T., et al., *Fetal Growth Restriction Alters Cerebellar Development in Fetal and Neonatal Sheep.* Front Physiol, 2019. **10**: p. 560.
162. Tahara, K., H. Yamamoto, and Y. Kawashima, *Cellular uptake mechanisms and intracellular distributions of polysorbate 80-modified poly (D,L-lactide-co-glycolide) nanospheres for gene delivery.* Eur J Pharm Biopharm, 2010. **75**(2): p. 218-24.
163. Machado-Pereira, M., et al., *Intravenous administration of retinoic acid-loaded polymeric nanoparticles prevents ischemic injury in the immature brain.* Neuroscience Letters, 2018. **673**: p. 116-121.
164. Chen, H., et al., *Nanoerythropoietin is 10-times more effective than regular erythropoietin in neuroprotection in a neonatal rat model of hypoxia and ischemia.* Stroke, 2012. **43**(3): p. 884-7.
165. Pham, H., et al., *Impact of inhaled nitric oxide on white matter damage in growth-restricted neonatal rats.* Pediatr Res, 2015. **77**(4): p. 563-9.
166. Bilati, U., E. Allemann, and E. Doelker, *Poly(D,L-lactide-co-glycolide) protein-loaded nanoparticles prepared by the double emulsion method--processing and formulation issues for enhanced entrapment efficiency.* J Microencapsul, 2005. **22**(2): p. 205-14.
167. Liu, Y. and X. Deng, *Influences of preparation conditions on particle size and DNA-loading efficiency for poly(dl-lactic acid–polyethylene glycol) microspheres entrapping free DNA.* Journal of Controlled Release, 2002. **83**(1): p. 147-155.
168. Navarro-Tovar, G., et al., *Chapter 7 - Surface functionalization of nanoparticles: Structure determines function*, in *Antimicrobial Activity of Nanoparticles*, G. Guisbiers, Editor. 2023, Elsevier. p. 203-248.
169. Danhier, F., et al., *Paclitaxel-loaded PEGylated PLGA-based nanoparticles: In vitro and in vivo evaluation.* Journal of Controlled Release, 2009. **133**(1): p. 11-17.
170. Betancourt, T., B. Brown, and L. Brannon-Peppas, *Doxorubicin-Loaded PLGA Nanoparticles by Nanoprecipitation: Preparation, Characterization and In Vitro Evaluation.* Nanomedicine, 2007. **2**(2): p. 219-232.
171. Cheng, J., et al., *Formulation of functionalized PLGA–PEG nanoparticles for in vivo targeted drug delivery.* Biomaterials, 2007. **28**(5): p. 869-876.
172. Çavuşoğlu, H., *Evaluating the influence of polyethylene glycol as a surfactant on CdO films grown by SILAR method.* Journal of Physics and Chemistry of Solids, 2019. **124**: p. 67-72.
173. Ramge, P., et al., *Polysorbate-80 coating enhances uptake of polybutylcyanoacrylate (PBCA)-nanoparticles by human and bovine primary brain capillary endothelial cells.* Eur J Neurosci, 2000. **12**(6): p. 1931-40.
174. Sharma, S. and S. Dang, *Polysorbate 80 surface modified PLGA nanoparticles: an in-vitro evaluation of cellular uptake and cytotoxicity on neuro-2a cells.* Journal of Microencapsulation, 2023. **40**(7): p. 534-548.
175. Alexis, F., et al., *Factors Affecting the Clearance and Biodistribution of Polymeric Nanoparticles.* Molecular Pharmaceutics, 2008. **5**(4): p. 505-515.
176. Keles, H., et al., *Investigation of factors influencing the hydrolytic degradation of single PLGA microparticles.* Polymer Degradation and Stability, 2015. **119**: p. 228-241.
177. Swider, E., et al., *Forster Resonance Energy Transfer-Based Stability Assessment of PLGA Nanoparticles in Vitro and in Vivo.* ACS Appl Bio Mater, 2019. **2**(3): p. 1131-1140.
178. Crowe, T.P., et al., *Mechanism of intranasal drug delivery directly to the brain.* Life Sci, 2018. **195**: p. 44-52.

179. Lofts, A., et al., *Using the Intranasal Route to Administer Drugs to Treat Neurological and Psychiatric Illnesses: Rationale, Successes, and Future Needs.* CNS Drugs, 2022. **36**(7): p. 739-770.
180. Mistry, A., et al., *Effect of physicochemical properties on intranasal nanoparticle transit into murine olfactory epithelium.* J Drug Target, 2009. **17**(7): p. 543-52.
181. Albarki, M.A. and M.D. Donovan, *Bigger or Smaller? Size and Loading Effects on Nanoparticle Uptake Efficiency in the Nasal Mucosa.* AAPS PharmSciTech, 2020. **21**(8): p. 294.
182. Adhipandito, C.F., et al., *Atypical Renal Clearance of Nanoparticles Larger Than the Kidney Filtration Threshold.* Int J Mol Sci, 2021. **22**(20).
183. Alqahtani, M.S., R. Syed, and M. Alshehri, *Size-Dependent Phagocytic Uptake and Immunogenicity of Gliadin Nanoparticles.* Polymers (Basel), 2020. **12**(11).
184. Zha, S., et al., *Functionalized Nanomaterials Capable of Crossing the Blood-Brain Barrier.* ACS Nano, 2024. **18**(3): p. 1820-1845.
185. Ohta, S., et al., *Investigating the optimum size of nanoparticles for their delivery into the brain assisted by focused ultrasound-induced blood-brain barrier opening.* Sci Rep, 2020. **10**(1): p. 18220.
186. Su, Y., et al., *Intranasal Delivery of Targeted Nanoparticles Loaded With miR-132 to Brain for the Treatment of Neurodegenerative Diseases.* Front Pharmacol, 2020. **11**: p. 1165.
187. Yousfan, A., et al., *Intranasal delivery of phenytoin-loaded nanoparticles to the brain suppresses pentylenetetrazol-induced generalized tonic clonic seizures in an epilepsy mouse model.* Biomater Sci, 2021. **9**(22): p. 7547-7564.
188. Zha, S., K.L. Wong, and A.H. All, *Intranasal Delivery of Functionalized Polymeric Nanomaterials to the Brain.* Adv Healthc Mater, 2022. **11**(11): p. e2102610.
189. Lee, D. and T. Minko, *Nanotherapeutics for Nose-to-Brain Drug Delivery: An Approach to Bypass the Blood Brain Barrier.* Pharmaceutics, 2021. **13**(12).
190. Meng, Q., et al., *Intranasal delivery of Huperzine A to the brain using lactoferrin-conjugated N-trimethylated chitosan surface-modified PLGA nanoparticles for treatment of Alzheimer's disease.* Int J Nanomedicine, 2018. **13**: p. 705-718.
191. Henkin, R.I., *Intranasal delivery to the brain.* Nat Biotechnol, 2011. **29**(6): p. 480.
192. Jeong, S.H., J.H. Jang, and Y.B. Lee, *Drug delivery to the brain via the nasal route of administration: exploration of key targets and major consideration factors.* J Pharm Investig, 2023. **53**(1): p. 119-152.
193. Gizurarson, S., *Anatomical and histological factors affecting intranasal drug and vaccine delivery.* Curr Drug Deliv, 2012. **9**(6): p. 566-82.
194. Buchner, K., et al., *A quantitative study of anterograde and retrograde axonal transport of exogenous proteins in olfactory nerve C-fibers.* Neuroscience, 1987. **22**(2): p. 697-707.
195. Misan, N., et al., *Blood-Brain Barrier Disintegration in Growth-Restricted Fetuses with Brain Sparing Effect.* Int J Mol Sci, 2022. **23**(20).
196. Wu, X., et al., *Functionalized lipid nanoparticles modulate the blood-brain barrier and eliminate α-synuclein to repair dopamine neurons.* Asian Journal of Pharmaceutical Sciences, 2024. **19**(2): p. 100904.
197. Del Amo, L., et al., *Surface Functionalization of PLGA Nanoparticles to Increase Transport across the BBB for Alzheimer's Disease.* Applied Sciences, 2021. **11**(9): p. 4305.
198. Kessler, J., et al., *Fetal Growth Restriction Is Associated With Prioritization of Umbilical Blood Flow to the Left Hepatic Lobe at the Expense of the Right Lobe.* Pediatric Research, 2009. **66**(1): p. 113-117.
199. Senra, J.C., et al., *Kidney impairment in fetal growth restriction: three-dimensional evaluation of volume and vascularization.* Prenat Diagn, 2020. **40**(11): p. 1408-1417.
200. Gu, X., et al., *Clearance of two organic nanoparticles from the brain via the paravascular pathway.* J Control Release, 2020. **322**: p. 31-41.

201. Lu, H. and S. Rosenbaum, *Developmental pharmacokinetics in pediatric populations.* J Pediatr Pharmacol Ther, 2014. **19**(4): p. 262-76.
202. Shoaf, S.E., W.S. Schwark, and C.L. Guard, *Pharmacokinetics of sulfadiazine/trimethoprim in neonatal male calves: effect of age and penetration into cerebrospinal fluid.* Am J Vet Res, 1989. **50**(3): p. 396-403.
203. van Donge, T., et al., *Key Components for Antibiotic Dose Optimization of Sepsis in Neonates and Infants.* Front Pediatr, 2018. **6**: p. 325.
204. Mian, P., et al., *Therapeutic Drug Monitoring in Neonates: What Makes them Unique?* Curr Pharm Des, 2017. **23**(38): p. 5790-5800.
205. Faix, R.G., et al., *Whole-Body Hypothermia for Neonatal Encephalopathy in Preterm Infants 33 to 35 Weeks' Gestation: A Randomized Clinical Trial.* JAMA Pediatr, 2025. **179**(4): p. 396-406.
206. Hewlings, S.J. and D.S. Kalman, *Curcumin: A Review of Its Effects on Human Health.* Foods, 2017. **6**(10).
207. Obeid, M.A., M. Alsaadi, and A.A. Aljabali, *Recent updates in curcumin delivery.* J Liposome Res, 2022: p. 1-12.
208. Xu, N., et al., *Nano-formulated curcumin uptake and biodistribution in the fetal growth restricted newborn piglet brain.* Drug Deliv Transl Res, 2025.
209. Juul, S.E., et al., *Microarray analysis of high-dose recombinant erythropoietin treatment of unilateral brain injury in neonatal mouse hippocampus.* Pediatr Res, 2009. **65**(5): p. 485-92.
210. Sabir, H., et al., *Immediate hypothermia is not neuroprotective after severe hypoxia-ischemia and is deleterious when delayed by 12 hours in neonatal rats.* Stroke, 2012. **43**(12): p. 3364-70.
211. Serdar, M., et al., *Early Pro-inflammatory Microglia Activation After Inflammation-Sensitized Hypoxic-Ischemic Brain Injury in Neonatal Rats.* Front Cell Neurosci, 2019. **13**: p. 237.
212. Ziemka-Nalecz, M., J. Jaworska, and T. Zalewska, *Insights Into the Neuroinflammatory Responses After Neonatal Hypoxia-Ischemia.* J Neuropathol Exp Neurol, 2017. **76**(8): p. 644-654.
213. Biegon, A., *Considering Biological Sex in Traumatic Brain Injury.* Front Neurol, 2021. **12**: p. 576366.
214. Ziemka-Nalecz, M., et al., *Sex Differences in Brain Disorders.* Int J Mol Sci, 2023. **24**(19).
215. Beheshti, I., S. Booth, and J.H. Ko, *Differences in brain aging between sexes in Parkinson's disease.* npj Parkinson's Disease, 2024. **10**(1): p. 35.
216. Liu, F. and L.D. McCullough, *Inflammatory responses in hypoxic ischemic encephalopathy.* Acta Pharmacol Sin, 2013. **34**(9): p. 1121-30.
217. Zhao, M., et al., *Oxidative Stress in Hypoxic-Ischemic Encephalopathy: Molecular Mechanisms and Therapeutic Strategies. LID - 2078.* (1422-0067 (Electronic)).
218. Mallard, C., C.J. Ek, and Z.S. Vexler, *The myth of the immature barrier systems in the developing brain: role in perinatal brain injury.* J Physiol, 2018. **596**(23): p. 5655-5664.
219. Fernández-López, D., et al., *Blood-brain barrier permeability is increased after acute adult stroke but not neonatal stroke in the rat.* J Neurosci, 2012. **32**(28): p. 9588-600.
220. Nance, E., et al., *Nanoscale effects in dendrimer-mediated targeting of neuroinflammation.* Biomaterials, 2016. **101**: p. 96-107.
221. Mastenbroek, L.J.M., et al., *The role of microglia in early neurodevelopment and the effects of maternal immune activation.* Semin Immunopathol, 2024. **46**(1-2): p. 1.
222. Kim, I., et al., *A postnatal peak in microglial development in the mouse hippocampus is correlated with heightened sensitivity to seizure triggers.* Brain Behav, 2015. **5**(12): p. e00403.
223. Soch, A., et al., *The role of microglia in the second and third postnatal weeks of life in rat hippocampal development and memory.* Brain Behav Immun, 2020. **88**: p. 675-687.
224. Pierre, W.C., et al., *Neonatal microglia: The cornerstone of brain fate.* Brain Behav Immun, 2017. **59**: p. 333-345.
225. Bilbo, S.D. and J.M. Schwarz, *Early-life programming of later-life brain and behavior: a critical role for the immune system.* Front Behav Neurosci, 2009. **3**: p. 14.

226. Lembo, C., G. Buonocore, and S. Perrone, *Oxidative Stress in Preterm Newborns.* Antioxidants (Basel), 2021. **10**(11).
227. Carrascal, L., et al., *Age-Dependent Vulnerability to Oxidative Stress of Postnatal Rat Pyramidal Motor Cortex Neurons.* Antioxidants (Basel), 2020. **9**(12).
228. Wilhelm, J., et al., *Oxidative Stress in the Developing Rat Brain due to Production of Reactive Oxygen and Nitrogen Species.* Oxid Med Cell Longev, 2016. **2016**: p. 5057610.
229. Indrio, F., et al., *Development of the Gastrointestinal Tract in Newborns as a Challenge for an Appropriate Nutrition: A Narrative Review.* Nutrients, 2022. **14**(7).
230. Van Den Driessche, M. and G. Veereman-Wauters, *Gastric emptying in infants and children.* Acta Gastroenterol Belg, 2003. **66**(4): p. 274-82.
231. Tóthová, C., et al., *Changes in the concentrations of serum proteins in calves during the first month of life.* 2015
232. O'Hara, K., et al., *Pharmacokinetics in neonatal prescribing: evidence base, paradigms and the future.* Br J Clin Pharmacol, 2015. **80**(6): p. 1281-8.
233. Batchelor, H.K. and J.F. Marriott, *Paediatric pharmacokinetics: key considerations.* Br J Clin Pharmacol, 2015. **79**(3): p. 395-404.
234. Yang, X., et al., *Knockdown of interleukin-6 plays a neuroprotective role against hypoxia-ischemia in neonatal rats via inhibition of caspase 3 and Bcl-2-associated X protein signaling pathway.* Ibrain, 2022. **8**(3): p. 413-428.
235. Orrock, J.E., et al., *Association of brain injury and neonatal cytokine response during therapeutic hypothermia in newborns with hypoxic-ischemic encephalopathy.* Pediatr Res, 2016. **79**(5): p. 742-7.
236. Andersson, E.A., C. Mallard, and C.J. Ek, *Circulating tight-junction proteins are potential biomarkers for blood-brain barrier function in a model of neonatal hypoxic/ischemic brain injury.* Fluids Barriers CNS, 2021. **18**(1): p. 7.
237. Hagberg, H., et al., *PARP-1 gene disruption in mice preferentially protects males from perinatal brain injury.* J Neurochem, 2004. **90**(5): p. 1068-75.
238. Renolleau, S., S. Fau, and C. Charriaut-Marlangue, *Gender-related differences in apoptotic pathways after neonatal cerebral ischemia.* Neuroscientist, 2008. **14**(1): p. 46-52.
239. Renolleau, S., et al., *'Sex, neuroprotection, and neonatal ischemia'.* Dev Med Child Neurol, 2007. **49**(6): p. 477; author reply 477-8.
240. Mirza, M.A., et al., *Sexually dimorphic outcomes and inflammatory responses in hypoxic-ischemic encephalopathy.* J Neuroinflammation, 2015. **12**: p. 32.
241. Al Mamun, A., et al., *Inflammatory Responses are Sex Specific in Chronic Hypoxic-Ischemic Encephalopathy.* Cell Transplant, 2018. **27**(9): p. 1328-1339.
242. Zhou, K.Q., J.O. Davidson, and A.J. Gunn, *Does sex materially modulate responses to therapeutic hypothermia?* Pediatr Res, 2023. **94**(4): p. 1259-1260.
243. Wood, T.R., et al., *Variability and sex-dependence of hypothermic neuroprotection in a rat model of neonatal hypoxic-ischaemic brain injury: a single laboratory meta-analysis.* Sci Rep, 2020. **10**(1): p. 10833.
244. Hurn, P.D., S.J. Vannucci, and H. Hagberg, *Adult or perinatal brain injury: does sex matter?* Stroke, 2005. **36**(2): p. 193-5.
245. Brotfain, E., et al., *Neuroprotection by Estrogen and Progesterone in Traumatic Brain Injury and Spinal Cord Injury.* Curr Neuropharmacol, 2016. **14**(6): p. 641-53.
246. Nakano, T., et al., *Testosterone exacerbates neuronal damage following cardiac arrest and cardiopulmonary resuscitation in mouse.* Brain Res, 2010. **1357**: p. 124-30.

Appendix A: Supplementary Information for Chapter 1

Table S1-1. Systemically administered therapeutic nanoparticles in clinical trials.

Name	Particle type/drug	Application	Clinical trial identifier
Anti-EGFR immunoliposomes	Anti-EGFR immunoliposomes loaded with doxorubicin	Solid tumors	2007: NCT01702129 (phase 1): completed
NL CPT-11	CPT-11 encapsulated liposome nanoparticle	Recurrent high-grade gliomas	2008: NCT00734682 (phase 1): completed
CALAA-01	siRNA nanoparticle	Solid tumors	2008: NCT00689065 (phase 1): terminated
Nanoxel	Paclitaxel nanoparticle	Advanced breast cancer	2009: NCT00915369 (phase 1): unknown status
Paclical®	Paclitaxel micellar nanoparticle	Ovarian cancer	2009: NCT00989131 (phase 3): completed
Nanoparticle Albumin-Bound (Nab)	Nab paclitaxel/cyclophosphamide	Early-Stage Breast Cancer	2010: NCT00629499 (phase 2): completed
Docetaxel-PNP	Polymeric nano-formulation of docetaxel	Solid tumors	2010: NCT01103791 (phase 1): completed 2014: NCT02274610 (phase 1): completed
TKM 080301	siRNA lipid nanoparticles	Liver cancer	2011: NCT01437007 (phase 1): completed
NK105	Paclitaxel-incorporating micellar nanoparticle	Metastatic or recurrent breast cancer	2012: NCT01644890 (phase 3): completed
BIND-014	Docetaxel nanoparticles	Urothelial carcinoma, cholangiocarcinoma, prostate/lung/cervical/head/neck cancer	2011: NCT01300533 (phase 1): completed 2013: NCT01812746, NCT01792479 (phase 2): completed 2014: NCT02283320 (phase 2): completed

			2015: NCT02479178 (phase 2): terminated
CRLX101 (NLG207)	20(S)-camptothecin conjugated to cyclodextrin-polyethylene glycol-based polymer	Lung/ovarian/tubal/peritoneal/rectal/prostate cancer	2011: NCT01380769 (phase 2): completed 2012: NCT01652079 (phase 2): completed 2013: NCT02010567 (phase 1, phase 2): terminated 2019: NCT03531827 (phase 2): terminated
EGEN-001	IL-12 plasmid formulated with PEG-PEI-Cholesterol lipopolymer	Ovarian epithelial, fallopian tube, or primary peritoneal cancer	2012: NCT01489371 (phase 1): completed
RSV-F Vaccine	RSV-F protein nanoparticle	RSV	2012: NCT01709019 (phase 1): completed, NCT01704365 (phase 2): completed 2013: NCT01960686 (phase 2): completed 2014: NCT02296463 (phase 1): completed, NCT02247726 (phase 2): completed 2015: NCT02593071 (phase 2): completed, NCT02624947 (phase 3): completed
Magnetic nanoparticles	Magnetic nanoparticles	Prostate cancer	2013: NCT02033447 (phase 1): completed
Vitamin D encapsulated in casein micelles	Vitamin D encapsulated in casein micelles	Vitamin D deficiency	2013: NCT01807845: unknown status
ND-L02-s0201	Vitamin A-coupled lipid nanoparticle containing siRNA against HSP47	Moderate to extensive hepatic fibrosis	2013: NCT01858935 (phase 1): completed 2014: NCT02227459 (phase 1): completed

TUSC2-nanoparticles	TUSC2-nanoparticles	Lung cancer	2014: NCT01455389 (phase 1, phase 2): terminated
SGT-53	Cationic liposome encapsulating DNA	Recurrent glioblastoma	2014: NCT02340156 (phase 2): terminated
TargomiRs	Targeted minicells containing a microRNA mimic	Recurrent malignant pleural mesothelioma and non-small cell lung cancer	2014: NCT02369198 (phase 1): completed
DCR-MYC	Double stranded RNA formulated in a liposomal nanoparticle	Solid tumors	2014: NCT02110563 (phase 1): terminated 2015: NCT02314052 (phase 1, phase 2): terminated
NC-6004	Cisplatin contained polymeric nanoparticle	Solid tumors	2014: NCT02240238 (phase 1, phase 2): completed 2016: NCT02817113 (phase 1): terminated
BikDD nanoparticle	Cholesterol liposome-based nanoparticles	Advanced pancreatic cancer	2015: NCT00968604 (phase 1): withdrawn
EBOV GP vaccine	Ebola virus GP nanoparticle	Ebola	2015: NCT02370589 (phase 1): completed
CriPec® docetaxel	Docetaxel containing nanoparticles	Solid tumors	2015: NCT02442531 (phase 1): completed 2018: NCT03712423 (phase 1): completed, NCT03742713 (phase 2): completed 2015: NCT02379845 (phase 2, phase 3): completed
NBTXR3 nanoparticle	Hafnium oxide-containing nanoparticles	Solid tumors	2016: NCT02721056 (phase 1, phase 2): terminated

			2017: NCT02805894 (phase 1, phase 2): terminated 2020: NCT04484909 (phase 1): recruiting, NCT04615013 (phase 1): recruiting 2021: NCT04505267 (phase 1): recruiting NCT04862455 (phase 2): recruiting, NCT04834349 (phase 2): withdrawn 2023: NCT05039632 (phase 1, phase 2): recruiting
Targeting-Enhancing Nanoparticles of Paclitaxel	Paclitaxel nanoparticles	Advanced solid tumor	2016: NCT02979392 (phase 1): terminated
EP0057	Sugar molecule cyclodextrin linked to camptothecin	Lung cancer	2016: NCT02769962 (phase 1, phase 2): recruiting
PAN-301-1 (SNS-301)	Human aspartyl-asparaginyl-β-hydroxylase directed nanoparticle	Prostate cancer	2016: NCT03120832 (phase 1): completed
AZD4635	AZD4636 nanoparticle	Advanced solid malignancies	2016: NCT02740985 (phase 1): completed
Phospholipovit	Nanoemulsion of phospholipids	Combined hyperlipidemia	2016: NCT05742022 (phase 2, phase 3): completed
PLM60	Mitoxantrone Hydrochloride Liposome	Non-Hodgkin's Lymphoma	2016: NCT02856685 (phase 1, phase 2): unknown
SOR007	Uncoated nanoparticle paclitaxel	Plaque psoriasis	2016: NCT03004339 (phase 1): completed

MTL-CEBPA	Double stranded RNA formulated in a liposomal nanoparticle	Advanced liver cancer	2016: NCT02716012 (phase 1): active, not recruiting
EGFR(V)-EDV-Dox	Doxorubicin nanoparticle	Recurrent glioblastoma	2016: NCT02766699 (phase 1): unknown status
Tri-NIV	Recombinant trivalent nanoparticle	Influenza	2017: NCT03293498 (phase 1, phase 2): completed
NU-0129	Spherical nucleic acid arranged on the surface of spherical gold nanoparticles	Glioblastoma	2017: NCT03020017 (phase 1): completed
NC-6300	Nanoparticle epirubicin	Advanced solid tumors or soft tissue sarcoma	2017: NCT03168061 (phase 1, phase 2): unknown status
AZD2811	AZD2811 nanoparticle	Acute myeloid leukemia	2017: NCT03217838 (phase 1): terminated
IT141	Nanoparticle formulation of SN-38	Advanced cancer	2017: NCT03096340 (phase 1): terminated
mRNA-2416	mRNA lipid nanoparticle	Advanced malignancies	2017: NCT03323398 (phase 1, phase 2): terminated
STP705	siRNA histidine-lysine co-polymer peptide nanoparticles	Hypertrophic scar	2017: NCT02956317 (phase 1, phase 2): completed
MM-398	Liposomal irinotecan	Solid tumors	2017: NCT02631733 (phase 1): active, not recruiting 2018: NCT03337087 (phase 1, phase 2): active, not recruiting

			2019: NCT03736720 (phase 1): active, not recruiting 2020: NCT03739801 (phase 1, phase 2): withdrawn 2021: NCT04753216 (phase 2): completed
mRNA-2752	Lipid nanoparticle encapsulating mRNAs encoding human OX40L, IL-23, and IL-36γ	Advanced malignancies	2018: NCT03739931 (phase 1): active, not recruiting
IMX-110	Nanoparticle encapsulating a Stat3/NF-kB/poly-tyrosine kinase inhibitor	Advanced solid tumor	2018: NCT03382340 (phase 1, phase 2): active, not recruiting
Quad-NIV (NanoFlu™)	Recombinant quadrivalent nanoparticle	Influenza	2018: NCT03658629 (phase 2): terminated 2019: NCT04120194 (phase 3): completed
MTX110	Panobinostat nanoparticle	Diffuse intrinsic pontine glioma	2018: NCT03566199 (phase 1, phase 2): completed 2020: NCT04264143 (phase 1): completed
AGuIX® nanoparticles	Nanoparticles based on polysiloxane and gadolinium chelates	Solid tumors	2016: NCT02820454 (phase 1): completed 2018: NCT03308604 (phase 1): recruiting 2019: NCT03818386 (phase 2): recruiting 2020: NCT04094077 (phase 2): terminated 2021: NCT04789486 (phase 1, phase 2): recruiting, NCT04899908 (phase 2): recruiting 2022: NCT04881032 (phase 1, phase 2): recruiting 2024: NCT04784221 (phase 2): not yet recruiting
Paclitaxel-LDE	Paclitaxel carried by a lipid nanoparticle	Atherosclerotic	2019: NCT04148833 (phase 2, phase 3): unknown status

Laboratory Biomarker Analysis	Vincristine Sulfate Liposome	Recurrent Adult Acute Myeloid Leukemia	2019: NCT02337478 (phase 2): terminated
MRT5201	Codon-optimized human ornithine transcarbamylase mRNA with lipid-based nanoparticles	Ornithine transcarbamylase deficiency	2019: NCT03767270 (phase 1, phase 2): withdrawn
CNM-Au8	Gold nanocrystals	Amyotrophic Lateral Sclerosis, multiple sclerosis, Parkinson's disease	2019: NCT04098406, NCT03815916 (phase 2): completed, NCT03993171 (phase 2): recruiting 2020: NCT03843710 (phase 2): withdrawn
Methotrexate-loaded nanoparticles	Methotrexate-loaded nanoparticles	Inflammatory reaction of Covid-19 infection	2020: NCT04352465 (phase 1, phase 2): unknown status
NanoPac	Paclitaxel nanoparticle	Prostate cancer	2020: NCT04221828 (phase 2): terminated
Cetuximab nanoparticle	Cetuximab loaded polymeric nanoparticles	Colon cancer	2020: NCT03774680 (phase 1): unknown status
INT-1B3	Lipid nanoparticle formulated microRNA (miR-193a-3p) mimic	Advanced solid tumor	2020: NCT04675996 (phase 1): terminated
Gold factor	Gold nanoparticles	Knee joint health and function	2020: NCT05347602: completed
BNT165b1	RNA-lipid nanoparticle	Malaria	2020: NCT05581641 (phase 1): active, not recruiting
AgNPs	Silver nanoparticle	Covid-19	2020: NCT04978025: unknown status
NTLA-2001	Clustered regularly interspaced short palindromic repeats	Hereditary transthyretin	2020: NCT04601051 (phase 1): active, not recruiting

	(CRISPR)/Cas9 gene editing system delivered by lipid nanoparticles	amyloidosis with polyneuropathy, cardiomyopathy, or wild type cardiomyopathy	
ARCT-810	mRNA coding for cystic fibrosis transmembrane conductance regulator (CFTR) protein formulated in a lipid nanoparticle	Ornithine transcarbamylase deficiency	2020: NCT04416126 (phase 1): completed, NCT04442347 (phase 1): active, not recruiting 2022: NCT05526066 (phase 2): recruiting
MTX-LDE	Methotrexate carried by a lipid nanoparticle	Covid-19, atherosclerotic	2020: NCT04610567 (phase 1, phase 2): unknown status NCT04616872 (phase 2, phase 3): unknown status
GBP510	SK SARS-CoV-2 recombinant protein nanoparticle	Covid-19	2020: NCT04368988 (phase 1, phase 2): completed 2021: NCT04742738 (phase 1, phase 2): completed, NCT04750343 (phase 1, phase 2): active, not recruiting, NCT05007951 (phase 3): active, not recruiting 2022: NCT05175950 (phase 2): active, not recruiting
EP0057	Nanoparticle-drug conjugate	Advanced gastric and ovarian cancer, small cell lung cancer	2020: NCT04669002 (phase 2): completed 2023: NCT05411679 (phase 2): withdrawn
PRECIOUS-01	Invariant natural killer T cell (iNKT) activator threitolceramide-6 (ThrCer6, IMM60) and the New York esophageal squamous cell carcinoma-1 (NY-ESO-1) cancer-testis antigen peptides	Advanced solid tumor	2021: NCT04751786 (phase 1): recruiting

	encapsulated in PLGA nanoparticles		
ChulaCov19 vaccine	SARS-CoV-2 wild type S-spike mRNA lipid nanoparticle	Covid-19	2021: NCT04566276 (phase 1, phase 2): completed
CoV2 SAM	Self-amplifying mRNA lipid nanoparticle	Covid-19	2021: NCT04758962 (phase 1): completed
SpFN	SARS-CoV-2-spike-ferritin nanoparticle	Covid-19	2021: NCT04784767 (phase 1): unknown status
DS-5670a	mRNA lipid nanoparticles	Covid-19	2021: NCT04821674 (phase 1, phase 2): completed
UFluA	Influenza A hemagglutinin stabilized stem nanoparticle	Influenza	2021: NCT05155319 (phase 1): completed
ICC vaccine	Influenza quadrivalent hemagglutinin nanoparticle and SARS-CoV-2 rS nanoparticle	Covid-19, influenza	2021: NCT04961541 (phase 1, phase 2): completed 2022: NCT05519839 (phase 2): active, not recruiting
PepGNP	Gold nanoparticle plus peptides	Dengue virus, Covid-19	2021: NCT04935801 (phase 1): completed 2022: NCT05113862 (phase 1): completed 2023: NCT05633446 (phase 1, phase 2): not yet recruiting
Quaratusugene ozeplasmid (Reqorsa)	DNA plasmid with the TUSC2 tumor suppressor gene encapsulated lipid nanoparticles	Non-small cell lung cancer	2021: NCT04486833 (phase 1, phase 2): recruiting 2022: NCT05062980 (phase 1, phase 2): recruiting 2024: NCT05703971 (phase 1, phase 2): recruiting
Nano-QUT	Quercetin-encapsulated PLGA-PEG nanoparticles	Oral cancer	2022: NCT05456022 (phase 2): not yet recruiting

Carbon nanoparticle-loaded iron [CNSI-Fe(II)]	Carbon nanoparticle-loaded iron	Advanced solid tumor	2022: NCT06048367 (phase 1): recruiting
WGI-0301	Lipid Nanoparticle Suspension of Akt-1 Antisense Oligonucleotide	Advanced solid tumors or non-small cell lung, biliary and bladder cancer	2022: NCT05267899 (phase 1): recruiting
BL 1.33	Bupivacaine Liposome	Osteoarthritis of the shoulder	2022: NCT04134442 (phase 4): withdrawn
GF-AuKHC46	Gold Factor (gold nanoparticles, AuNPs)	Knee Osteoarthritis	2022: NCT05347602 (phase 1, phase 2, phase 3): completed
mRNA-3745	Lipid nanoparticle	Glycogen storage disease	2022: NCT05095727 (phase 1): recruiting
OTX-2002	mRNA lipid nanoparticles	Solid tumor	2022: NCT05497453 (phase 1, phase 2): recruiting
HDT-301	Replicon RNA (repRNA) SARS-CoV-2 nanoparticle	Covid-19	2022: NCT04844268 (phase 1): recruiting, NCT05132907 (phase 1): active, not recruiting
QTP104	repRNA lipid-inorganic nanoparticle	Covid-19	2022: NCT05876364 (phase 1): active, not recruiting
Covovax®	Recombinant spike protein nanoparticle	Covid-19	2022: NCT05112848 (phase 2): completed, NCT05433285 (phase 3): completed
Epstein-Barr Virus (EBV) gp350-Ferritin Vaccine	Helicobacter pylori non-heme ferritin fused to EBV gp350 which self-assembles to nanoparticles	EBV infection	2022: NCT04645147 (phase 1): active, not recruiting 2023: NCT05683834 (phase 1, phase 2): recruiting 2022: NCT05639894 (phase 1, phase 2): active, not recruiting
RSV mRNA vaccine	RSV mRNA lipid nanoparticles	RSV	2024: NCT06237296 (phase 1): not yet recruiting

V3G CH848 Pr-NP1	mRNA lipid nanoparticles	HIV	2023: NCT05903339 (phase 1): recruiting
OP-101-004	OP-101 (Dendrimer N-acetyl-cysteine)	COVID-19	2023: NCT04458298 (phase 1): terminated
D-4517.2	Hydroxyl dendrimer VEGFR tyrosine kinase inhibitor	Neovascular age-related macular degeneration / Diabetic macular edema	2023: NCT05387837 (phase 2): recruiting
DCVC H1 HA mRNA vaccine	DCVC H1 HA mRNA lipid nanoparticle	Influenza	2023: NCT05945485 (phase 1): recruiting
HA mRNA vaccines	mRNA lipid nanoparticles	Influenza	2023: NCT05829356 (phase 1): active, not recruiting
H1ssF-3928	mRNA lipid nanoparticles	Influenza	2023: NCT05755620 (phase 1): recruiting
BNT165e	RNA-lipid nanoparticles	Malaria	2023: NCT06069544 (phase 1, phase 2): recruiting
PLZ4-coated paclitacel-loaded micelles (PPM)	PPM	Recurrent or refractory non-muscle invasive bladder cancer	2023: NCT06173349 (phase 1): recruiting
Irinotecan liposome injection	Convection enhanced delivery (CED) of nanoliposomal irinotecan (nal-IRI)	Diffuse intrinsic pontine glioma	2023: NCT03086616 (phase 1): completed

Nanoparticle Albumin-Bound (Nab)	Nab-paclitaxel/Rituximab-coated Nanoparticle AR160	Relapsed or Refractory B-Cell Non-Hodgkin Lymphoma	2023: NCT03003546 (phase 1): completed
ARCT-032	mRNA coding for OTC formulated in a lipid nanoparticle	Cystic fibrosis	2023: NCT05712538 (phase 1): recruiting
TI-0010	circRNA lipid nanoparticle	Covid-19	2023: NCT06205524 (phase 1): recruiting
BIO 300 oral suspension	Genistein nanoparticles	Covid-19	2023: NCT04482595 (phase 2): recruiting
XBB.1.5 Vaccine	SARS-CoV-2 rS protein nanoparticle	Covid-19	2023: NCT05925127 (phase 2, phase 3): active, not recruiting, NCT05975060 (phase 2, phase 3): recruiting
PTX-COVID19-B	mRNA lipid nanoparticles	Covid-19	2023: NCT05534035, NCT05534048 (phase 3): not yet recruiting
MT-302	TROP2-FcA mRNA lipid nanoparticle	Advanced or metastatic epithelial tumors	2023: NCT05969041 (phase 1): recruiting
RNA-nanoparticle vaccine	Autologous total tumor mRNA loaded DOTAP liposome	Melanoma	2024: NCT05264974 (phase 1): recruiting

siRNA: small interfering RNA. Nab: Nanoparticle Albumin-Bound. RSV: Respiratory Syncytial Virus. GP: glycoprotein. mRNA: messenger RNA. HIV: Human Immunodeficiency Virus. circRNA: Circular RNA.

Appendix B: Supplementary Information for Chapter 2

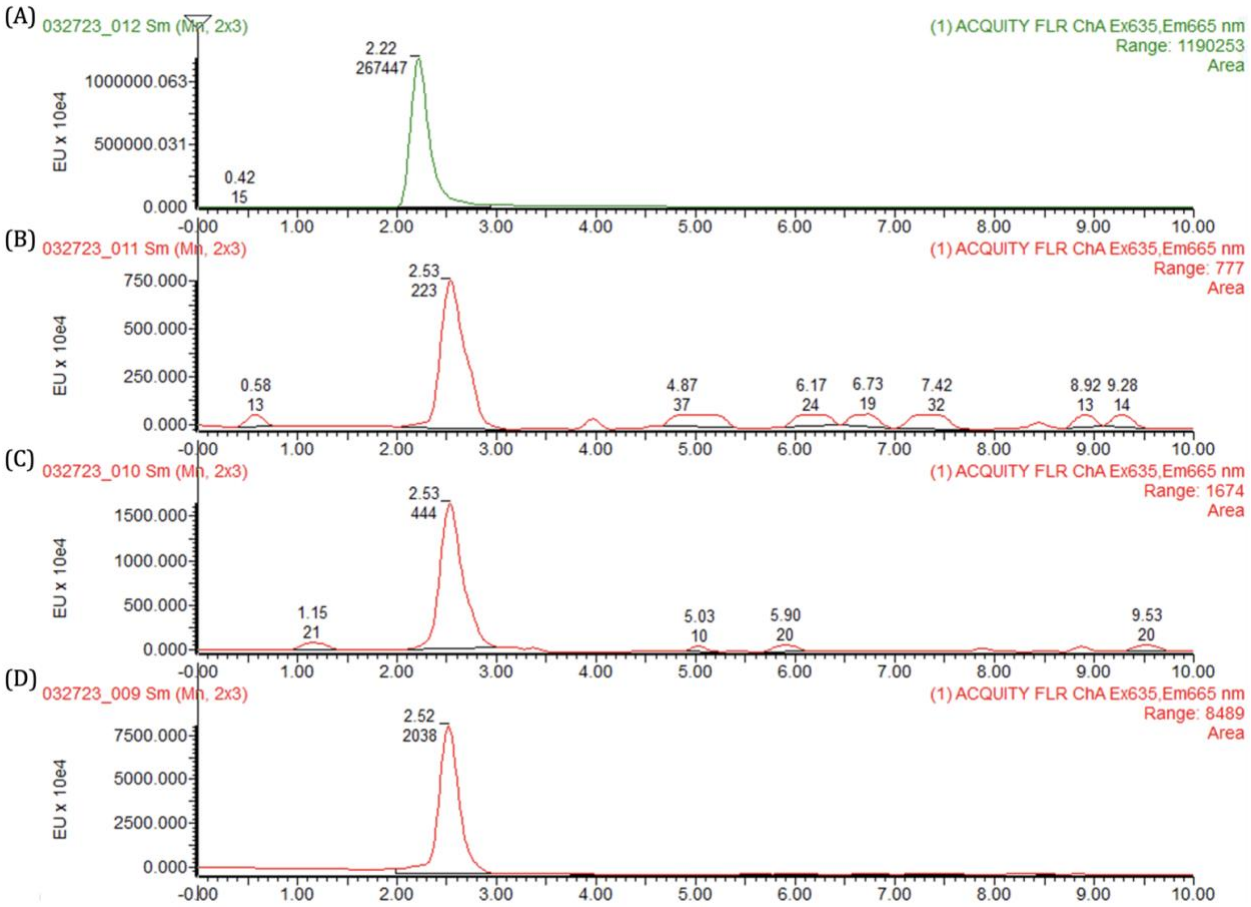

Figure S2-1. Representative HPLC chromatograms acquired based on Ex/Em at 635 nm/665 nm for: (A) Free CF647 dye at a 20 nmol/mL concentration, (B) blank serum extracts, (C) serum extracts obtained from rat 4 h post injection of PLGA-PEG/F127 at a 150 mg/kg dosage, and (D) serum extracts obtained from rat 4 h post injection of PLGA-PEG/P80 at a 150 mg/kg dosage. The retention time for the serum extracts is different than the free CF647, indicating that there was no CF647 detected in serum extracts.

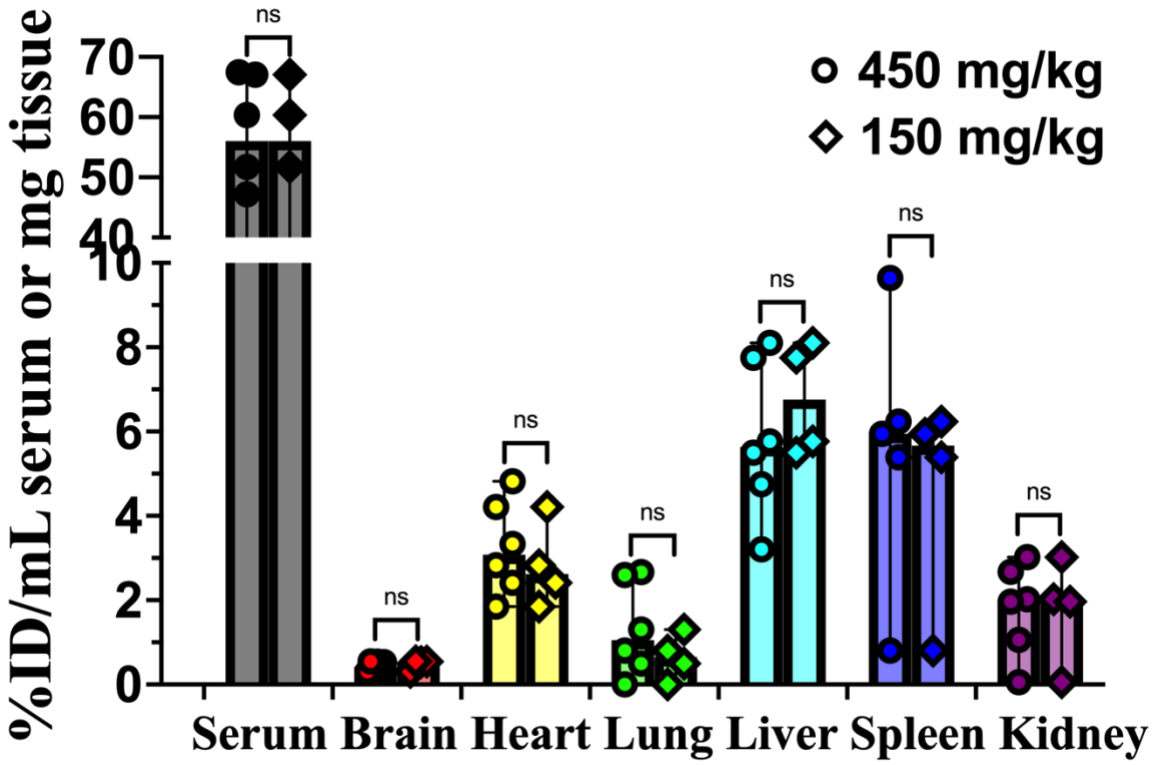

Figure S2-2. Biodistribution of PLGA-PEG/P80 at 4 h after i.p. injection with 450 mg/kg i.p. dosage versus 150 mg/kg i.p. dosage in healthy P10 rat (n≥4 per timepoint). Graph displays median ± 95% confidence interval. Group differences were evaluated by Welch's t-test, ns: not significant.

Appendix C: Supplementary Information for Chapter 3

Table S3-1. Physicochemical properties of curcumin-loaded PLGA-PEG formulated via standard nanoprecipitation technique after lyophilization. All values are reported as mean ± standard error of the mean (SEM) (n = 3).

Curcumin-loaded PLGA-PEG	Size ± SEM (nm)	PDI ± SEM	Zeta potential ± SEM (mV)	Curcumin release after lyophilization
Before lyophilization	63.9 ± 1.5	0.06 ± 0.02	-4.6 ± 0.7	
Lyophilized without cryoprotectant	187.4 ± 110.2	0.47 ± 0.02	-4.9 ± 0.3	Yes
Lyophilized with 5% sucrose	72.4 ± 7.8	0.39 ± 0.01	-3.5 ± 0.2	Yes
Lyophilized with 5% F68	74.2 ± 8.8	0.36 ± 0.07	-5.5 ± 0.5	Yes
Lyophilized with 5% F127	64.4 ± 3.7	0.48 ± 0.01	-5.6 ± 0.2	Yes
Lyophilized with 5% inulin	75.6 ± 8.0	0.19 ± 0.02	-3.8 ± 0.5	Yes
Lyophilized with 5% trehalose	77.4 ± 11.8	0.51 ± 0.07	-6.0 ± 1.8	Yes

Table S3-2. Physicochemical properties of curcumin-loaded PLGA-PEG formulated with 20 mg/mL PLGA-PEG and curcumin (20: 20). All values are reported as mean ± standard error of the mean (SEM) (n = 3).

Curcumin-loaded PLGA-PEG	Size ± SEM (nm)	PDI ± SEM	Zeta potential ± SEM (mV)
Before lyophilization	74.9 ± 7.0	0.11 ± 0.02	-6.4 ± 1.3
Lyophilized with 5% sucrose	32.0 ± 6.7	0.75 ± 0.03	-8.0 ± 1.7

Table S3-3. Physicochemical properties of fluorescent dye-labeled curcumin-loaded PLGA-PEG nanoparticles. Initial concentration of curcumin: 13.3 mg/mL, initial concentration of PLGA-PEG: 20 mg/mL; organic solution: aqueous solution = 1: 10; 0.1% F127 was used as aqueous solution. All values are reported as mean ± standard error of the mean (SEM) (n = 3).

Dye-labeled curcumin-loaded PLGA-PEG	Size ± SEM (nm)	PDI ± SEM	Zeta potential ± SEM (mV)
CF555	53.9 ± 5.9	0.17 ± 0.03	-1.6 ± 0.6
CF647	54.6 ± 5.8	0.14 ± 0.01	-3.9 ± 2.7

Table S3-4. Comparison of curcumin-loaded PLGA-PEG nanoparticles formulated via sequential nanoprecipitation and standard nanoprecipitation technique.

Formulation technique	Sequential nanoprecipitation	Standard nanoprecipitation
Drug loading	39 %	5 % - 10 %
Drug encapsulation efficiency	> 95 %	~ 50 %
Nanoparticle size	More tunable	Less tunable
Polydispersity index	< 0.2	< 0.2
Zeta potential	0 - -10 mV	0 - -10 mV
Release profile	Sustained release up to 8 days	80% released in 24 h

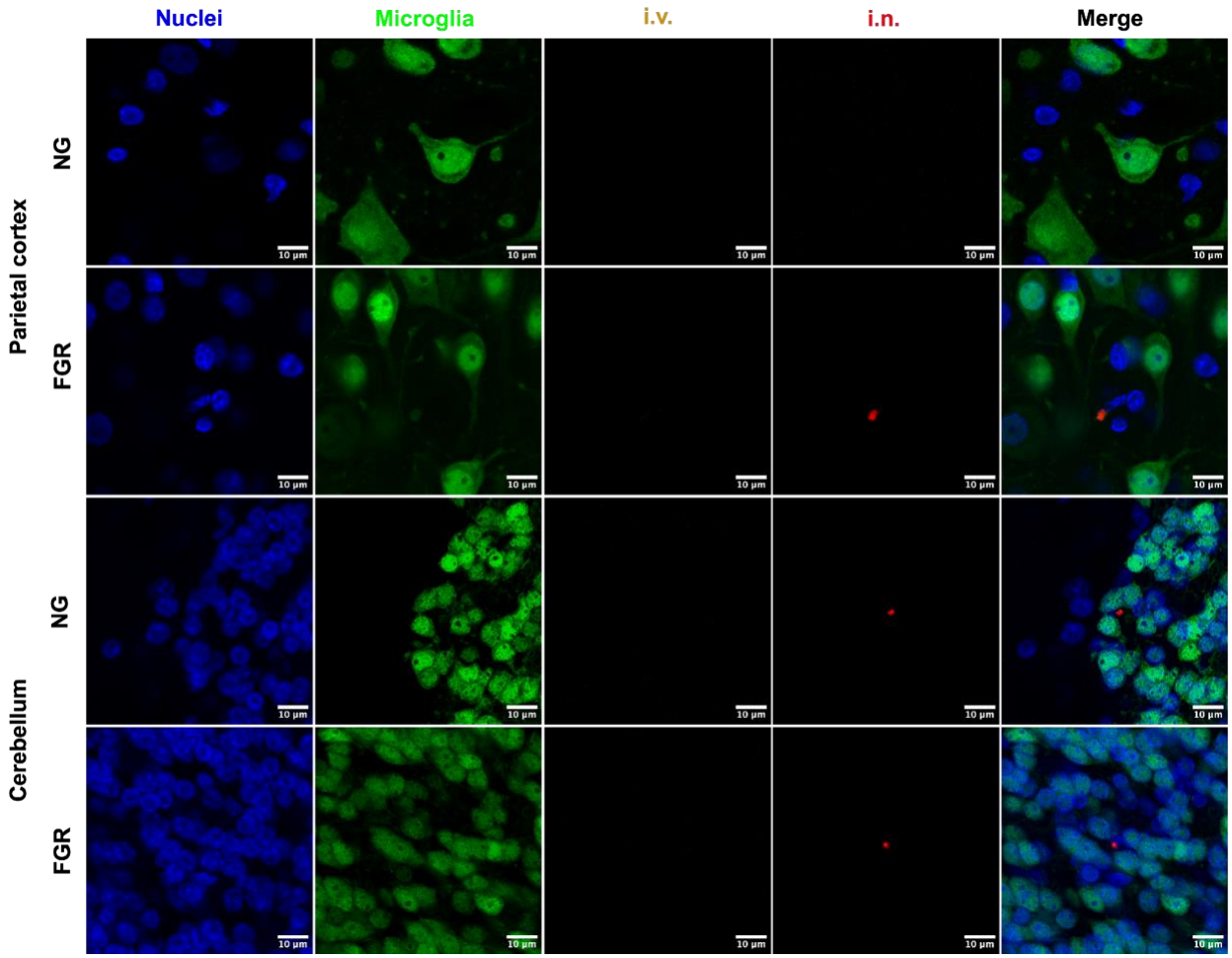

Figure S3-1. Curcumin-loaded PLGA-PEG accumulation in parietal cortex and cerebellum at 4 h after i.v. (orange) and i.n. (red) administration. Small amount of particles were found in extracellular space of neurons in NG and FGR piglet brains. Scale bars: 10 μm. Blue: DAPI nuclei stain. Green: NeuN neuron stain.

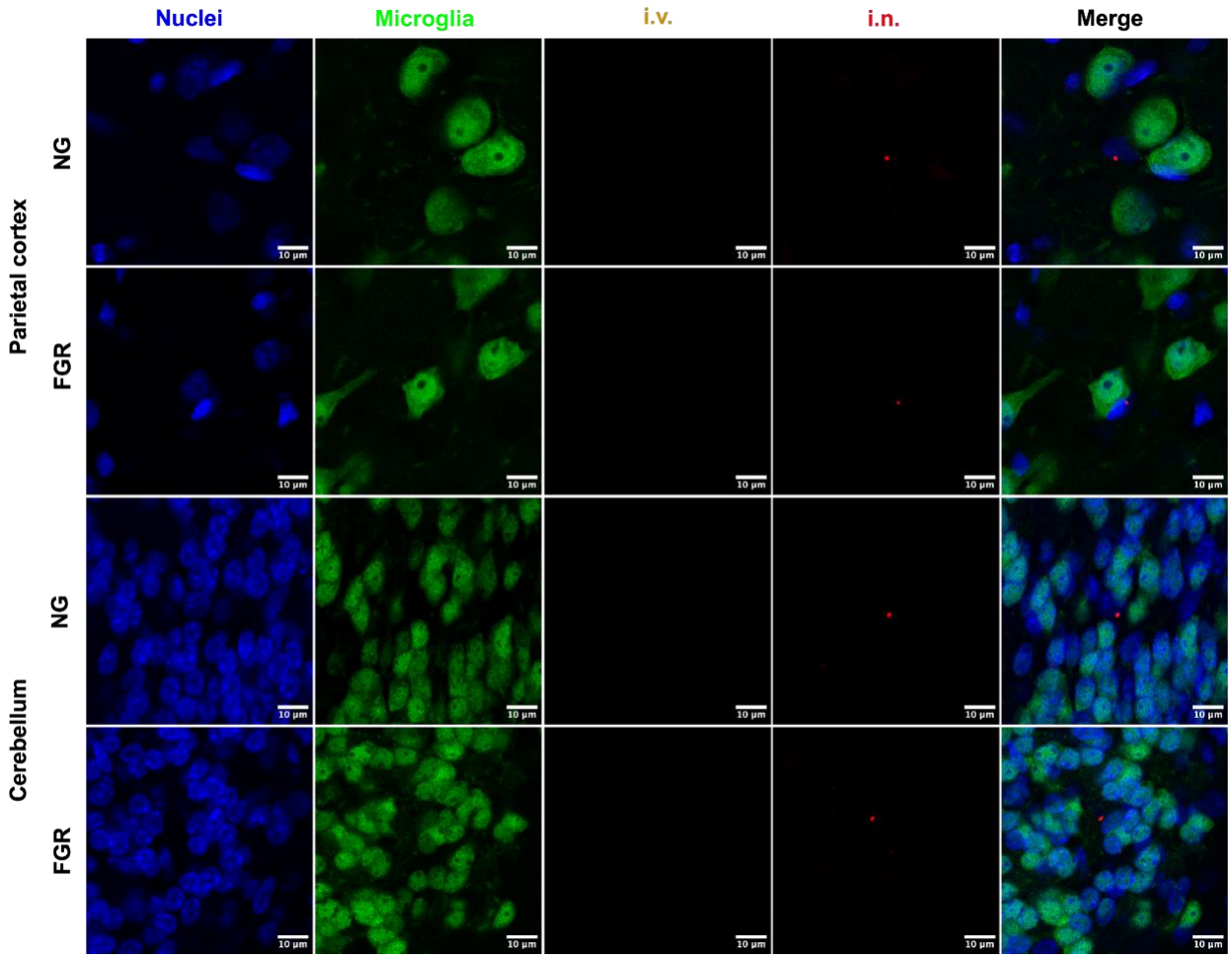

Figure S3-2. Curcumin-loaded PLGA-PEG accumulation in parietal cortex and cerebellum at 48 h after i.v. (orange) and i.n. (red) administration. Small amount of particles were found in extracellular space of neurons in NG and FGR piglet brains. Scale bars: 10 μm. Blue: DAPI nuclei stain. Green: NeuN neuron stain.

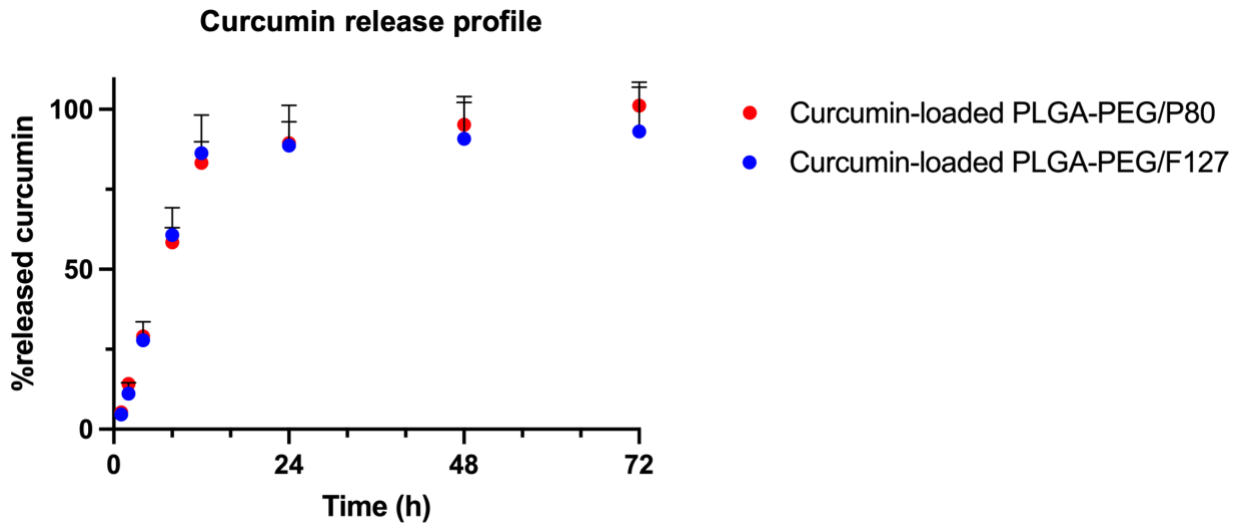

Figure S3-3. Curcumin release profiles for curcumin-loaded PLGA-PEG nanoparticles formulated with 1% P80 (curcumin-loaded PLGA-PEG/P80) and 1% F127 (curcumin-loaded PLGA-PEG/F127) via standard nanoprecipitation.

Curriculum Vitae

Nuo Xu

Benson Hall #239
University of Washington nuoxu@uw.edu
Seattle, WA 98105 (206) 288-3338

I. EDUCATION

Ph.D. in Chemical Engineering **06/21 – Present**
University of Washington, Seattle, WA
Expected Defense: June 9th, 2025
Thesis title: Pharmacokinetics and efficacy of a tunable curcumin-loaded polymeric nanoparticle for neonatal neuroprotection

Master of Science in Chemical Engineering **09/19 – 06/21**
University of Washington, Seattle, WA
Thesis title: Bupivacaine loaded nanoparticles coated on microneedle arrays for nerve block

Bachelor of Science in Pharmacy **09/15 – 06/19**
East China University of Science and Technology, Shanghai, China
Thesis title: Application of mesoporous silica nanocarriers in insect RNA interference

II. SUMMARY OF SKILLS

- Experimental Skills – nanoparticle formulation and characterization, nanoparticle functionalization, nanoparticle lyophilization, colloidal stability evaluation, drug loading and release analysis, polymer conjugation and functionalization, RNA extraction, RT-qPCR, immunofluorescent imaging and imaging analysis, wet chemistry.
- Spectroscopy and Chromatography – UV-Vis spectroscopy, confocal microscopy, spectrophotometer, DLS, nanoparticle tracking analysis (NTA), HPLC, LC-MS.
- In Vivo and Ex Vivo Expertise – handling and procedures on rats and mice (intraperitoneal and oral administration, blood collection, tissue harvesting), *in vivo* pharmacokinetics, *in vivo* pharmacology, preclinical animal models, tissue slicing and culturing.
- Computer and Instrumentation Software – Microsoft office (word, excel, power point), GraphPad Prism, Fiji, Python, Matlab, Chemdraw.
- Professional Skills – project management, technical writing.

III. RESEARCH EXPERIENCE

Ph.D. student, graduate research Assistant; Advisor: Dr. Elizabeth Nance, University of Washington, Seattle, WA

06/21 – Present

- Characterized the neonatal pharmacokinetic (PK) profiles and biodistribution of polymeric nanoparticles, effect of surfactant, and relationship between surfactant and protein corona composition on PLGA-PEG nanoparticles.
- Evaluated the neuroprotection effects of different drug-loaded PLGA-PEG nanoparticles in different neonatal age groups, and designed the optimal dosage and dosing interval for HI treatment in neonatal rats with HI injury.

- Developed a tunable, controllable, reproducible, and scalable PLGA-PEG-based nanoplatform with good shelf-life stability.
- In collaboration with Perinatal Research Centre in University of Queensland, assessed the therapeutic efficacy of the optimized curcumin-contained formulation in piglet model, and compared the neuroprotection effects of nanomedicine administrated via different routes.

Master student; Advisor: Dr. Elizabeth Nance, University of Washington, Seattle, WA

03/20 – 06/21

Project: Bupivacaine loaded nanoparticles coated on microneedle arrays for nerve block

- Developed a bupivacaine-loaded polymer nanoparticle for encapsulation into flexible microneedle array electrodes to achieve sustained and controlled drug delivery of bupivacaine in a rat model of spinal cord injury.
- Altered biodegradable particle surface properties to determine optimal nanoparticle loading and release from flexible microneedle array electrodes.
- In collaboration with Neurosurgery, evaluated the efficacy of the polymer nanoparticle-coated flexible microneedle array electrodes in reducing pain response in spinal cord injury.

Undergraduate research Assistant; Advisor: Dr. Zhiping Xu, East China University of Science and Technology, Shanghai, China

09/18 – 07/19

- Extracted RNA from *Culex pipiens*, and prepared dsRNA of chitin synthase gene (CHS1) through reverse transcription, TA cloning, and plasmid preparation.
- Loaded dsRNA into mesoporous silica nanocarriers and verified vector stability through agarose gel electrophoresis.

Undergraduate research Assistant; Advisor: Dr. Jinxing Ye, East China University of Science and Technology, Shanghai, China

09/17 – 05/19

- Developed the first two steps of a green synthesis method of a broad-spectrum antibacterial drug draxacin by optimizing the original synthesis process to reduce the cost of expensive intermediates and the generation of toxic intermediates.

IV. PUBLICATIONS

5. Parrot, M., **Xu, N.**, Nance, E., Adnan, M., Cave, J., Ghandehari, H., Yellepeddi, V. From Bench to Bedside: Overcoming Translational Hurdles in Nanoparticle Research with Pharmacokinetic Modeling. Manuscript in preparation.
4. **Xu, N.**, Wixey, J., Chand, K., Wong, M., Nance, E. Nano-formulated curcumin uptake and biodistribution in the fetal growth restricted newborn piglet brain. *Drug Delivery and Translational Research* 2025, 1-15.
3. **Xu, N.**, Wong, M., Balistreri, G., Nance, E. Neonatal Pharmacokinetics and Biodistribution of Polymeric Nanoparticles and Effect of Surfactant. *Pharmaceutics* 2023, 15, 1176.
2. Joseph, A., Simo, G. M., Gao, T., Alhindi, N., **Xu, N.**, Graham, D. J., Nance, E. Surfactants influence polymer nanoparticle fate within the brain. *Biomaterials* 2021, Vol. 277 Pages 121086.
1. Helmbrecht, H., **Xu, N.**, Liao, R., Nance, E. Data management schema design for effective nanoparticle formulation for neurotherapeutics. *AIChE J.* 2021, 67(12):e17459.

V. PRESENTATIONS

Oral presentations ǂpresenting author

3. **Xu, N.**, Wixey, J., Chand, Kirat., Nance, Eǂ. Nano-formulated curcumin uptake and biodistribution in the fetal growth restricted newborn piglet brain. AIChE Annual Meeting, San Diego, CA; October 31, 2024.
2. **Xu, N.**ǂ, Wong, M., Chand, K., Wixey, J., Nance, E. Neonatal pharmacokinetics and biodistribution of polymeric nanoparticles. 2023 BMES Annual Meeting, Seattle, WA; October 13, 2023.
1. **Xu, N.**ǂ, Wong, M., Nance, E. Neonatal pharmacokinetics and biodistribution of polymeric nanoparticles and effect of surfactant. AIChE Annual Meeting, Phoenix, AZ; November 15, 2022.

Poster presentations ǂpresenting author

3. **Xu, N.**ǂ, Wixey, J., Chand, Kirat., Nance, E. Nano-formulated curcumin uptake and biodistribution in the fetal growth restricted newborn piglet brain. Drug Carriers in Medicine and Biology Gordon Research Conference, Portland, ME; August 7 – 8, 2024.
    2. Wixey, J., **Xu, N.**, Chand, Kirat., Colditz, P., Nance, E. Curcumin-loaded nanoparticles rapidly accumulate in the fetal growth restricted newborn brain. The 14th Hershey Conference on Developmental Brain Injury, Marstrand, Sweden; June, 2024.
1. **Xu, N.**ǂ, Wong, M., Nance, E. Neonatal pharmacokinetics and biodistribution of polymeric nanoparticles. Controlled Release Society Annual Meeting, Montreal, Canada; July 14, 2022.

VI. HONORS AND AWARDS

2023 Barbara Krieger-Brockett Travel Award; University of Washington, Seattle, WA

2018 The Second Prize Scholarship (10%); East China University of Science and Technology, Shanghai, China

2017 The Second Prize Scholarship (10%); East China University of Science and Technology, Shanghai, China

2016 The Third Prize Scholarship (20%); East China University of Science and Technology, Shanghai, China

VII. TEACHING AND MENTORING

University of Washington, Department of Chemical Engineering, Teaching Assistant for Unit Operation I
Spring 2023

University of Washington, Department of Chemical Engineering, Teaching Assistant for Unit Operation I
Spring 2022

Trainees

Sofia Dahlgren, Chemical Engineering, Mary Gates Research Scholar, Goldwater Scholar (2025)
2024 - Present

Megan Wong, Chemical Engineering, NIH fellow, Honor's Thesis
2020 - 2024

Danielle Bondurant, Chemical Engineering, NIH fellow
2021- 2022